

DETERMINATION OF ADSORPTION AND SEPARATION OF CO₂/N₂ AND H₂S/CH₄
MIXTURES IN POROUS MATERIALS BY MOLECULAR SIMULATION



A Dissertation Submitted in Partial Fulfillment of the Requirements
for the Degree of Doctor of Philosophy in Petrochemistry and Polymer Science

Field of Study of Petrochemistry and Polymer Science

FACULTY OF SCIENCE

Chulalongkorn University

Academic Year 2021

Copyright of Chulalongkorn University

การตรวจสอบการดูดซับและการแยกของผสม CO_2/N_2 และ $\text{H}_2\text{S}/\text{CH}_4$ ในวัสดุรูพรุนด้วยการจำลอง
แบบทางโมเลกุล.



วิทยานิพนธ์นี้เป็นส่วนหนึ่งของการศึกษาตามหลักสูตรปริญญาวิทยาศาสตรดุษฎีบัณฑิต
สาขาวิชาปิโตรเคมีและวิทยาศาสตร์พอลิเมอร์ สาขาวิชาปิโตรเคมีและวิทยาศาสตร์พอลิเมอร์
คณะวิทยาศาสตร์ จุฬาลงกรณ์มหาวิทยาลัย
ปีการศึกษา 2564
ลิขสิทธิ์ของจุฬาลงกรณ์มหาวิทยาลัย

Thesis Title	DETERMINATION OF ADSORPTION AND SEPARATION OF CO ₂ /N ₂ AND H ₂ S/CH ₄ MIXTURES IN POROUS MATERIALS BY MOLECULAR SIMULATION
By	Mr. Tanawut Ploymeerusmee
Field of Study	Petrochemistry and Polymer Science
Thesis Advisor	Professor Dr. SUPOT HANNONGBUA
Thesis Co Advisor	Associate Professor Dr. Tatiya Chokbunpiam

Accepted by the FACULTY OF SCIENCE, Chulalongkorn University in Partial
Fulfillment of the Requirement for the Doctor of Philosophy

..... Dean of the FACULTY OF SCIENCE
(Professor Dr. POLKIT SANGVANICH)

DISSERTATION COMMITTEE

..... Chairman
(Professor Dr. PATTARAPAN PRASASSARAKICH)

..... Thesis Advisor
(Professor Dr. SUPOT HANNONGBUA)

..... Thesis Co-Advisor
(Associate Professor Dr. Tatiya Chokbunpiam)

..... Examiner
(Professor Dr. Voravee Hoven)

..... Examiner
(Associate Professor Dr. Somsak Pianwanit)

..... External Examiner
(Assistant Professor Dr. Tawun Remsungnen)

ธนาวุฒิ พลอยมีร์คีมี : การตรวจสอบการดูดซับและการแยกของผสม CO_2/N_2 และ $\text{H}_2\text{S}/\text{CH}_4$ ในวัสดุรูพรุนด้วยการจำลองแบบทางโมเลกุล.. (DETERMINATION OF ADSORPTION AND SEPARATION OF CO_2/N_2 AND $\text{H}_2\text{S}/\text{CH}_4$ MIXTURES IN POROUS MATERIALS BY MOLECULAR SIMULATION) อ.ที่ปรึกษาหลัก : ศ. ดร.สุพจน์ หารหนองบัว, อ.ที่ปรึกษาร่วม : รศ. ดร.ตติยา ไชคุญญเปี่ยม

แหล่งพลังงานหลักของโรงไฟฟ้าในโลกพึ่งพาด่านหินและก๊าซธรรมชาติซึ่งมีความคุ้มค่าเชิงเศรษฐศาสตร์สำหรับการผลิตไฟฟ้า ก๊าซไอเสียส่วนใหญ่คือ N_2 และ CO_2 ถูกผลิตและปล่อยสู่ชั้นบรรยากาศ โครงข่ายซีโอไลติกอิมิดาโซเลต - 90 (ซีฟ-90) มีศักยภาพสูงในฐานะตัวเลือกสำหรับการใช้งานที่หลากหลาย ดังนั้น ความรู้พื้นฐานเกี่ยวกับการดูดซับและการแพร่กระจายของก๊าซในวัสดุนี้เป็นปัจจัยสำคัญในการปรับปรุงเทคนิคการแยกก๊าซนี้ โมเลกุล CO_2 ที่ดูดซับบนโครงสร้างของ ZIF-90 ส่งผลให้สามารถเกิดการเปิดประตูได้ขึ้นกับปริมาณของโมเลกุลที่ดูดซับและอุณหภูมิ แต่ปรากฏการณ์นี้ไม่สามารถพบได้สำหรับโมเลกุลไนโตรเจน เส้นผ่านศูนย์กลางหน้าต่างเพิ่มขึ้นสูงสุดที่ 4.43 อังสตรอม ตามการเพิ่มขึ้นของอุณหภูมิ ปัจจัยการแยกสารของแก๊สผสม CO_2/N_2 ในรูปแบบของการเลือกจำเพาะแบบดูดซับและแบบแพร่แสดงค่าสูงสุดประมาณ 6 และ 12 ที่ 298 เคลวิน ตามลำดับ นอกจากนี้ วัสดุดีบุกหลักอันดับสองสำหรับโรงไฟฟ้าคือก๊าซธรรมชาติซึ่งต้องไม่มี H_2S ก่อนนำไปใช้งาน วัสดุทั้งหมดที่เลือกมาทดสอบมีความเหมาะสมในการแยกแต่มีประสิทธิภาพต่างกัน สำหรับ MIL-127(Fe) ความสามารถในการคัดเลือกจำเพาะ $\text{CH}_4/\text{H}_2\text{S}$ มีค่าประมาณ 250 ที่ 2 บาร์และ 250 เคลวิน ผลลัพธ์ที่ได้สามารถสรุปได้ในขั้นต้นว่าพลังงานศักย์ของคู่แก๊ส/วัสดุแต่ละคู่ พื้นที่ว่างภายในวัสดุและโลหะออกไซด์มีค่าเท่ากับ กุญแจสำคัญในการดูดซับและแยก H_2S จาก CH_4

สาขาวิชา ปีโตรเคมีและวิทยาศาสตร์พอลิ ลายมือชื่อนิสิต

เมอร์

ปีการศึกษา 2564

ลายมือชื่อ อ.ที่ปรึกษาหลัก

ลายมือชื่อ อ.ที่ปรึกษาร่วม

5872812223 : MAJOR PETROCHEMISTRY AND POLYMER SCIENCE

KEYWORD: adsorption, diffusion, separation, porous material

Tanawut Ploymeerusmee : DETERMINATION OF ADSORPTION AND SEPARATION OF CO₂/N₂ AND H₂S/CH₄ MIXTURES IN POROUS MATERIALS BY MOLECULAR SIMULATION. Advisor: Prof. Dr. SUPOT HANNONGBUA Co-advisor: Assoc. Prof. Dr. Tatiya Chokbunpiam

The major resources of power plant in the world rely on coal and natural gas which are economical for generating electricity. Flue gases, mainly N₂ and CO₂, are produced and released into the atmosphere. The zeolitic imidazolate framework-90 (ZIF-90) obtains a high potential as being a candidate for several applications. Consequently, the basic knowledge of adsorption and diffusion of gases in this material is the key factor of improving this gas separation technique. The effect of adsorbed CO₂ molecules on the lattice structure of ZIF-90 can lead to gate opening depending on the amount of adsorbed guest molecules and the temperature but this is not observed for N₂ molecules. The window diameter is increased up to 4.43 Å with increasing temperature. The separation factors of the CO₂/N₂ mixture in form of adsorption and diffusion selectivity show the highest values of about 6 and 12 at 298 K, respectively. In addition, the second major feedstock for power plants is natural gas which must be freed from H₂S before using. All investigated materials are suited for the separation, but with different efficiency. For MIL-127(Fe) the CH₄/H₂S selectivity reaches values of about 250 at 2 bar and 250 K. The results can be initially concluded that the potential energy of each gas/material pair, free space inside the material and metal oxide are important keys for adsorption and separation of H₂S from CH₄.

Field of Study: Petrochemistry and
Polymer Science

Student's Signature

Academic Year: 2021

Advisor's Signature

Co-advisor's Signature

ACKNOWLEDGEMENTS

This dissertation would not be possible and feasible without people who have supported and encouraged me. Therefore, in this acknowledgment, I would like to name and thank the people who have contributed to my work.

First of all, I would like to appreciatively thank my advisor Prof. Dr. rer. nat. Supot Hannongbua and also my co-advisors consisting of Assoc Prof. Dr. Tatiya Chokbunpiam for giving me the opportunity to study at Chulalongkorn University where I was able to learn and complete my Doctor of Philosophy Program under their kind encouragement and constant help.

I would like to take this opportunity to thank Priv-Doz. Dr. rer. nat. habil. Siegfried Fritzsche, Asst. Prof. Dr. Tawun Remsungnen for many good ideas, discussions and encouragement in difficult times. Furthermore, I would like to thank Professor Dr. Voravee P. Hoven, Assoc. Prof. Dr. Somsak Pianwanit, who act as the thesis committee. Special thanks to my family and protectors such as Asst. Prof. Dr. Siriphan Nilpairach and Asst. Prof. Dr. Krisana Siralermukul who supported me during this work. Their unconditional love is the source of my strength.

Lastly, I also would like to acknowledge the Malaysia-Thailand Joint Authority (MTJA) Research Cess Fund (RCF) and Petroleum, Petrochemicals, and Advanced Materials for financial supporting. All facilities and computing resources are offered by the Computational Chemistry Unit Cell (CCUC) at Department of Chemistry, Faculty of Science, Chulalongkorn University and the High Performance Computing Cluster of Assoc Prof. Dr. Tatiya Chokunpiam at the Department of Chemistry, Faculty of Science, Ramkhamhaeng University.

Tanawut Ploymeerusmee

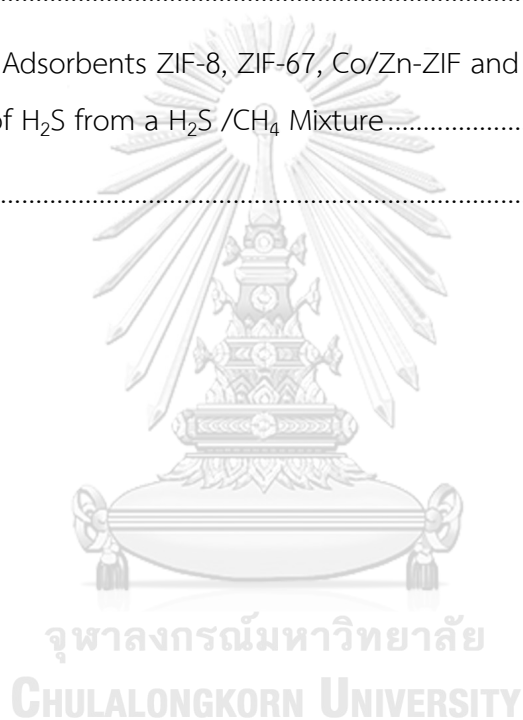
TABLE OF CONTENTS

	Page
.....	iii
ABSTRACT (THAI).....	iii
.....	iv
ABSTRACT (ENGLISH).....	iv
ACKNOWLEDGEMENTS.....	v
TABLE OF CONTENTS.....	vi
LIST OF TABLES.....	x
LIST OF FIGURES.....	xi
CHAPTER 1.....	1
INTRODUCTIONS.....	1
1.1. Research rationale.....	1
1.2. Zeolitic Imidazolate Frameworks (ZIFs).....	6
1.3. Literature reviews.....	9
1.4. Scope of this study.....	12
CHAPTER II.....	13
THEORY BACKGROUND.....	13
2.1. Molecular simulation techniques.....	13
2.1.1. Force field interactions.....	13
2.1.1.1. The intramolecular potential.....	13
2.1.1.2. The intermolecular potential.....	15
2.1.2. Periodic Boundary Conditions (PBC).....	17

2.1.3. Ensembles.....	18
2.1.4. Radial Distribution Function (RDF).....	19
2.1.5. Adsorption, diffusion and permeation	20
2.2. Gibbs ensemble Monte Carlo (GEMC) simulation	23
2.3. Molecular dynamics simulations	24
2.3.1. Classical mechanics.	25
2.3.2. Integration algorithms.....	27
CHAPTER III.....	30
CALCULATION DETAILS	30
3.1. CO ₂ and N ₂ in ZIF-90.....	30
3.1.1. Force Field Validation.....	30
3.1.2. Gibbs ensemble Monte Carlo simulations	32
3.1.3. Molecular dynamics (MD) simulations	33
3.2. H ₂ S and CH ₄ in ZIFs and MIL-127 materials.....	33
3.2.1. Gibbs ensemble Monte Carlo simulations.	37
3.2.2. Molecular dynamics (MD) simulations.	38
CHAPTER IV	40
RESULTS AND DISCUSSION.....	40
4.1. CO ₂ and N ₂ in ZIF-90	40
4.1.1. Verifying force field of CO ₂ and N ₂ in ZIF-90 by using Gibbs ensemble Monte Carlo simulations.....	40
4.1.2. Adsorption isotherm and adsorption selectivity of CO ₂ /N ₂ mixture in ZIF- 90 material.....	41
4.1.3. Effect of the number of adsorbed gas molecules (CO ₂) by Molecular Dynamics (MD) simulations.....	44

4.1.4. Temperature effect on CO ₂ adsorption by Molecular Dynamics (MD) simulations.....	45
4.1.5. Effect of the number of adsorbed gas molecules (N ₂) by Molecular Dynamics (MD) simulations.....	47
4.1.6. Self-diffusion coefficient of CO ₂ and N ₂ in ZIF-90 by Molecular Dynamics (MD) simulations	49
4.1.7. Radial distribution functions and Density Plots by Molecular Dynamics (MD) simulations	52
4.2. H ₂ S/CH ₄ in ZIFs and MIL-127 materials.....	56
4.2.1. Adsorption Isotherms and Adsorption Selectivity	56
4.2.1.1. Pure Gases	56
4.2.1.2. H ₂ S/ CH ₄ Mixture in ZIF-8.....	59
4.2.1.3. H ₂ S/ CH ₄ Mixture in ZIF-67	60
4.2.1.4. H ₂ S/ CH ₄ Mixture in Co/Zn-ZIF	61
4.2.1.5. H ₂ S/ CH ₄ Mixture in MIL-127(Fe).....	63
4.2.2. Enthalpy of adsorption.....	64
4.2.3. Radial distribution functions (RDFs)	65
4.2.3.1. H ₂ S/CH ₄ mixture in ZIF-8 at 250 K.....	66
4.2.3.2. H ₂ S/CH ₄ mixture in MIL-127(Fe) at 250 K	67
4.2.4. The average numbers of adsorbed molecules in the ZIFs and MIL-127 materials.....	68
4.2.5. Dynamic property	70
4.2.5.1. Self-diffusion	70
4.2.5.2. Selectivityies.....	71
CHAPTER V	73

CONCLUSIONS	73
REFERENCES	75
APPENDICES.....	87
APPENDIX A	88
CO ₂ induced swing effect at imidazolate of zeolitic imidazolate framework-90 using molecular simulations	88
APPENDIX B	91
Porous Material Adsorbents ZIF-8, ZIF-67, Co/Zn-ZIF and MIL-127(Fe) for separation of H ₂ S from a H ₂ S /CH ₄ Mixture.....	91
VITA.....	100



LIST OF TABLES

	page
Table 3.1 Lennard-Jones parameters and charge of all atom types in ZIF-90.	30
Table 3.2 Lennard-Jones parameters and charge of all atom types for CO ₂ and N ₂ ...	31
Table 3.3 Lennard-Jones parameters [82, 83] and charge of all atom types in ZIF-8 [82], ZIF-67 [84] and Co/Zn ZIFs [82]......	34
Table 3.4 Bond lengths (Å) and force constants (kcal/mol/Å ²) of ZIF-8, ZIF-67 and Co/Zn ZIFs [82, 83, 85].	34
Table 3.5 The bending angles (deg) and force constants (kcal/mol/deg ²) of ZIF-8, ZIF-67 and Co/Zn ZIFs [82, 83, 85]......	35
Table 3.6 The torsional angles ϕ_0 (deg) and torsion force constants k_ϕ (kcal/mol) of ZIF-8, ZIF-67 and Co/Zn ZIFs [82, 83, 85]......	35
Table 3.7 Lennard-Jones parameters, charge and coordinate for gas molecules were loaded in ZIFs.....	36
Table 3.8 Lennard-Jones parameters [88] and charge of all atom types in MIL-127 (Fe) material [48]......	36
Table 4.1 The average gas adsorption capacities of CO ₂ /N ₂ mixture gas in ZIF-90.....	42
Table 4.2 Diffusion selectivity of CO ₂ /N ₂ mixture in ZIF-90.....	52
Table 4.3 Enthalpy of adsorption in kJ/mol for CH ₄ and H ₂ S at 250 K.	64
Table 4.4 Average gas adsorption capacities in ZIFs and MIL-127 by GEMC 4x4x4 = 64 unit cells and MD 2x2x2 = 8 unit cells.	69
Table 4.5 Diffusion of mixture between CH ₄ and H ₂ S in porous materials as a function of the pressure and temperature.....	70
Table 4.6 Adsorption, diffusion and membrane selectivities of mixture between CH ₄ and H ₂ S in porous materials as a function of the pressure and temperature.....	71

LIST OF FIGURES

	Page
Figure 1.1 The chemical composition of natural gas.....	3
Figure 1.2 The bridging angles in metal IMs (1) and zeolites (2) [38].....	6
Figure 1.3 The structure of Zeolitic Imidazolate Framework-90.....	7
Figure 1.4 (a) Metal tetrahedral (b) 2-methylimidazolate (c) Schematic view of the ZIF-8 (d) Schematic view of the ZIF-67. (e) Schematic view of the Co/ZnZIF. Zn ²⁺ , Co ²⁺ , carbon, oxygen and nitrogen atoms are represented in gray polyhedra, blue polyhedral, grey, red and blue, respectively.....	8
Figure 1.5 (a) Fe(iii) octahedra trimers (b) 3,3',5,5'-azobenzenetetracarboxylic acid (H4-TazBz) (c) Schematic view of the iron(iii) MIL-127. Iron(iii) trimers, iron, carbon, oxygen and nitrogen atoms are represented in gold polyhedra, yellow, grey, red and blue, respectively.....	9
Figure 2.1 The bonded potential; (a) The bond-stretching potential. (b) The angle bending potential. (c) The torsional potential (also called dihedral potential) [52].....	14
Figure 2.2 Periodic boundary conditions. A central box is surrounded by copies of itself. The arrows show the shortest distance between particles 1 and 3 [55].	18
Figure 2.3 The radial distribution function g(r) describes the local density at distance r from a central particle [55].....	20
Figure 2.4 The step of a GEMC simulation	23
Figure 4.1 Calculated adsorption isotherms of CO ₂ in ZIF-90 using GEMC (FF1 –FF4) compared with experiment (x symbol) [43] at 303 K.	40
Figure 4.2 Calculated adsorption isotherms of N ₂ in ZIF-90 using GEMC (FF1 –FF3) at 303 K compared with 2 experiments (x and ■ symbols) [43].	41
Figure 4.3 Calculated adsorption isotherms of CO ₂ /N ₂ mixture in ZIF-90 using GEMC at 298, 323 and 358 K.....	42

Figure 4.4 Adsorption selectivity of CO ₂ and N ₂ mixture in ZIF-90 as a function of the mixture ratio and temperature.....	43
Figure 4.5 Distributions of the window diameter of ZIF-90 for different loadings of CO ₂ as well as empty lattice in range of 100 to 473 K.....	45
Figure 4.6 Distributions of the window diameter at 25 CO ₂ / cage for 5 temperatures.	47
Figure 4.7 Distributions of the window diameter of ZIF-90 for different loadings of N ₂ as well as in range of 300 to 473 K.....	48
Figure 4.8 Distributions of the window diameter at 30 N ₂ / cage for 3 temperatures. 49	
Figure 4.9 The calculated D_s for CO ₂ loadings of 0.5 to 30 molecules/cage in ZIF-90 frameworks at 300, 373, 473K by MD simulation.....	50
Figure 4.10 The calculated D_s for N ₂ loadings of 0.5 to 30 molecules/cage in ZIF-90 frameworks at 300, 373, 473K by MD simulation.....	51
Figure 4.11 The calculated D_s for CO ₂ and N ₂ in two ratios of CO ₂ /N ₂ mixture for 298 and 323 K.....	52
Figure 4.12 The RDFs of lattice atoms with CO ₂ and CO ₂ itself at loadings of 5, 25 and 30 molecules/cage in ZIF-90 frameworks at 300 K.....	54
Figure 4.13 The RDFs of lattice atoms with N ₂ and N ₂ itself at loadings of 5, 25 and 30 molecules/cage in ZIF-90 frameworks at 300 K.....	55
Figure 4.14 Density plots of CO ₂ in the x-y plane of the last 0.5 ns, 300K at loading of 5, 15, 30 molecules/cage.....	56
Figure 4.15 Adsorbed amounts of the pure gases (a) H ₂ S and (b) CH ₄ in several materials at 300 K for various pressures.....	56
Figure 4.16 Adsorbed amounts of pure gases (a) H ₂ S and (b) CH ₄ in several materials at 250 K for various pressures.....	57
Figure 4.17 (a) Adsorbed amounts and (b) adsorption selectivity of CH ₄ and H ₂ S in ZIF-8 as a function of the pressure and temperature.....	59

Figure 4.18 (a) Adsorbed amounts and (b) adsorption selectivity of CH ₄ and H ₂ S in ZIF-67 as a function of the pressure and temperature.....	60
Figure 4.19 (a) Adsorbed amounts and (b) adsorption selectivity of CH ₄ and H ₂ S in Co/Zn ZIF as a function of the pressure and temperature.....	61
Figure 4.20 (a) Adsorbed amounts and (b) adsorption selectivity of CH ₄ and H ₂ S in MIL-127(Fe) as a function of the pressure and temperature.	63
Figure 4.21 Radial distribution functions (a) between different atoms of the guest molecules, (b) between the C atom in CH ₄ with different atoms of the ZIF-8 lattice, that are defined in the inlet picture above, (c) between the S atom of H ₂ S with these lattice atoms.....	66
Figure 4.22 Radial distribution functions (a) between different atoms of the guest molecules, (b) between the C atom in CH ₄ with different atoms of the MIL-127(Fe) lattice, that are defined in the inlet picture above, (c) between the S atom of H ₂ S with these lattice atoms.	67

CHAPTER 1

INTRODUCTIONS

1.1. Research rationale

The major resources of power plant in the world rely on coal and natural gas because these materials are economical for generating electricity. Due to this process, CO₂ is under considerable attention because it contributes to greenhouse gas and climate change that affect human life. In power plant processing, CO₂ captures were classified in three strategies, oxy-combustion, pre-combustion CO₂ capture and post-combustion CO₂ capture [1]. Looking at the end of the pipe, flue gases were produced and released into atmosphere. The components of flue gas are mainly N₂, about 4 - 30% of CO₂ and little of H₂O and O₂. Normally, CO₂ (kinetic diameter = 3.30 Å) diffuses faster than N₂ (kinetic diameter = 3.64 Å) in many materials. Then a CO₂/N₂ mixture can feasibly be separated by membrane in the post-combustion CO₂ capture process. This procedure has a high performance because it is compatible with retrofit structure and easy operation in the existing plant [2, 3]. The separation efficiency bases on the difference in diffusion of each gas in membrane materials. The essential properties of membrane are durable membranes, high selectivity, thermal and physical stability in combustion flue gas condition. To improve the performance of membrane, the various kinds of them were characteristically considered in two main parameters, permeability and selectivity. Polymer membrane, Polaris™ and Polyactive® are commercial products, with high selectivity and permeability of CO₂ over N₂. They are easily fabricated but membrane thickness and reliability need to be improved. The silica and zeolite membranes have better properties than polymer membrane. However, the production of the large surface area is more difficult. Metal organic frameworks (MOFs) membranes are of tremendous attention in this area because of their easy

tunable porosity allows for their properties to be adjusted to suit promising targets [4-7].

A new subclass of MOFs which has zeolitic structure, called zeolitic imidazolate frameworks (ZIFs) has been synthesized. Having good properties of both MOFs and zeolites, not only inherent properties, large surface areas, pore volume, but also an excellent chemical and thermal stability, it is no surprise that ZIFs are emerging in material research in recent years. Due to their fascinating properties, the scientists are extensively studying, for example, the separation of CO_2/H_2 , N_2/H_2 , CH_4/H_2 and CO_2/CH_4 . These systems can be treated by ZIF-90 [8, 9]. Beyond the experimental research, computational methods which have high performance and accuracy but low price are a great choice to discover their basic properties. This can help the experimentalists to proofing adsorption mechanism or to elucidate unclear information by an easier approach than some experiments [10].

Moreover, natural gas plays the significant role for driving the country's economic which is a second large usage in the world electricity generation. The chemical composition of natural gas is primarily composed of methane compound (CH_4), with some ethane (C_2H_6), propane (C_3H_8), impurities of carbon dioxide, hydrogen sulphide and nitrogen as shown in Figure 1.1 [11]. The major pollutant gas of natural gas contains a CO_2 and H_2S . The high amount of CO_2 can reduce the burn-rate of natural gas [12]. The significant amount of H_2S can be many problems not only in transportation but also the engine because the highly corrosive may cause internal corrosion of the pipelines and the engines, respectively. Therefore, removal of H_2S and CO_2 from natural gas is typically considered as the first step of the utilization of sour gas for power generation.

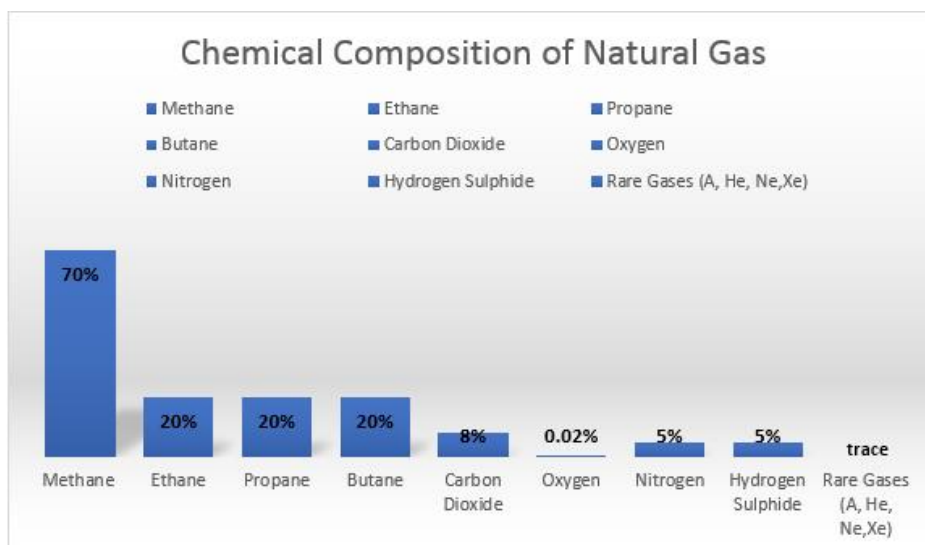


Figure 1.1 The chemical composition of natural gas.

The natural gas treatment process includes different techniques [13-24]. (i) Physical absorption that relies on physical solvents *e.g.* dimethyl ethers of polyethylene glycol (DEPG) shows no reaction between solvent and sour gas via counterflow. In this process, it is sometimes required to decrease the operating temperature to rise sour gas solubility and to reduce the solvent circulation rate. (ii) Chemical absorption involves the formation of reversible chemical bonds between the sour gas and the base solvent such as monoethanolamine (MEA), diethanolamine (DEA), diglycolamine (DGA) and sodium hydroxide (NaOH). In the process, the solvent itself undergoes regeneration, which involves bond breaking. The chemical solvent is good for removing sour gas but still has a problem with the separation of by-products from the solution *i.e.* salt. (iii) Adsorption processes that use solid adsorbents such as activated carbon. The activated carbon is impregnated with alkaline solutions, such as sodium hydroxide (NaOH), potassium hydroxide (KOH), and potassium carbonate (K_2CO_3). Potassium carbonate was proven to be the best alkaline-impregnated activated carbon for effective adsorption capacity. However, disadvantages are the need of chemical inputs and the high cost of activated carbon

via alkaline solutions. (iv) Use of granulates of solids that adsorb impurities *e.g.* metal oxides or molecular sieves like zeolites or Metal-Organic Frameworks (MOFs). (v) Capillary condensation [22] (vi) Use of membranes that act as molecular sieves. The gas is adsorbed at the membrane surface and it diffuses through barriers where some of the gases can move through the membrane more easily whereas other gases cannot pass or can pass in a lower amount. Membrane research for eliminating hydrogen sulfide requires many parameters to study such as pressure, temperature, concentration of the permeants and types of membrane [25]. For the separation of components, the permeability is ruled by selectivity (selectivity coefficient, separation coefficient).

Based on the information above, such techniques have attracted the attention of many scientists for reviewing and discussing, different processes. All have advantages and disadvantages. These must be investigated in order to increase efficiency and reduce the cost of separation procedures. The adsorption and membrane flow processes by porous materials seem to be very promising for the elimination of hydrogen sulfide from methane. The efficiency of porous materials depends on the surface area, porosity, specific function group of adsorbents, and upon the temperature, pressure and concentration of hydrogen sulfide. Separation of components of gas mixtures using porous materials was already investigated in several experimental and simulation studies [8, 26-29]. The separation has been examined under the influence of an additional chemical reaction [30]. Several materials have extensively attracted scientists for studied the separation of H₂S/CH₄ mixture, for instance, UiO-66(Zr) [31], MIL [32, 33], zeolite [34], and molecular sieves [35] which be the candidate materials in this field.

With all above remarks, ZIF-90 gives a good CO₂ permeability so that it has a potential in CO₂/N₂ mixture separation. For better understanding of the separation process on a molecular level, in this challenging work, effects of temperature and

number of gases loading in ZIF-90 were examined by using Monte Carlo simulations and Molecular Dynamic simulations. Moreover, the adsorption and diffusion results of single gases, N_2 and CO_2 , and CO_2/N_2 mixture were expected to provide the information of adsorption site and selectivity in ZIF-90. The flexibility of the ZIF structure has important influence on the diffusivity of gases through frameworks. Therefore, the structural changes have been examined during all of the simulations. The outcomes hopefully can be useful for the design of the novel material in real industrial and power plant of CO_2 capture application.

The aim of the second work is to compare the separation of H_2S impurity from methane if some porous materials are in use. We consider Zeolitic Imidazolate Frameworks (ZIFs) *i.e.* ZIF-8, ZIF-67, Co/Zn-ZIF and a MOF, namely, Materials of Institute Lavoisier-127 (MIL-127(Fe)). ZIF-8 has been chosen because it is one of the most common MOFs and one of the few MOFs that are already commercially produced and sold. Thus, it may be of considerable interest to find out its performance for important technical processes. ZIF-67 and Co/Zn-ZIF are modifications of ZIF-8 and it is not only of scientific but also of practical interest if such modifications improve its performance for our purpose. As a contrast to this structure, we have additionally examined MIL-127(Fe) which showed good separation performance in previous study by our group. This may help to decide if the ZIF-8 - like structures are really optimal. Furthermore, the separation selectivity is offered on the pair of interested gases. If the computational simulation is intensively only the selected gases in term or equimolar ratio, it may not representative the real system because there are various type and amount of gas composition in nature. Considering at this point, the binary mixture of gases are verified with the real ratio of gases by ZIFs and MIL materials using computational simulation.

1.2. Zeolitic Imidazolate Frameworks (ZIFs).

Zeolitic Imidazolate Frameworks (ZIFs) are the new subclass of Metal Organic Frameworks (MOFs) that are embraced of imidazolate or derivative of imidazolate joined with tetrahedral metal ions (e.g. Zn, Co, Cu, Fe, etc.). Interestingly, the metal-imidazole-metal angle of ZIFs is approximately 145° that similar to Si-O-Si angle in zeolites as shown in Figure 1.2 . ZIFs show zeolite-like topologies and can tailor by varieties divertive of imidazole and many type of metal, 105 ZIF topologies have been reported in the literature [36, 37]. The combination of the advantage of zeolite and MOFs properties leading ZIFs have properties of two materials such as robust porosity, resistance to thermal changes, and chemical stability, ZIFs are being investigated for applications such as gas storage and separation.

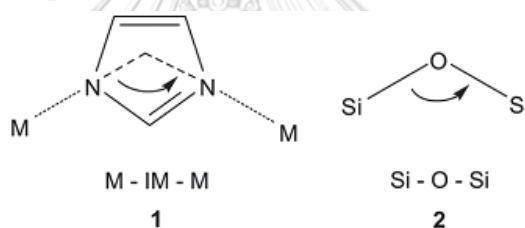


Figure 1.2 The bridging angles in metal IMs (1) and zeolites (2) [38].

Zeolitic imidazolate framework - 90 (ZIF-90) was firstly synthesized in 2008, it is composed of tetrahedral metal ion (ZnN_4) with linker imidazolate-2-carboxyaldehyde (Ica). The framework has two aperture types which are including four linkers (4-member ring) and six linkers (6-member ring) as in Figure 1.3. The largest cavity diameter up to 11.0 \AA and window size (6-member ring) is 3.5 \AA [39].

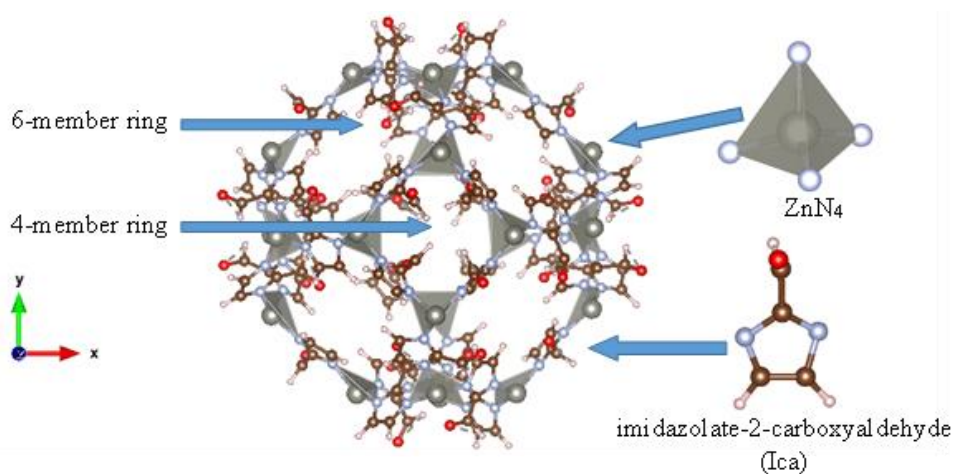


Figure 1.3 The structure of Zeolitic Imidazolate Framework-90.

Zeolitic imidazolate framework - 8 (ZIF-8), was composed of the 2-methylimidazolate linked together with tetrahedral metal ion (ZnN_4) to constructing a sodalite (SOD) topology) that features a space group of interconnected six membered ring windows with an accessible diameter and pore width of 3.4 Å and 11.6 Å, respectively [38].

Zeolitic imidazolate framework -67 (ZIF-67) has the same topology of ZIF-8 but the metal was changed from Zn to Co. The largest cavity diameter up to 11.6.0 Å and window size (6-member ring) is 3.5 Å. Co/Zn Zeolitic imidazolate framework (Co/Zn-ZIF) is a mixed material between ZIF-8 and ZIF-67 which is synthesized from both tetrahedral Zn and Co metal with 2-methylimidazolate. The all frameworks are presented in Figure 1.4. Because the ionic radii of Co^{2+} (0.72 Å) and Zn^{2+} (0.74 Å) are comparable, the Co/Zn-ZIF is expected to be achievable due to the isostructural feature of ZIF-8 and ZIF-67 [40].

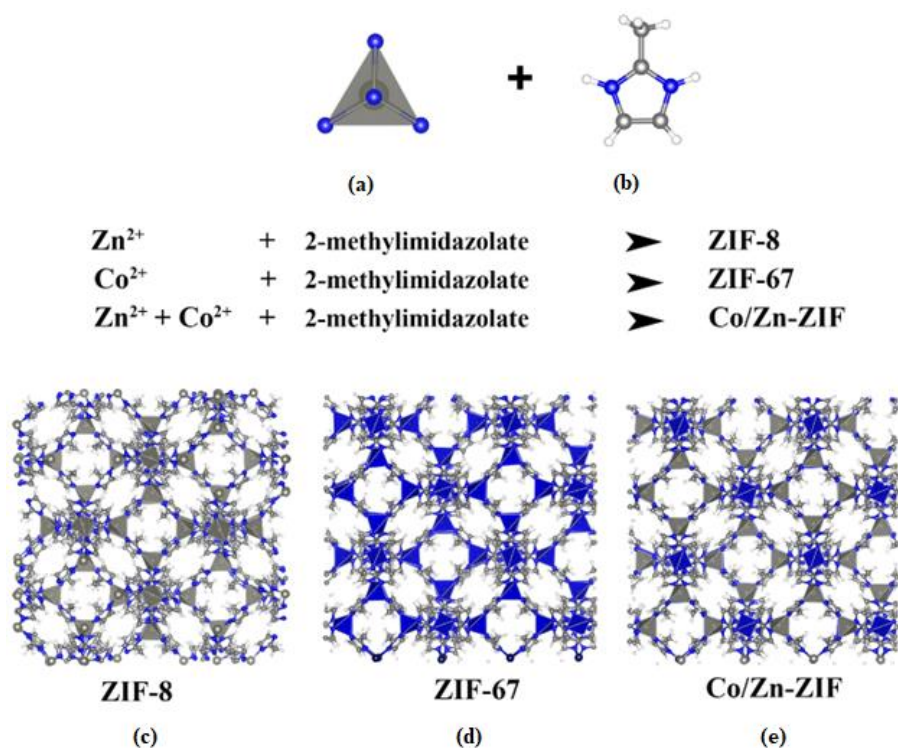


Figure 1.4 (a) Metal tetrahedral (b) 2-methylimidazolate (c) Schematic view of the ZIF-8 (d) Schematic view of the ZIF-67. (e) Schematic view of the Co/ZnZIF. Zn^{2+} , Co^{2+} , carbon, oxygen and nitrogen atoms are represented in gray polyhedra, blue polyhedral, grey, red and blue, respectively.

Material of Institute Lavoisier-127 (MIL-127) is one of porous metal organic frameworks which is composed of trimers of iron (III) linked together with 3,3',5,5'-azobenzenetetracarboxylate anions as shown in Figure 1.5. There are two types of pores in this structure, including for a 1-D channel with pore diameter around 6 Å and cage with 10 Å diameter [41].

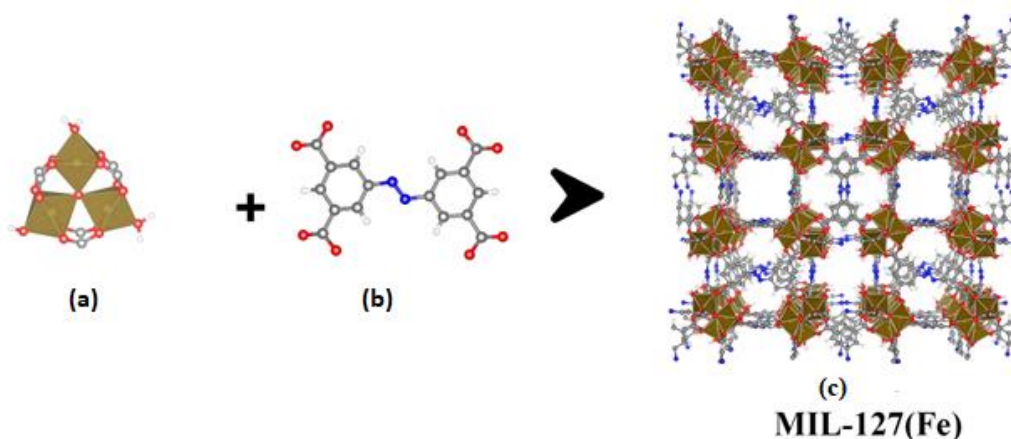


Figure 1.5 (a) Fe(III) octahedra trimers (b) 3,3',5,5'-azobenzene tetracarboxylic acid (H₄-TazBz) (c) Schematic view of the iron(III) MIL-127. Iron(III) trimers, iron, carbon, oxygen and nitrogen atoms are represented in gold polyhedra, yellow, grey, red and blue, respectively.

1.3. Literature reviews.

In 2012, Atci and Keskin investigated the performance of adsorbing and diffusing single gas or mixture gas in 15 different ZIFs, some of whom were examined in their previous work [42]. UFF force field again was used in this work for simulations and compared with DREIDING force field. Their models were treated with Grand canonical Monte Carlo (GCMC) and equilibrium molecular dynamics (EMD) simulations and they predict the adsorption-based, permeation-based, permeability. Furthermore, a good agreement is obtained between performing simulations and calculating by mixing theories for estimate diffusion-based selectivity. Nevertheless, when comparing with experiment, they found the underestimation of CH₄ and N₂ permeance in mixture and therefore it will lead to overestimation of the selectivity in gas mixtures. The main reason came from their assumption that frameworks could be rigid for saving computational cost and examining a lot of ZIFs. Hence, gas molecules that have larger diameters than pore size of ZIFs wouldn't pass or permeate through the membrane but, of course, in reality, frameworks are flexible.

In 2012, Nair's group described properties of adsorption of CH_4 , CO_2 , N_2 in two MOFs, one of them is ZIF-90 [43]. The experiment was carried out for a range of temperature from 30 to 70 °C at pressure from 0.3 to 110 psi. Both of these MOFs have the same trend for gas solubility which is $\text{CO}_2 > \text{CH}_4 > \text{N}_2$. However, while $\text{Cu}(4,4'-(\text{hexafluoroisopropylidene})\text{bisbenzoate})_{1.5}$ (referred to a Cu-hfipbb) showed a good presentation with mono-layer coverage in Langmuir model, ZIF-90 only followed this rule at low pressure due to its capacity for multi-layer at high and moderate pressure which can be explained by the large pore volume inside and small window size (three dimensions).

In 2014, Zhang et al. [44] have examined a series of ZIFs to study about the important role of functional groups in bio-fuel purification. Ethanol, water and mixture between them were simulated with UFF force field. Because of the results from the above mentioned work which states that flexibility hasn't affected significantly on the adsorption so in this work, they assume that framework to be rigid. Using molecular simulation results, they proposed ZIF-8 might be a good candidate for bio-fuel purification while ZIF-90 in this work shows a good capacity for the adsorption of both ethanol and water because of the hydrophilic functional group.

In 2016, Phuong et al. [45] validated force fields of ZIF-90 and CH_4 molecule compared with experimental data and the suitable one has been proposed to study adsorption and diffusion. Among tested force fields, the modified GAFF is the best ZIF-90 force field that gives agreement of the structural properties and adsorption isotherm with the experiment. The radial distribution functions show the adsorption site of CH_4 in ZIF-90 which is located near the organic linker at low loading of CH_4 and it was observed closer to the metal site and cage center at high loading.

In 2016, Sumer and Keskin [46] rank efficiency of MOF absorbent for CO_2 separations using Molecular Dynamic simulations. The separation of CO_2/CH_4 , CO_2/N_2 ,

and CO₂/H₂ mixtures, MOFs show better performance than well-known zeolites such as NaX, NaY. The adsorption selectivity of MOF membranes is slightly lower than those of NaX and NaY, but its permeability is much higher than those of zeolites. They can conclude that MOFs can be efficiently applied for membrane-based separations of CO₂ mixtures.

In 2017, Chokbunpiam et al. [47] examined the adsorption and diffusion of a H₂/CH₄ mixture in ZIF-90 at 3 temperatures using GEMC and MD simulations. The results show that high temperature can induce structural changes in ZIF-90 without influence of gas loading. The membrane H₂/CH₄ selectivity is predicted to increase from 3.9 to 9.1 increasing with the temperature from 300 to 473 K. That agrees well with experimental data. It means that we can enhance the membrane selectivity by increased temperature.

In 2014, Hafez and Mohammad [48] were successfully synthesized high silica CHA-type membrane which can separate both acid (H₂S, CO₂) gases from methane. The ternary (H₂S-CO₂-CH₄) gas mixtures, with the real compositions of sour natural gas (CO₂:2.13 mol%, H₂S:0.3 mol% and CH₄:97.57 mol %), at 298K and 400 kPa. The results revealed that both acid gases can be removed from CH₄ simultaneously with H₂S/CH₄ selectivity of 3.24.

In 2017, Pongsajanukul et. al. [48] investigated the carbon dioxide adsorption and diffusion in MIL-127 by using molecular simulation. The results show that the gas molecules were filled in the central regions of the channels. The self-diffusion coefficient obtained the highest value at loading of 5 molecules/unit cell while for higher concentrations it decreases because of mutual hindrance of guest molecules.

In 2019, Jafarzadeh et.al. [49] used the molecular simulation for seeking the performance of graphene membrane for the separation of CH₄ /H₂S mixture. The effect of functional group (-OH and -F) on the edge of pore can make the selective

separation of CH_4 out of $\text{CH}_4/\text{H}_2\text{S}$ mixture. The best performance is obtained at 0 MPa with the selectivity of 12.4.

Due to the low performance of $\text{CH}_4/\text{H}_2\text{S}$ selectivities in the previous works are not good enough, the new challenge for finding the better is the mission of this work.

1.4. Scope of this study.

In this challenging work, effects of temperature and number of gas molecules in ZIF-90 were examined by using Monte Carlo simulations and Molecular Dynamic simulations. Moreover, the adsorption and diffusion results of single gases, N_2 and CO_2 , and CO_2/N_2 mixture were expected to provide information of adsorption site and selectivity in ZIF-90. The flexibility of the ZIF structure has an important influence on the diffusivity of gases through frameworks. Therefore, the structural changes have been examined during all of the simulations. The outcomes can be useful for the design of the novel material in industrial and power plant of CO_2 capture application.

Furthermore, the four materials (i.e., ZIF-8, ZIF-67, Co/Zn-ZIF and MIL-127) are also examined the separation of impurity (H_2S) from natural gas (CH_4) by using Monte Carlo simulations and Molecular Dynamic simulations of the selected gas.

CHAPTER II

THEORY BACKGROUND

The molecular dynamics are the one of the most prominent techniques in a variety of science fields to understand the physical and dynamic properties at the intra-, inter-, and supramolecular scales and insightful tool of investigating crystal formation. The achievement of the predictions of molecular simulations depends on the reliability and accuracy of the chosen force fields. Thus, the quantification of uncertainties associated with the form of force fields and their parameters is a fundamental part of molecular modeling.

2.1. Molecular simulation techniques

2.1.1. Force field interactions

The force field is the set of potential energy functions used to define the interactions between atoms within molecule and also between molecules. These may have a wide variety of analytical forms, with some basis in chemical physics, which must be parameterized to give the correct energy and forces. Commonly, there are two terms of functions which are intramolecular (bonded) and intermolecular (non-bonded) as seen in equation 2.1.

$$U_{total} = \sum U_{bonded} + \sum U_{non-bonded} \quad (2.1)$$

2.1.1.1. The intramolecular potential

The intermolecular potential is the interaction between atom within molecule which are including two-, three- and four- body potentials referred to bond-stretching, angle-bending and torsion potentials, respectively as shown in

Figure 2.1. The energy U_{bonded} is calculated as a sum of U_{bond} , U_{angle} and $U_{torsion}$. [50, 51].

$$U_{bonded} = U_{bond} + U_{angle} + U_{torsion} \quad (2.2)$$

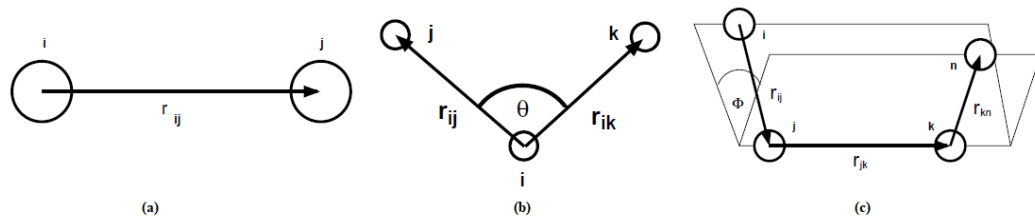


Figure 2.1 The bonded potential; (a) The bond-stretching potential. (b) The angle bending potential. (c) The torsional potential (also called dihedral potential) [52].

Two-body potential or bonded potential describes the explicit bond between the specific pair atom. There are several potential functions such as harmonic potential, Morse potential, 12-6 potential bond or restrained harmonic potential. The common potential that widely use is harmonic potential as shown in equation (2.2)

$$U_{bond} = \sum \text{bonds } k_r (r_{ij} - r_0)^2 \quad (2.2)$$

When r_{ij} being the absolute value of $\vec{r}_{ij} = \vec{r}_i - \vec{r}_j$. In these formular r_{ij} is the absolute value of the distance between atoms labelled i and j . The configurational energy of a bond is a function of the deviation of the bond length from the “equilibrium” value (r_0). The force constant (k_r) indicates the strength of the bond.

Three-body potential or angle-bending potential energy (U_{angle}) equation is the energy change associated with two bonds forming an angle with each other by three atoms ($i-j-k$), where there is a bond between i and j , and between j and k . This is also a harmonic potential. where θ_0 is the equilibrium angle and k_θ a

constant which describes the angular dependence well. This leads to the following equation (2.3).

$$U_{angle} = \sum_{angles} k_{\theta} (\theta_{ijk} - \theta_0)^2 \quad (2.3)$$

The bond and angular terms were already familiar from the potentials for solids. In the physics and chemistry of molecules there are many important effects which cannot be described by only these terms. The most fundamental of these is probably torsion. This refers to the rotations of one part of a molecule with respect to another. Four-body potential or torsion potential energy ($U_{torsion}$) in equation (2.4) describes the part of the energy change associated with rotation in a four-atom sequence $i-j-k-l$, where $i-j$, $j-k$ and $k-l$ are bonded. The rotational motion associated with this term is described by a dihedral angle and a coefficient of symmetry m (periodicity), around the central bond $j-k$. This potential is supposed to be periodic and is regularly represented by a cosine function as given in equation (2.4).

$$U_{torsion} = \sum_{torsions} k_{\phi} [1 + \cos(m\phi_{ijkl} - \phi_0)] \quad (2.4)$$

The values of force constant (k_{ϕ}) can be obtained from experimental data (such as infrared spectral frequencies) or from quantum mechanical calculations.

2.1.1.2. The intermolecular potential

Intermolecular potentials or non-bonded potentials ($U_{non-bonded}$) [53, 54] involve electrostatic and Van Der Waals potentials. A typical expression for such a potential is:

$$U_{non-bonded} = U_{Van Der Waals} + U_{electrostatic} \quad (2.5)$$

For pair potentials, the total potential energy of a system can be calculated from the sum of the energy contributions from pairs of atoms and it depends only on the distance between atoms. One example of a pair potential is the *Lennard-Jones potential* which is shown in equation (2.6) and is the most commonly used form.

$$U_{Van Der Waals} = \sum_{i < j} 4\varepsilon_{ij} \left[\left(\frac{\sigma_{ij}}{r_{ij}} \right)^{12} - \left(\frac{\sigma_{ij}}{r_{ij}} \right)^6 \right] \quad (2.6)$$

When ε_{ij} is the value of the minimum depth of the potential energy for the interaction involving atom i and j , σ_{ij} (the equilibrium distance) and r_{ij} shows the distance between the atom centers. In this study, Lorentz–Berthelot mixing rules are used, which are:

$$\sigma_{ij} = \frac{1}{2}(\sigma_{ii} + \sigma_{jj}) \quad (2.7)$$

and

$$\varepsilon_{ij} = \sqrt{\varepsilon_{ii} \varepsilon_{jj}} \quad (2.8)$$

Where σ_{ii} , σ_{jj} , ε_{ii} and ε_{jj} are the LJ diameters for the interaction of i - i atoms and so on. The $(\sigma/r)^{12}$ term describes the repulsive force due to overlapping of electron orbitals (Pauli repulsion) and does not have a true physical motivation, other than that the exponent must be larger than 6 to get a potential well. One often uses 12 because it can be calculated efficiently (square of 6). The term $(\sigma/r)^6$ describes the attractive force (Van der Waals) and can be derived classically by considering how two charged spheres induce dipole-dipole interactions into each other.

Another intermolecular potential is the electrostatic interaction ($U_{electrostatic}$) between a pair of atoms. The charge group scheme is more cpu intensive than a simple atomistic cutoff scheme as more computation is required to determine whether or not to include a set of interactions. The fundamental equation of electrostatics is Coulomb's law as shown in equation (2.9), which describes the force between two point charges. ϵ_0 is the effective dielectric function for the medium and r_{ij} is the distance between two atoms with charges q_i and q_j .

$$U_{Coulomb} = \sum_{i < j} \frac{1}{4\pi\epsilon_0} \frac{q_i q_j}{r_{ij}} \quad (2.9)$$

The derivations of the potential energy function with respect to the atomic coordinates yield the forces needed in a Molecular Dynamic simulation.

2.1.2. Periodic Boundary Conditions (PBC)

In most cases we want to simulate a system in realistic environment, such as solution. The simulation is needed to preserve thermodynamic properties like temperature, pressure and density for the contained molecules in boundary. The periodic boundary conditions are a set of boundary conditions that can be used to simulate a large system (i.e. bulk material) simply by modeling using a small part (unit cell). A unit cell in MD is usually referred to as periodic box. PBC has been favored among many researchers and practicing engineers in the study of various materials. When a molecule leaves the box, one of its images will enter through the opposite site with exactly the same way and direction. The molecules in the simulation box will conserve and the system can be thought of as having no surface. There are several different periodic boundary conditions, which are defined by the shape and size of the simulation cell such as cubic, orthorhombic, hexagonal prism

etc. Figure 2.2 presents the cubic periodic boundaries that is the most commonly used in simulation and has the advantage of great simplicity.

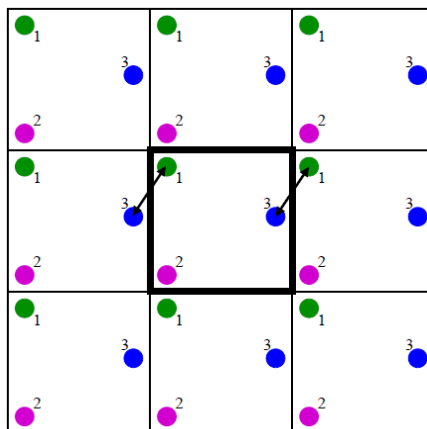


Figure 2.2 Periodic boundary conditions. A central box is surrounded by copies of itself. The arrows show the shortest distance between particles 1 and 3 [55].

Simulations requiring no periodic boundaries are best suited to *in vacuo* simulations, such as the conformational study of an isolated polymer molecule or study in a solvent.

2.1.3. Ensembles

In MD was for the “typical” MD ensemble, that keeps the particle number, system volume and total energy constant (NVE). In addition, the total momentum is conserved in the common NVE-MD. There are three important ensembles in the theory of statistical thermodynamics, and they are classified according to what is held constant in each system as follows [56].

- Microcanonical ensemble (NVE): The thermodynamic state is determined by a fixed number of atoms (N), a fixed volume (V), and a fixed energy (E). This corresponds to an isolated system.

- Canonical ensemble (NVT): This ensemble describes a system in contact with a heat bath. Its thermodynamic state is defined by a fixed number of atoms (N), a fixed volume (V), and a fixed temperature (T). Energy can be exchanged with the bath which has the desired temperature.
- Isobaric-isothermal ensemble (NPT): This ensemble is characterized by the number of atoms (N), the pressure (P), and the temperature (T). The energy can be exchanged with the heat bath and volume can be exchanged with the “pressure” bath.

2.1.4. Radial Distribution Function (RDF)

Radial distribution function is the one statistic mechanic that described how the density of surrounding matter varies as a function of the distance from the particular point. It gives the information concerning the frequency with which certain distances occur. In MD simulation, the RDF is calculated by counting the number of the atom pairs between given ranges of separation. The results can be transferred to the average density of atoms as a function of distance. The general expression to calculate the RDF $G(r)$ is:

$$g(r) = \frac{V}{N} \langle \sum_{i=1}^N \delta(r - r_i) \times \sum_{j=1}^N \delta(r - r_j) \rangle \quad (2.10)$$

in which $\delta(x)$ is Dirac's δ function. By definition, $g(r) = 1$ for an ideal gas. The radial distribution function (or its Fourier transform) can be measured in (scattering) experiments. Moreover, the $g(r)$ plays a key role in many liquid state theories.

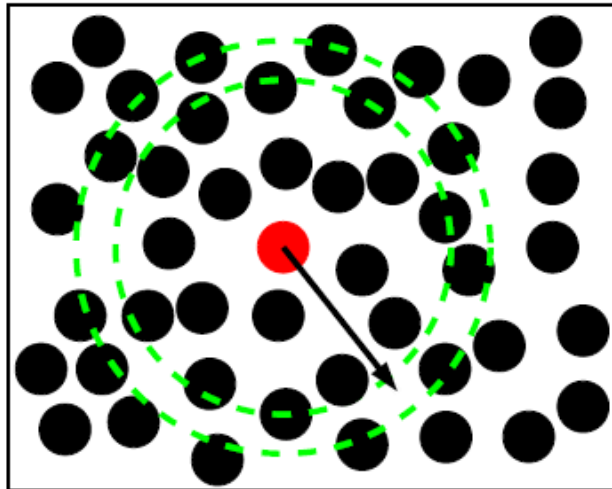


Figure 2.3 The radial distribution function $g(r)$ describes the local density at distance r from a central particle [55].

The concept for calculating a radial distribution function is very simple. Firstly, the reference atom which the RDF will be calculated are chosen. For every value of r , construct a spherical shell of radius r and width dr centered on your chosen atom, then calculate the density (e.g., in atoms per cubic centimeter) within that spherical shell as shown in Figure 2.3.

2.1.5. Adsorption, diffusion and permeation

To determine the selectivity of material in this work adsorption and diffusion will be consider [55, 57]. Adsorption is mainly two interaction such as electrostatic or Van Der Waals forces. The separation factor for mixture is focus in term of adsorption selectivity that can be evaluated as equation 2.11.

$$S_{adsorption(i/j)} = \frac{x_i/x_j}{y_i/y_j} \quad (2.11)$$

Where x is the molar fraction of the adsorbed phase and y is the molar fraction of the bulk gas phase. With this equation that can be obtained the adsorption selectivity not only via Gibbs ensemble Monte Carlo simulation but also by Molecular simulation and experiment.

Diffusion is the process whereby an initially nonuniform concentration profile (e.g. an ink drop in water) evolves in time. Diffusion is caused by the thermal motion of the particles in the fluid. The macroscopic law that describes diffusion is known as Fick's law, which states that the flux j of the diffusing species is proportional to the negative gradient in the concentration of that species:

$$j = -D\nabla c \quad (2.12)$$

In this chapter, we limit ourselves to self-diffusion. This means that we study the diffusion of a labeled species among other identical species. We now compute the concentration profile of the labeled species assuming that, the labeled species was concentrated at the origin at time $t = 0$. To compute the time evolution of the concentration profile, we combine Fick's law with conservation of the total amount of labeled material: where the proportionality constant D is the diffusion coefficient.

$$\frac{\partial \langle r^2(t) \rangle}{\partial t} = 6D \quad (2.13)$$

The diffusion coefficient was calculated using the Einstein relation that was first derived by Einstein around 1905. It relates the diffusion coefficient D to the width of the concentration profile. We stress that D is a macroscopic transport coefficient, whereas $\langle r^2(t) \rangle$ is a microscopic property as it is the mean-squared distance over which the tagged particles have moved in a time t . In a computer

simulation, D can be measured by measuring for every particle i the distance traveled in time t , $\Delta r_i(t)$. To be more specific, we plot the mean-squared displacement as a function of t .

$$\Delta \langle r(t)^2 \rangle = \frac{\sum_{i=1}^N \Delta \langle r_i(t)^2 \rangle}{N} \quad (2.14)$$

More information on computing diffusivities can be found in Ref. [58]. In mixture, diffusion selectivity can be evaluated like that, in which self-diffusivities measured in mixture

$$S_{\text{diffusion}(i/j)} = \frac{D_{s,i,(i,j)}}{D_{s,j,(i,j)}} \quad (2.15)$$

In porous material, the gas transport mechanism inside follows the surface diffusion due to the porous structure. Therefore, the permeance can be predicted by the combination of the adsorption and the self-diffusion coefficient as the following equation

$$P_i = \Pi_i l = D_{s,i} \phi \frac{c}{f} : \text{ where } \Pi_i = N_i \Delta P_i \quad (2.16)$$

ϕ is void fraction, c (mol.m^{-3}) is equilibrium gas concentration, f (Pa) is the fugacity. Furthermore, permeation selectivity can also be evaluated by the relation

$$\begin{aligned} S_{\text{permeation}} &= S_{\text{adsorption}(i/j)} \times S_{\text{diffusion}(i/j)} \\ &= \frac{x_i/x_j}{y_i/y_j} \cdot \frac{D_{s,i,(x_i,x_j)}}{D_{s,j,(x_i,x_j)}} \end{aligned} \quad (2.17)$$

$S_{\text{adsorption}(i/j)}$, $S_{\text{diffusion}(i/j)}$ are adsorption selectivity and self-diffusion selectivity respectively.

2.2. Gibbs ensemble Monte Carlo (GEMC) simulation

Gibbs ensemble Monte Carlo (GEMC) simulation has been specifically designed to characterize phase transitions. The Gibbs ensemble method was proposed by Panagiotopoulos [59] in 1987 for simulation of the gas-liquid and liquid-liquid equilibria and extended to calculation of gas-solid phase equilibria [60]. As in the conventional Gibbs ensemble method, it is performed in 2 boxes simultaneously in one simulation at given initial density of gas at desired temperature and volume.

One of the boxes contains the crystalline structure and adsorbed gas molecules, while the gas phase of the desired gas forms the other simulation box. The temperature, which is an input quantity in MC, is equal in both boxes. When simulation was started, the chemical potentials and pressures in 2 boxes should turn into equal according to the conditions for phase coexistence. Metropolis MC consists of a random movement of random gas particles within both simulation boxes that occur gas displacement inside of each box or gas exchange between 2 boxes as shown in Figure 2.4. The total number of gas particles within 2 boxes will be constant during each simulation run. Each box was simulated within standard periodic boundary conditions.

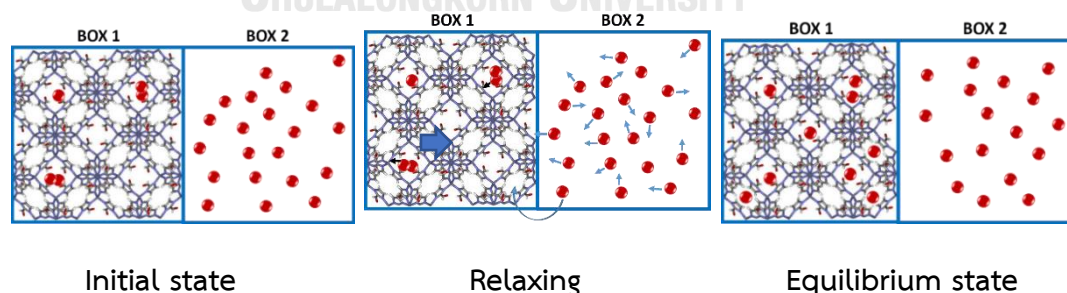


Figure 2.4 The step of a GEMC simulation.

The 3 steps of an GEMC simulation are

1. Creating an initial situation.
2. Relaxing the initial situation to a true equilibrium situation.
3. Main part: Long simulations in equilibrium in order to explore the equilibrium system.

The particle exchanges lead to equilibrium between the gas phase and the adsorbed phase. The GEMC simulation does not require knowledge of pressure or chemical potential. Instead, the state of the gas box is determined by the temperature and n particle densities. Thus $(n+1)$ intensive variables determine the gas phase in agreement with Gibbs rule. The state of the adsorbed phase is determined by the condition of equilibrium with the gas phase. But the pressure can be evaluated additionally if wished. This is desirable in order to compare the adsorption isotherms with experiments because the particle densities in the gas box are commonly not used (although known) for the abscissa in the presentation of adsorption isotherms by experimentalists or by engineers. The plotting of pressure vs amount of adsorbed at each point was compared with the experimental data for verifying parameter of simulation.

2.3. Molecular dynamics simulations

Molecular dynamics is the science of simulating the time dependent behavior of a system of particles. The time evolution of the set of interacting atoms is followed by integrating their equation of motion with boundary conditions appropriate for the geometry or symmetry of the system. In order to calculate the microscopic behavior of a system from the laws of classical mechanics, MD requires, as an input, a description of the interaction potential (or force field). The quality of the results of an MD simulation depends on the accuracy of the description of inter-

particle interaction potential. The adsorption and diffusion of gases in porous material with time dependence can be investigated by Molecular Dynamic (MD) simulation [61].

2.3.1. Classical mechanics.

Basically, the MD simulation consists in calculation of the particle trajectories using Newton's second law. Newton's second law is an equation of motion that is solved for the equilibrium system. Knowledge of the forces acting on the individual atoms and the configuration energy is required. Integration of the Newton's second law equations then yields a trajectory that gives the advance positions, velocities and accelerations of the atoms with time. Using this trajectory, the average values of the properties can be estimated. The positions and velocities of the individual atoms in the system can be calculated at any time during the simulation time.

The essential elements for a molecular dynamics simulation are (i) the interaction potential (i.e., potential energy) for the particles, from which the forces can be calculated, and (ii) the equations of motion governing the dynamics of the particles. We follow the laws of classical mechanics, mainly Newton's law that is given by equation (2.18) when \vec{F}_i is the total force of atom i , m_i is the mass of atom i and \vec{a}_i is the acceleration of atom i .

$$\vec{F}_i = m_i \vec{a}_i \quad (2.18)$$

The force on an atom can be calculated as the derivative of energy with respect to the change in the atom's position. Then, the force can be calculated from the gradient of the potential energy by equation (2.19). Afterward, combining these two equations yields from (2.18) and (2.19) are giving in equation (2.20) when U is the potential or configurational energy of the system. Therefore, Newton's

equations of motion related with the potential energy for changing the position as a function of time are:

$$\vec{F}_i = -\nabla_i U \quad (2.19)$$

$$\vec{F}_i = -\frac{\partial U}{\partial \vec{r}_i} = m_i \frac{\partial^2 \vec{r}_i}{\partial t^2} = m_i \vec{a}_i \quad (2.20)$$

For a unique solution the knowledge of the initial positions and velocities of the atoms is necessary. Thus, positions and velocities at any time are determined by the initial positions and velocities. The average positions of the lattice atoms can be obtained from experimental structures such as the X-ray crystal structure determined by NMR spectroscopy. These can be used as initial position of the lattice atoms while the initial positions of the guests are chosen randomly.

The initial velocities (\vec{v}_{i0}) are usually selected randomly from a Maxwell-Boltzmann or Gaussian distribution at a given temperature, which gives the probability density (W) that an atom i has a velocity v_x in the x direction at a temperature (T) shown in equation (2.21).

$$W(\vec{v}_{ix}) = \left(\frac{m_i}{2\pi k_B T}\right)^{1/2} \exp\left(-\frac{1}{2} \frac{m_i \vec{v}_{ix}^2}{k_B T}\right). \quad (2.21)$$

The velocities are corrected to fulfill.

$$\vec{P} = \sum_{i=1}^N m_i \vec{v}_{i0} = 0 \quad (2.22)$$

The temperature can be estimated from the velocities using equation (2.23) when N is the number of atoms in the system using the equipartition theorem of statistical mechanics. k_B is Boltzmann constant.

$$T = \frac{1}{(3Nk_B)} \sum_{i=1}^N \frac{|\vec{p}_i \vec{v}_i|}{2m_i} \quad (2.23)$$

During the MD simulation the sites and velocities are stored. The trajectory can be used to evaluate configurational properties (positions, velocities and accelerations) and dynamic quantities like transport coefficients and time correlation functions of all N particles from the trajectory [41, 42].

2.3.2. Integration algorithms.

The integration algorithms in this MD simulation are based on the Verlet scheme, which is both time reversible and simple. It generates trajectories in the microcanonical (NVE) ensemble in which the total energy (kinetic plus potential energy) is conserved. The MD simulation program contains two versions of the Verlet algorithm. The first is the Verlet leapfrog (LF) algorithm and the second is the velocity Verlet (VV).

Verlet Leapfrog (LF) algorithm requires values of position (\underline{r}) and force (\underline{f}) at time t while the velocities (\underline{v}) are half a timestep behind. The first step is to advance the velocities to $t + \frac{1}{2}\Delta t$ by integration of the force:

$$\underline{v}\left(t + \frac{1}{2}\Delta t\right) \leftarrow \underline{v}\left(t - \frac{1}{2}\Delta t\right) + \Delta t \frac{\underline{f}(t)}{m} \quad (2.24)$$

where m is the mass of a site and Δt is the timestep.

The positions are then advanced using the new velocities:

$$\underline{r}(t + \Delta t) \leftarrow \underline{r}(t) + \Delta t \underline{v}\left(t + \frac{1}{2}\Delta t\right) \quad (2.25)$$

Molecular dynamics simulations normally require properties that depend on position and velocity *at the same time* (such as the sum of potential and kinetic energy). In the LF algorithm the velocity at time t is obtained from the average of the velocities half a timestep either side of time t :

$$\underline{v}(t) = \frac{1}{2} \left[\underline{v}\left(t - \frac{1}{2}\Delta t\right) + \underline{v}\left(t + \frac{1}{2}\Delta t\right) \right] \quad (2.26)$$

The VV algorithm assumes that positions, velocities and forces are known at each full timestep. The algorithm proceeds in two stages as follows.

In the first stage a half step velocity is calculated:

$$\underline{v}\left(t + \frac{1}{2}\Delta t\right) \leftarrow \underline{v}(t) + \frac{1}{2}\Delta t \frac{f(t)}{m} \quad (2.27)$$

and then the full timestep position is obtained:

$$\underline{r}(t + \Delta t) \leftarrow \underline{r}(t) + \Delta t \underline{v}\left(t + \frac{1}{2}\Delta t\right) \quad (2.28)$$

In the second stage, using the new positions, the next update of the forces $f(t + \frac{1}{2}\Delta t)$ is obtained, from which the full step velocity is calculated using:

$$\underline{v}(t + \Delta t) \leftarrow \underline{v}\left(t + \frac{1}{2}\Delta t\right) + \frac{1}{2}\Delta t \frac{f(t + \Delta t)}{m} \quad (2.29)$$

Thus, at the end of the two stages full synchronisation of the positions, forces and velocities is obtained. In its original form molecular velocities do not appear, in conflict with the attitude that the phase-space trajectory depends equally on positions and velocities. Modern formulations [62, 63] of the method often overcome this asymmetric view.



CHAPTER III

CALCULATION DETAILS

3.1. CO₂ and N₂ in ZIF-90

3.1.1. Force Field Validation

The structure of ZIF-90 was assembled from the x-ray structure that was taken from the CCDC database [39]. The simulation box consists of 2x2x2 unit cells in the Molecular Dynamics (MD) simulation and 4x4x4 unit cells in the Gibbs Ensemble Monte Carlo (GEMC) simulation. Because the lattice flexibility plays an important role in calculations of dynamic properties in several MOFs as shown in [5], a force field for a flexible lattice of ZIF-90 was applied in the MD simulations. Bonding interaction parameters, including bond stretching, bond bending and bond torsion, were taken from GAFF [64], which could lead to a stable lattice size and dynamic properties. The non-bonding interaction parameters were developed by our group and approved in CH₄ adsorption [65], seeing in Table 3.1. The 4 candidates of CO₂ parameters and 3 candidates of N₂ as shown in Table 3.2.

Table 3.2 are used to find the suitable force field of CO₂ and N₂ in the ZIF-90 system at 303 K by a comparison with the experimental data. These force fields were chosen from the best agreement with experiment of the results for adsorption isotherms and used to explore dynamic properties of the system.

Table 3.1 Lennard-Jones parameters and charge of all atom types in ZIF-90.

Atom	σ (Å)	ϵ (kcal/mol)	q (e)
C_CR	3.4	0.059	0.21
C_CC	3.4	0.059	-0.002
C_CT	3.4	0.059	0.258
H_H4	2.51	0.01	0.115

Atom	σ (Å)	ϵ (kcal/mol)	q (e)
H_HT	2.65	0.01	0.049
Zn	1.96	0.009	0.674
O	2.96	0.14	-0.410
N	3.25	0.11	-0.335

Table 3.2 Lennard-Jones parameters and charge of all atom types for CO₂ and N₂.

Force Fields	atom	σ (Å)	ϵ (kcal/mol)	q (e)
CO ₂				
FF1 (Liu D. et al.) [66]	C	3.43	0.10459	+0.544
	O	3.12	0.05974	-0.272
FF2 (Murthy C. S. et al.) [67]	C	2.785	0.057629	+0.596
	O	3.014	0.165138	-0.298
FF3 (Potoff, J. J. et al.) [68]	C	2.80	0.05343	+0.70
	O	3.05	0.15634	-0.35
FF4 (Zheng B. et al.) [69]	C	2.757	0.055 84	+0.6512
	O	3.033	0.15982	-0.3256
N ₂				
FF1 (Potoff, J. J. et al.) [68]	N	3.31	0.07154	-0.482
	Center	0	0	0.964
FF2 (Ravichandar Babarao) [70]	N	3.32	0.07233	-0.482
	Center	0	0	0.964
FF3 (Erhan Atci and Seda Keskin) [42]	N	3.31	0.07233	-0.400
	Center	0	0	0.800

3.1.2. Gibbs ensemble Monte Carlo simulations

All adsorption isotherms and adsorption selectivities in the porous materials examined in this work are calculated in Gibbs Ensemble Monte Carlo (GEMC) simulations by use of the homemade Gibbon software, that has been used successfully in several papers including [30, 47, 48, 71-74]. The Gibbon software performs Metropolis Monte-Carlo in 2 boxes simultaneously in one simulation at desired temperature. Equilibrium between the boxes is achieved by random particle exchange taking account of microscopic reversibility. The gas phase of the pure gas (CO_2 and N_2) and CO_2/N_2 mixture gas are simulated in box A while box B contains 64 ($4 \times 4 \times 4$) unit cells of the ZIF-90 with adsorbed gas. Within each box random displacements and random rotations are carried out ruled by the Metropolis algorithm. The Coulomb interactions are not calculated by Ewald summation but they are treated with a damping factor for larger distances improved by a method analogously to the charge group method [75] for long range interaction. Replacing the Ewald sum by such methods is extensively discussed in [76]. and our application is described in more detail in [45]. In this approximation the sum of the electrostatic potential of the three-point charges of each CO_2 and N_2 atoms are considered as an entity. The faster decaying sum is calculated within distances between the centers of masses of the two molecules smaller than the cutoff radius of 30 Å. Thus, the computer time needed in the GEMC simulation is reduced considerably.

Moreover, the CO_2/N_2 mixture gas was calculated in 2 temperature series related with the real condition for finding the adsorption selectivity for this separation. During GEMC simulation the structure was implicit as a rigid framework because of the effect of the lattice flexibility on adsorption was not significant difference in many ZIF's publication [42, 77].

3.1.3. Molecular dynamics (MD) simulations

The MD simulations have been carried out by use of the DL-POLY classic package [78]. Adsorbed amounts of CO₂ and N₂ in the range of 0.5 - 30 molecules per cage were investigated in 5 temperature series. All simulations started with NVT ensemble with Nosé–Hoover thermostat for 2 ns to control the temperature. After that NVE ensemble MD simulations were carried out during 25 ns to examine the dynamic properties. The effect of temperature and the amount of gas loading to the swinging of the imidazolate 6-member ring are examined in terms of window diameter distributions. The self-diffusion coefficients of CO₂ in ZIF-90 are evaluated.

The amount of CO₂ and N₂ mixture in ZIF-90, with ratio 1:1 and 1:2, in comparison with single gas results that obtained from GEMC, were used to evaluate the diffusion selectivity in MD simulation.

3.2. H₂S and CH₄ in ZIFs and MIL-127 materials

The binary mixture (CH₄/H₂S) is considered to evaluate the separation of the impurity in terms of adsorption isotherm and adsorption selectivity with porous materials. ZIF-8, ZIF-67, Co/Zn-ZIF and MIL-127(Fe) models are constructed from the XRD data of the Cambridge Crystallographic Data Center (CCDC)[40, 79-81]. The cubic frameworks of ZIF-8, ZIF-67 and Co/Zn-ZIF for simulations consist of 4x4x4 unit cells which have the corresponding lattice constants (unit cell edge lengths), of 16.9910 Å, 16.9589 Å, 17.099 Å and 21.985 Å, respectively. The structures are illustrated in Figure 1.4 and Figure 1.5. The interactions of Lennard-Jones parameters for the lattice atoms and its partial atomic charges as well as the parameters of CH₄ and H₂S are summarized in the Table 3.3. The adsorption selectivity and diffusion selectivity of all system are performed by Gibbs ensemble Monte Carlo and Molecular Dynamic Simulations.

Table 3.3 Lennard-Jones parameters [82, 83] and charge of all atom types in ZIF-8 [82], ZIF-67 [84] and Co/Zn ZIFs [82].

Atom	σ (Å)	ϵ (kcal/mol)	ZIF-8 q (e)	ZIF-67 q (e)	Co/Zn ZIF q (e)
CC	3.400	0.0860	-0.104	-0.0581	-0.104
CR	3.400	0.0860	+0.822	+0.7846	+0.822
CT	3.400	0.1094	-0.585	-0.3094	-0.585
HH	2.511	0.0150	+0.079	+0.0910	+0.079
HT	2.650	0.0157	+0.105	+0.0584	+0.105
N	3.250	0.1700	-0.751	-0.6956	-0.751
Zn	1.960	0.0125	+2.00	-	+2.00
Co	2.1856	0.0286	-	+1.3497	+2.00

Table 3.4 Bond lengths (Å) and force constants (kcal/mol/Å²) of ZIF-8, ZIF-67 and Co/Zn ZIFs [82, 83, 85].

Atom type		Force constants	Bond lengths
<i>i</i>	<i>j</i>	k_r	r_0
CC	CC	1036	1.371
CC	N	820	1.385
CC	HH	734	1.080
CT	HT	680	1.090
CR	N	996	1.335
Zn	N	160	2.050
Co	N	141	2.000
CR	CT	634	1.504

Table 3.5 The bending angles (deg) and force constants (kcal/mol/deg²) of ZIF-8, ZIF-67 and Co/Zn ZIFs [82, 83, 85].

Atom type			Force constants	Bending angles
<i>i</i>	<i>j</i>	<i>k</i>	k_{θ}	θ_0
CC	CC	N	140	120
CC	CC	HH	100	120
CR	CT	HT	100	109.5
HT	CT	HT	70	109.5
CC	N	Zn/Co	20	126
CR	N	Zn/Co	20	126
CC	N	CR	140	120
N	Zn/Co	N	20	109.5
N	CR	N	140	120
N	CR	CT	140	120
N	CC	HH	140	120

Table 3.6 The torsional angles ϕ_0 (deg) and torsion force constants k_{ϕ} (kcal/mol) of ZIF-8, ZIF-67 and Co/Zn ZIFs [82, 83, 85].

Atom type				Constant		
<i>l</i>	<i>j</i>	<i>k</i>	<i>l</i>	k_{ϕ}	n	ϕ_0
X	N	CC	X	6	2	180
X	CC	CC	X	21.5	2	180
X	CR	N	X	10	2	180

The interaction parameters and coordinate for gas molecules i.e. CH₄, and H₂S as show in Table 3.7.

Table 3.7 Lennard-Jones parameters, charge and coordinate for gas molecules were loaded in ZIFs.

Molecule	Atom types	σ (Å)	ϵ (kcal/mol)	q (e)	Coordinate (x,y,z)
CH ₄ [86]	C	3.730	0.2939	0.00	0.0, 0.0, 0.0
H ₂ S [87].	H	0.00	0.00	0.16	-1.34, 0.0, 0.0
	H	0.00	0.00	0.16	0.047, 1.339, 0.0
	S	3.700	0.5466	-0.32	0.0, 0.0, 0.0

Table 3.8 Lennard-Jones parameters [88] and charge of all atom types in MIL-127 (Fe) material [48].

Atom types	σ (Å)	ϵ (kcal/mol)	q (e)
O_Fe	3.118	0.060	-0.900
Fe_O	2.594	0.013	1.400
O_D	3.118	0.060	-0.930
H_D	2.571	0.044	0.387
O_W	3.118	0.060	-0.960
H_W	2.571	0.044	0.480
N_N	3.261	0.069	-0.210
C_N	3.431	0.105	0.330
C_H	3.431	0.105	-0.100
H_C	2.571	0.044	0.107
C_C	3.431	0.105	-0.200
C_O	3.431	0.105	1.070
O_C	3.118	0.060	-0.700

3.2.1. Gibbs ensemble Monte Carlo simulations.

In this work, the GEMC simulations have been done with rigid frameworks, which would not be possible for MD simulation of the diffusion of methane in ZIF-8, ZIF-67 and Co/Zn-ZIF. The diffusion selectivity depends strongly upon fluctuations of channel and aperture sizes in flexible frameworks. For example, for the separation of H_2/CH_4 , the flexibility of the ZIF-8 framework changed the membrane selectivity by orders of magnitude because CH_4 diffusion in the rigid framework is much smaller than in the flexible one [26]

The reason is that the size of the methane molecule is not very different from the size of the windows connecting adjacent cavities. The influence of the flexibility on adsorption is much smaller because the fluctuations of the window sizes influence the speed of approximation to the adsorption equilibrium, but they have a small influence on the adsorption equilibrium. However, this is true only for cases in which no phase transition of the structure of the MOF happens. Such phase transitions can happen in some cases (see *e.g.*[89, 90]). For the systems which are examined here, such effects have not been observed.

All adsorption isotherms (mixture gas *i.e.* CH_4/H_2S) and adsorption selectivities (CH_4/H_2S) in porous materials of this work were calculated using Gibbon 's in-house developed software for Gibbs Ensemble Monte Carlo (GEMC) that has been successfully used in several papers including [3-9]. The main feature of the GEMC simulation method [10-13] is that the equilibrium between a gas phase and an adsorbed phase (adsorbed in porous materials *i.e.* ZIF-8, ZIF-67, Co/Zn ZIF and MIL-127 (Fe)) is investigated directly. The GEMC simulations are first equilibrated at target temperatures using 21 runs of 10^8 simulation steps. Further, a run of 10^8 simulation steps is carried out for evaluation.

3.2.2. Molecular dynamics (MD) simulations.

Molecular Dynamics (MD) simulations examined the particle trajectories in system by using the Newton's second law of motion. All calculations in this work were calculated by DL-POLY program by following these steps. (i) Set the initial conditions for the simulation in terms of the initial coordinates and initial velocities of the particles in the system. (ii) The list of neighbor will be updated after every time step. (iii) Then solve the equations of motion to find the new positions and velocities. (iv) Update new configuration and velocities. (v) Perform pressure or temperature control depending on different ensembles. (vi) Repeat these processes until the time reach the time simulation that is set up at the beginning. (vii) From the trajectory, analyze the result to get physical quantities i.e. radial distribution functions (RDFs) and dynamical properties i.e. self-diffusion coefficient of the system.

The simulation boxes (ZIF-8, ZIF-67, Co/Zn-ZIF and MIL-127 (Fe)) consist of 2x2x2 unit cells in the MD simulations. This model could also describe well the ZIF lattice structure, particularly the size and shape of the windows. These MD simulations are done in the NVE ensemble. In this ensemble the simulation box size is constant and therefore agrees with X-ray data.

In this work, the MD simulation was conducted on flexible frameworks for ZIF-8, ZIF-67, Co/Zn ZIF but rigid framework for MIL-127. The numbers of gas mixture CH₄/H₂S are loaded in porous materials that deepened on the results of adsorption isotherms in results and discussion section for each temperature and pressure.

For ZIF-8, ZIF-67 and Co/Zn ZIF simulations were done by isochoric-isothermal ensemble (NVT) for 5 ns. After that, evaluation part of the run the simulations were examined 30 ns in the microcanonical ensemble (NVE) including 28 ns for equilibrate system and last 2 ns for interpreting results. For MIL-127 (Fe) simulations were studied for 25 ns by NVT ensemble that consists of 23 ns for

equilibrate system and last 2 ns for analyzing results. The simulation time step was 2 fs for all systems.



CHAPTER IV

RESULTS AND DISCUSSION

4.1. CO₂ and N₂ in ZIF-90

4.1.1. Verifying force field of CO₂ and N₂ in ZIF-90 by using Gibbs ensemble Monte Carlo simulations

The GEMC simulations yield the calculated adsorption isotherms of CO₂ in ZIF-90 at 303 K that are shown in Figure 4.1. By comparison of these adsorption isotherms, it turns out that the adsorption isotherm of FF1(■) presents good agreement with experiment (x) along the pressure range from 0.5 - 3.5 bar. On the other hand, the other force fields give overestimated adsorption. Hence the FF1 parameter set, that is from Liu *et.al.* [66] was selected to be used in the MD simulations.

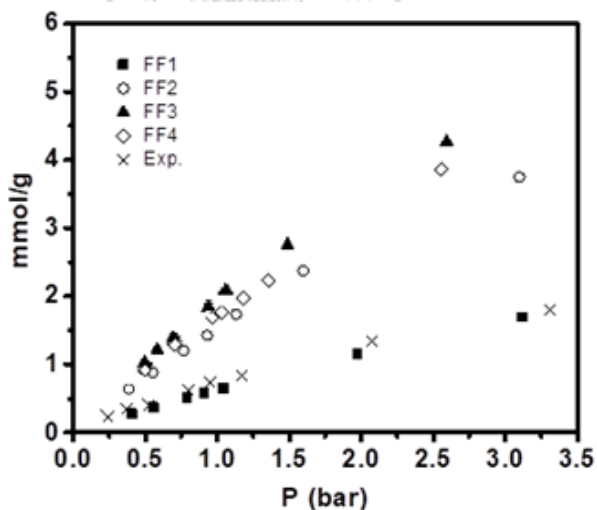


Figure 4.1 Calculated adsorption isotherms of CO₂ in ZIF-90 using GEMC (FF1 –FF4) compared with experiment (x symbol) [43] at 303 K.

As with CO₂, the force field of N₂ should be verified before use. The 3 force fields from well-known publications are selected for simulation and compared with

the experimental data, as seen in Figure 4.2. Note that the adsorption isotherm increases with increasing temperature. The results show that all simulated adsorption isotherms at 298K lie between two ranges of the experimental adsorption isotherms of 298 and 303 K. Then, the optimal force field of N₂ for studying the physical and dynamic properties of CO₂/N₂ mixture should be the FF1.

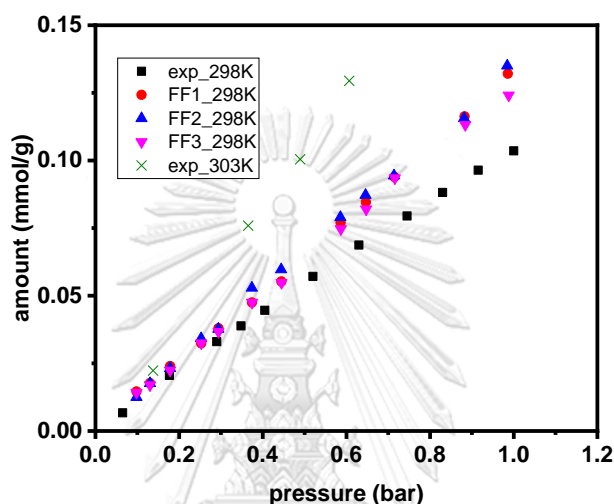


Figure 4.2 Calculated adsorption isotherms of N₂ in ZIF-90 using GEMC (FF1 –FF3) at 298 K compared with 2 experiments (x and ■ symbols) [43].

4.1.2. Adsorption isotherm and adsorption selectivity of CO₂/N₂ mixture in ZIF-90 material

After the force fields of CO₂ and N₂ were verified, the optimal parameters were chosen to simulate the adsorption isotherm of CO₂/N₂ mixture with two ratios: equimolar (1:1) and real (1:5) at each temperature of 298, 323 and 358 K. At equimolar ratio, CO₂ can adsorb about 5 times more than N₂ but CO₂ and N₂ are adsorbed almost equally in ZIF-90 for the real ratio. Due to the real ratio, the amount of N₂ is 5 times higher than the equimolar ratio, as seen in Figure 4.3.

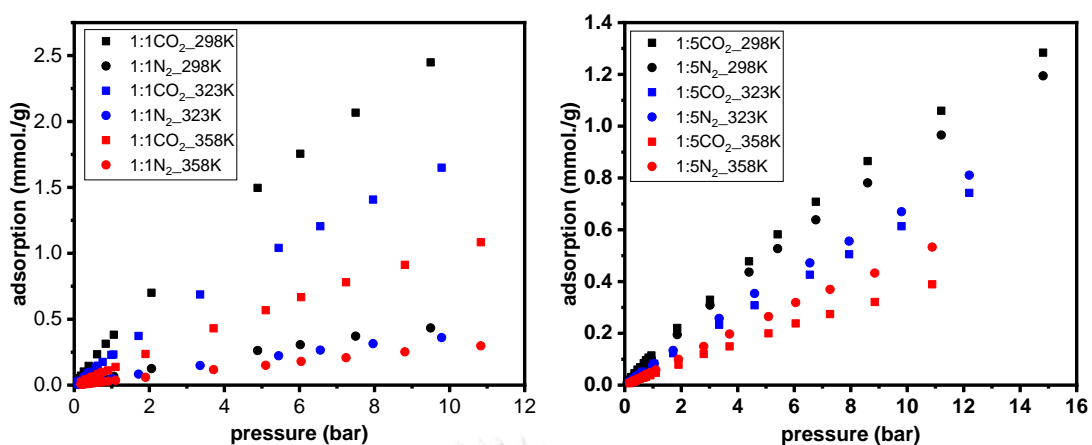


Figure 4.3 Calculated adsorption isotherms of CO_2/N_2 mixture in ZIF-90 using GEMC at 298, 323 and 358 K.

The average number of adsorbed molecules in ZIF-90 material that belong to the 1 bar of adsorption isotherms in Figure 4.3 are listed in Table 4.1. The information in the GEMC Column of Table 4.1 was used to be an average number of gas molecules that were loaded in ZIF-90 materials for MD simulations by $2 \times 2 \times 2 = 8$ unit cells. The average gas in the GEMC column was taken from the GEMC simulation results and must be divided by 8 to obtain the number of gases in the MD simulation.

Table 4.1 The average gas adsorption capacities of CO_2/N_2 mixture gas in ZIF-90.

Gas molecules	Number of gas molecule in GEMC		Number of gas molecule in MD	
	Temp. (K)			
	298	323	298	323
Equimolar ratio (1:1)				
CO_2	75	46	9	6
N_2	12	9.8	2	1

Gas molecules	Number of gas molecule in GEMC		Number of gas molecule in MD	
	Temp. (K)			
	298	323	298	323
Real ratio (1:5)				
CO ₂	23	16.2	3	2
N ₂	20	16.2	3	2

The adsorption selectivities of CO₂/N₂ mixtures were evaluated in Figure 4.4. The adsorption selectivity is about 4, 5 and 6 for the temperature of 358, 323 and 298, respectively, which may mean that lower temperature can induce higher selectivity. However, the adsorption selectivity of ZIF-90 is not good enough compared to other materials such as ZIF-8 or porous materials but still better than some polymer membranes.

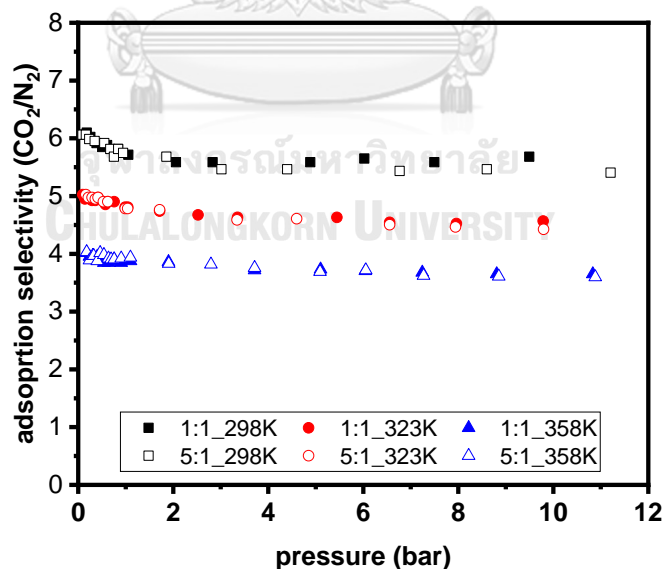


Figure 4.4 Adsorption selectivity of CO₂ and N₂ mixture in ZIF-90 as a function of the mixture ratio and temperature.

4.1.3. Effect of the number of adsorbed gas molecules (CO_2) by Molecular Dynamics (MD) simulations

Diffusion of CO_2 and dynamic properties of the ZIF-90 structure were monitored in terms of self-diffusion coefficient and windows diameter, respectively. The distributions of window diameters of the 6-membered ring at different temperatures were plotted in Figure 4.5. *E.g.* at 300 K for loadings from 0.5 to 22.5 CO_2/cage the diameter distributions of the 6-membered ring show a clear peak at around 3.49 - 3.53 Å. The peak is corresponding to the average experimental data of 3.50 Å [39]. But at 25 CO_2/cage a very broad peak has been found covering the whole region between 3.61 to 4.25 Å. It can be concluded that there are 2 phases of structure mixed together showing different form of rotation of the imidazolate group. The structure with lower window diameter is called “normal stage” and the one with higher window diameter is called “expanded stage”. However, for loadings higher than 25 CO_2 the height of the peak of the normal stage region decreases but the peak corresponding to the expanded stage region increases as established at window diameters of 4.22 Å at 27.5 CO_2/cage . Finally, the complete transformation of the structure to the expanded stage occurred at 30 CO_2/cage . It shows the highest peak at 4.34 Å which is a higher value than the one observed in previous work of ZIF-8 at 4.125 Å by around 0.21 Å. Thus, interestingly, the transition state of normal stage to expanded stage in this CO_2 -ZIF-90 system can be observed explicitly in the present work. The CO_2 molecules can induce the transition of the window diameter of ZIF-90 similar to in ZIF-8 [91] but in the previous CH_4 -ZIF-90 [45] examination no structure transition could be seen. For lower temperatures than 300 K the transition state is less pronounced but, a shoulder in the distributions can be seen.

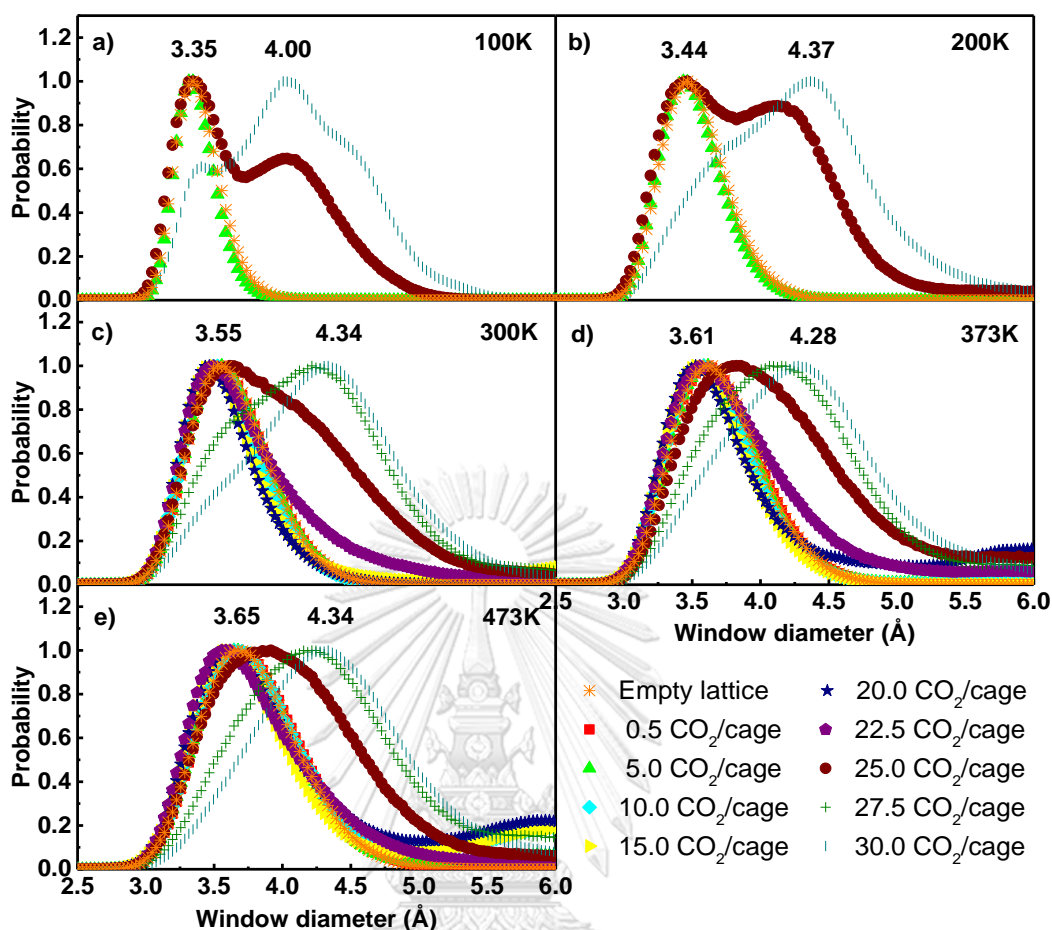


Figure 4.5 Distributions of the window diameter of ZIF-90 for different loadings of CO₂ as well as empty lattice in range of 100 to 473 K.

4.1.4. Temperature effect on CO₂ adsorption by Molecular Dynamics (MD) simulations

In Figure 4.5, even in the empty lattice (without CO₂ molecules in the framework) window diameters are gradually increased from 3.35 to 3.65 Å when the temperature is increased in the range of 100 to 473 K. The average window diameters under 25 CO₂/cage at a temperature range of 100 to 473 K show the same series like the empty lattice of around 3.35, 3.44, 3.55, 3.61 and 3.65 Å respectively. At a loading of 30 CO₂/cage, the structures were not completely transformed to the expanded stage at 100 and 200 K because 2 peaks appear. They are continuously

changed to reach the expanded stage at 300 K. The highest value of the window diameter at which a peak in the distribution at the expanded stage appears is 4.34 Å. It can be found at highest temperatures (473K). This is the highest value which has never been observed before in previous studies of ZIF-8 (300 K) [47].

Let us focus on the point of the first rapid increase of the windows diameters which happens at the same number of guest loading at 25 CO₂/cage for all temperatures. More details about the window diameter for 25 molecules per cage at different temperatures are explained in Figure 4.6. At a temperature of 100 K, 2 characteristic peaks of the window diameter can be observed. The first sharp peak appears at 3.35 Å and the second broad peak at 3.95 Å. When the temperature was increased, the second peak was also increased. Then it was blended with the first peak into the one very broad peak starting at 300 K. The average window diameters at 300 - 473 K were shifted from the first peak of 100 - 200 K (3.35 Å) to around 3.9 - 4.0 Å.

It is clearly to note that the rotation of the imidazolate, is the key of understanding the behavior of the window diameter, and can also be induced by temperature changes.

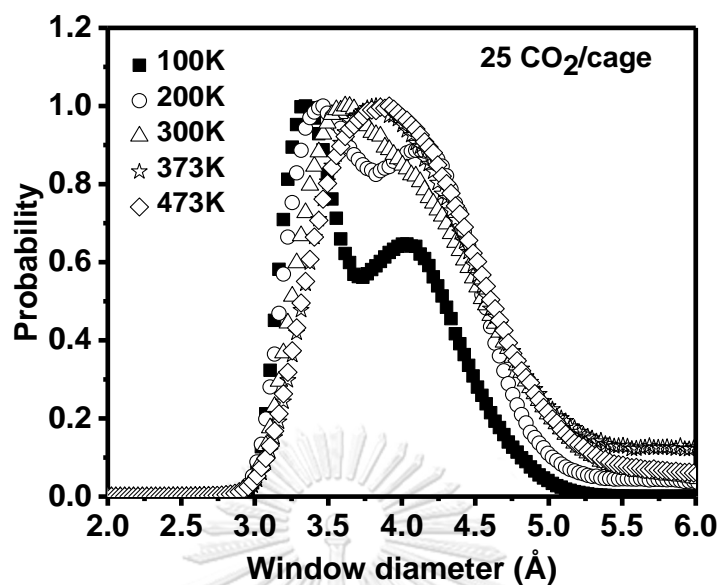


Figure 4.6 Distributions of the window diameter at 25 CO₂ / cage for 5 temperatures.

4.1.5. Effect of the number of adsorbed gas molecules (N₂) by Molecular Dynamics (MD) simulations

The distributions of window diameters of the 6-membered ring at different temperatures were plotted in Figure 4.7. For example, the diameter distributions of the 6-membered ring at 300 K for loadings from 0.5 to 30 N₂/cage show a clear peak at around 3.55 Å. The peak is consistent with the average experimental data of 3.50 Å [1]. This means that the N₂ cannot induce the transition of the window diameter of ZIF-90. When the temperature is increased in the range from 300 to 473 K, the average window diameters are similar for 300 and 373 K, but slightly increased up to 3.65-3.68 Å for 473 K. Due to the potential of mean force (PMF) as a function of dihedral angle are obtained at different temperatures, which shows that the “thermal swinging motion” is a soft vibration mode with large amplitude.

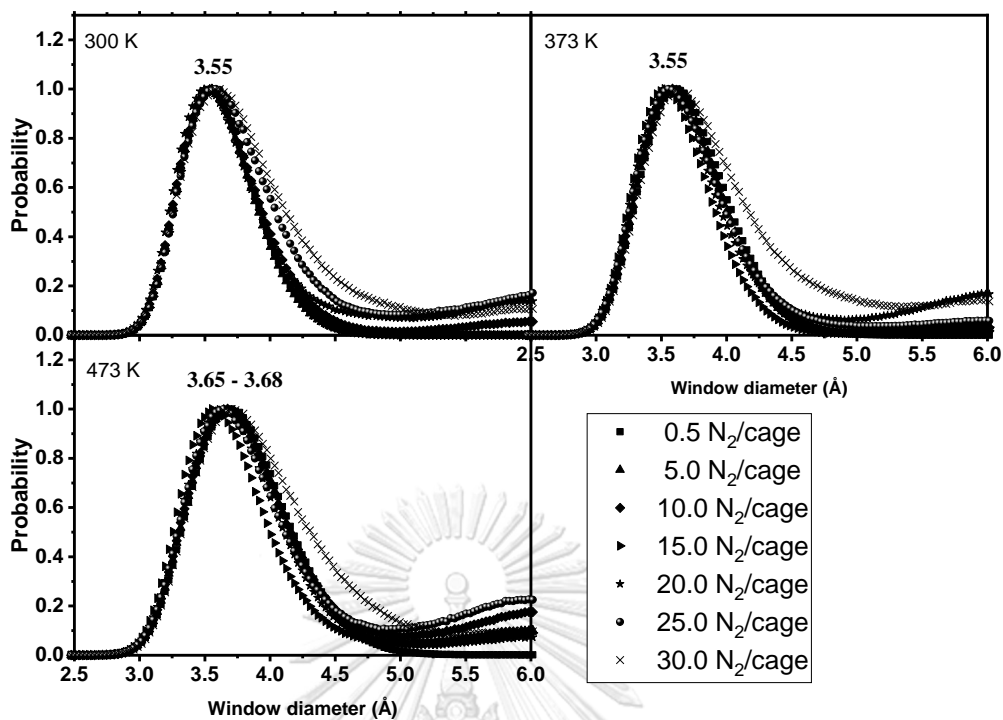


Figure 4.7 Distributions of the window diameter of ZIF-90 for different loadings of N₂ as well as in range of 300 to 473 K.

Figure 4.8 shows the distribution of the window diameter of ZIF-90 at 30 molecule/cage at different temperatures. The characteristic peak of ZIF-90 appears near 3.5 Å at 300 K, but gradually shifts to 3.7 Å as the temperature increases. It can be concluded that Zif-90 does not exhibit significant framework defects due to N₂ adsorption.

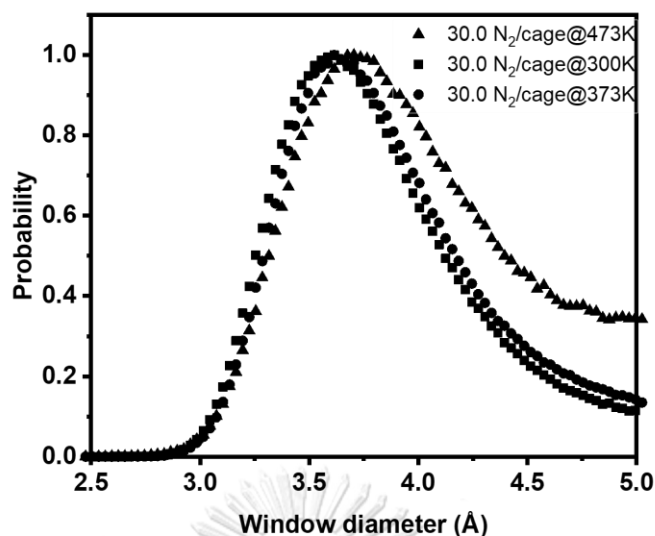


Figure 4.8 Distributions of the window diameter at 30 N₂ / cage for 3 temperatures.

4.1.6. Self-diffusion coefficient of CO₂ and N₂ in ZIF-90 by Molecular Dynamics (MD) simulations

In Figure 4.9, the diffusion of CO₂ was gradually increased from 1.65×10^{-10} to $1.90 \times 10^{-10} \text{ m}^2/\text{s}^{-1}$ at a loading range 0.5 to 15 molecules/cage for 300 K and started to decrease at 20 molecules/cage. The D_s was dropped down to $5.04 \times 10^{-12} \text{ m}^2/\text{s}^{-1}$ at 30 molecules/cage. This trend can also be observed at higher temperatures of 373 and 473 K. The D_s increases with increasing temperature, as expected due to the increased thermal motion. At very high CO₂ content the mutual hindrance of CO₂ molecules drops down the mobility.

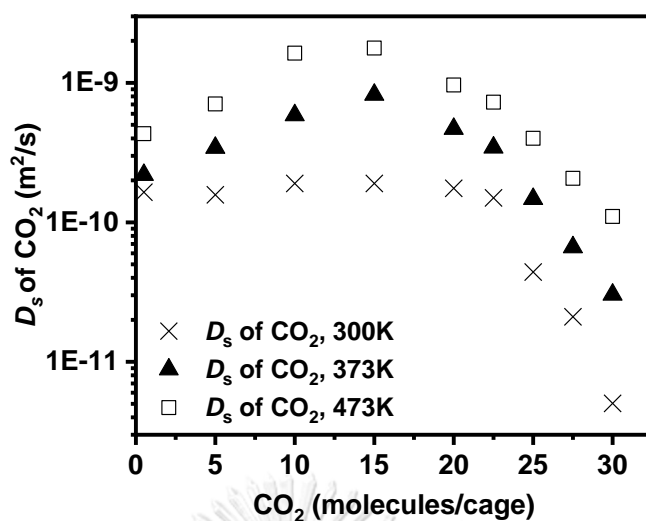


Figure 4.9 The calculated D_s for CO₂ loadings of 0.5 to 30 molecules/cage in ZIF-90 frameworks at 300, 373, 473K by MD simulation.

In Figure 4.10, the diffusion of N₂ was increased from 1.39×10^{-9} to 2.52×10^{-9} m²/s for a loading range of 0.5 to 15 molecules/cage for 300 K and started to decrease at 20 molecules/cage. The D_s was dropped down to 1.67×10^{-11} m²/s at 30 molecules/cage. This trend is also observed at higher temperatures of 373 and 473 K. The diffusion of N₂ is higher than that of CO₂ because the molecular weight of N₂ is lower. The D_s increases with increasing temperature, which is expected due to the increased thermal motion. At very high N₂ content the mutual hindrance of the N₂ molecules also reduces mobility.

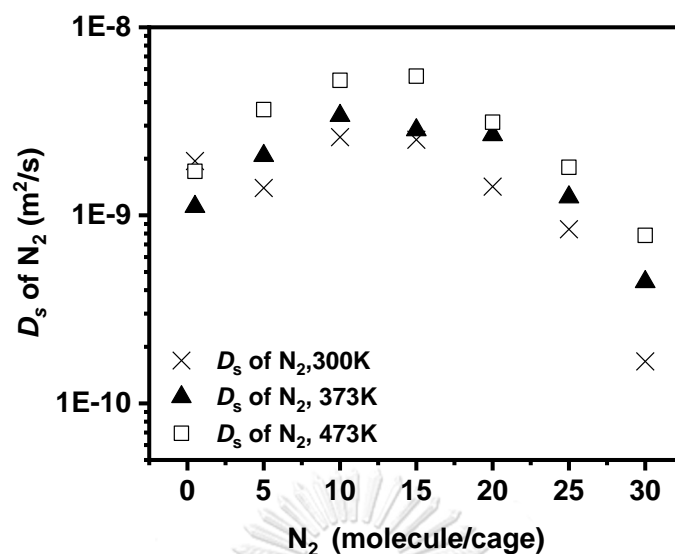


Figure 4.10 The calculated D_s for N_2 loadings of 0.5 to 30 molecules/cage in ZIF-90 frameworks at 300, 373, 473K by MD simulation.

The diffusion of CO_2 and N_2 in a CO_2/N_2 mixture at pressure of 1 bar was plotted in Figure 4.11 which shows the same trend as for pure gas, namely that the D_s of N_2 is higher than CO_2 for all conditions. Temperatures of 298 and 323 K were monitored, corresponding to conditions in the room and at the end of the chimney, respectively. Comparison of the two ratios at the same temperature shows that the 1:1 ratio gives the lower diffusion than 1:5 ratio for all temperatures. Note that the 1:1 ratio means equimolar adsorption while the 1:5 ratio means that the adsorption of N_2 is about five times that of CO_2 . To determine the separation factor from D_s the diffusion selectivity is calculated as declared in Table 4.2. The highest adsorption selectivity of CO_2/N_2 mixture is 12.39 at the 1:1 ratio and 298 K.

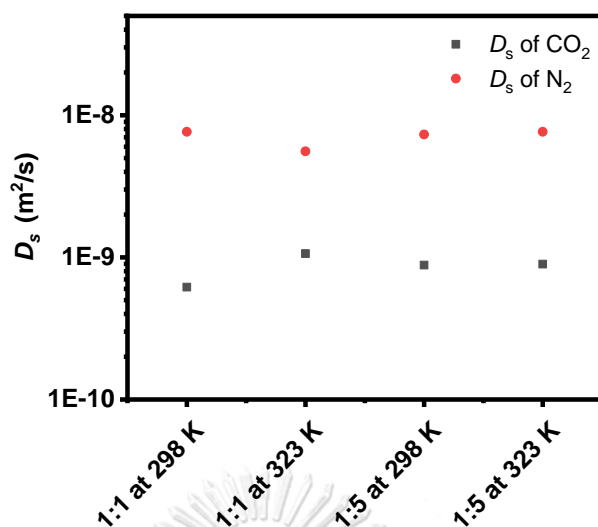


Figure 4.11 The calculated D_s for CO_2 and N_2 in two ratios of CO_2/N_2 mixture for 298 and 323 K.

Table 4.2 Diffusion selectivity of CO_2/N_2 mixture in ZIF-90.

Conditions	Diffusion selectivity
1:1 at 298 K	12.39
1:1 at 323 K	5.24
1:5 at 298 K	8.31
1:5 at 323 K	8.54

4.1.7. Radial distribution functions and Density Plots by Molecular Dynamics (MD) simulations

In order to check the distribution of guest molecules within the lattice and to identify adsorption centers the radial distribution functions (RDFs) and density plots have been examined. Figure 4.12 shows the pair correlation functions of atoms of CO_2 with various lattice atoms. It can be seen that the adsorption sites are not at the metal ion but at the O_OT atom of the linker. It was supported by the density plot in Figure 4.14 where the density of CO_2 scatters around the imidazolate-2-

carboxyaldehyde linkers at low concentration, while it is stronger at the center of the cage at higher concentration. The preferred orientation of CO_2 is so that the O and C atom of CO_2 is closer to the O_OT atom. As to be expected the adsorption centers are more pronounced at lower temperatures as can be seen in the appendix A.



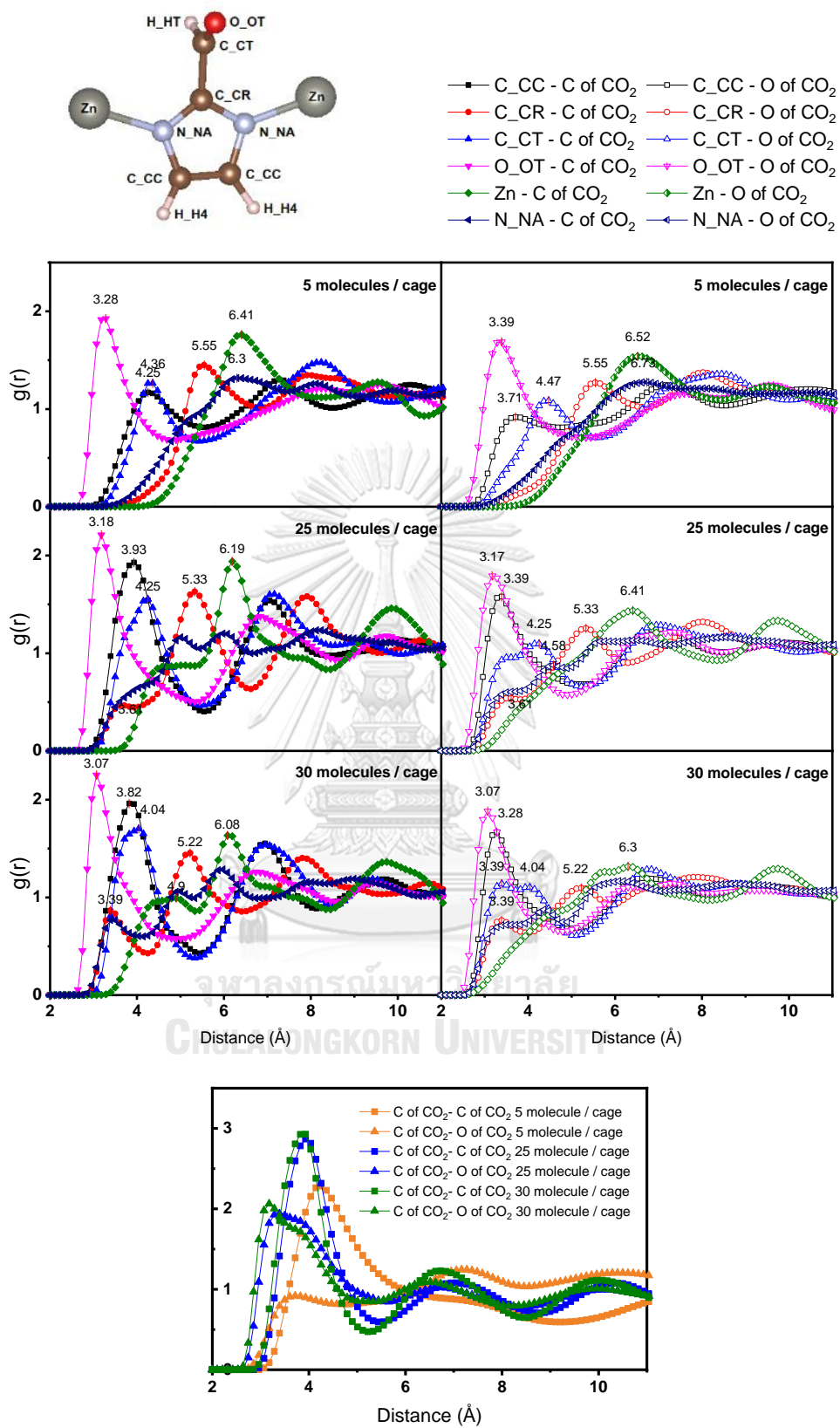


Figure 4.12 The RDFs of lattice atoms with CO₂ and CO₂ itself at loadings of 5, 25 and 30 molecules/cage in ZIF-90 frameworks at 300 K.

The RDFs of the weighty lattice atoms with N_2 and N_2 itself at loadings of 5, 25 and 30 molecules/cage in ZIF-90 frameworks at 300 K were plotted in Figure 4.13. The adsorption site of N_2 is close to the O_OT atoms of the imidazolate-2-carboxyaldehyde linkers about 3.2 Å, while the pair correlation functions of N_2 with Zn atom of ZIF-90 are above 6.1 Å. When the loading of N_2 in ZIF-90 is increased, the average distance between N_2 molecules is packed closer from 4.15 to 3.28 Å.

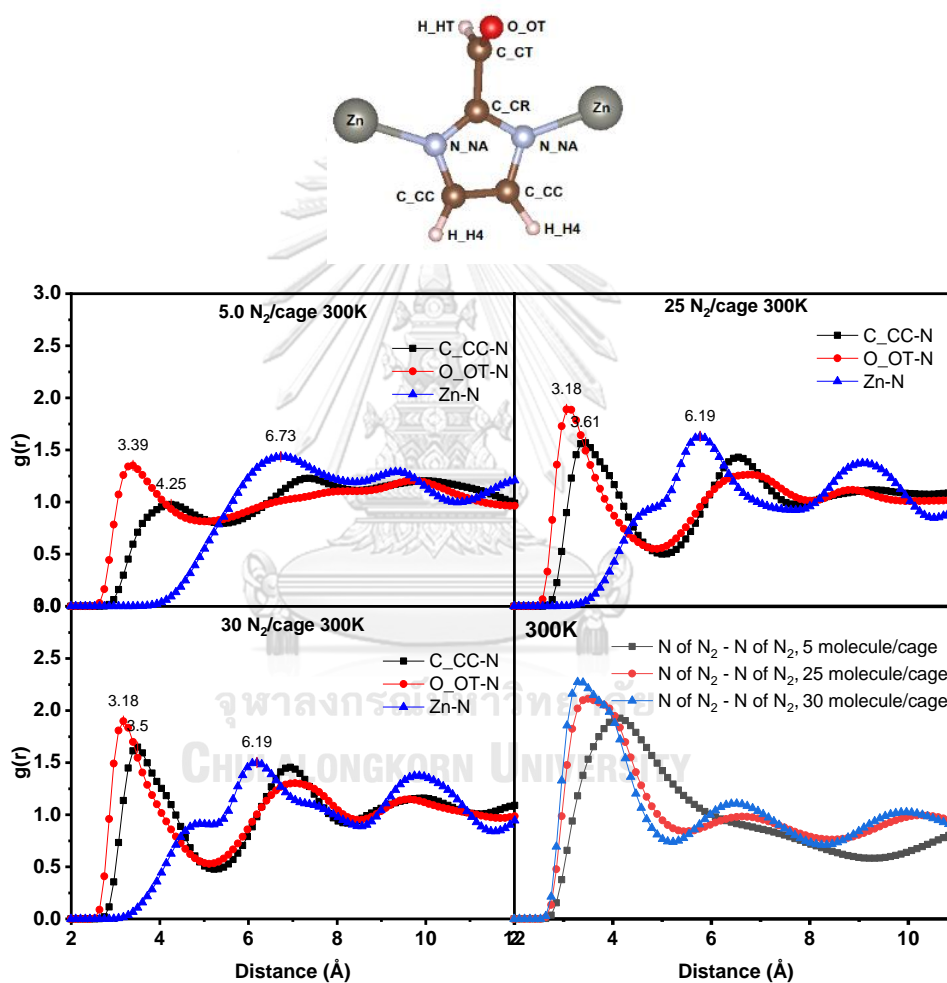


Figure 4.13 The RDFs of lattice atoms with N_2 and N_2 itself at loadings of 5, 25 and 30 molecules/cage in ZIF-90 frameworks at 300 K.

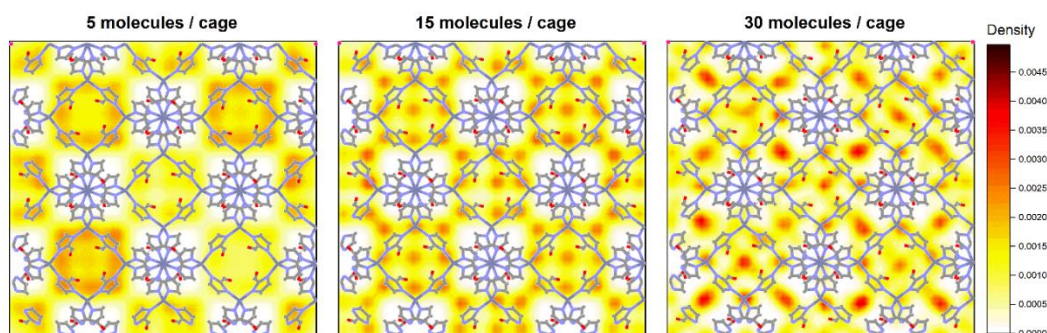


Figure 4.14 Density plots of CO_2 in the x-y plane of the last 0.5 ns, 300K at loading of 5, 15, 30 molecules/cage.

4.2. $\text{H}_2\text{S}/\text{CH}_4$ in ZIFs and MIL-127 materials

4.2.1. Adsorption Isotherms and Adsorption Selectivity

4.2.1.1. Pure Gases

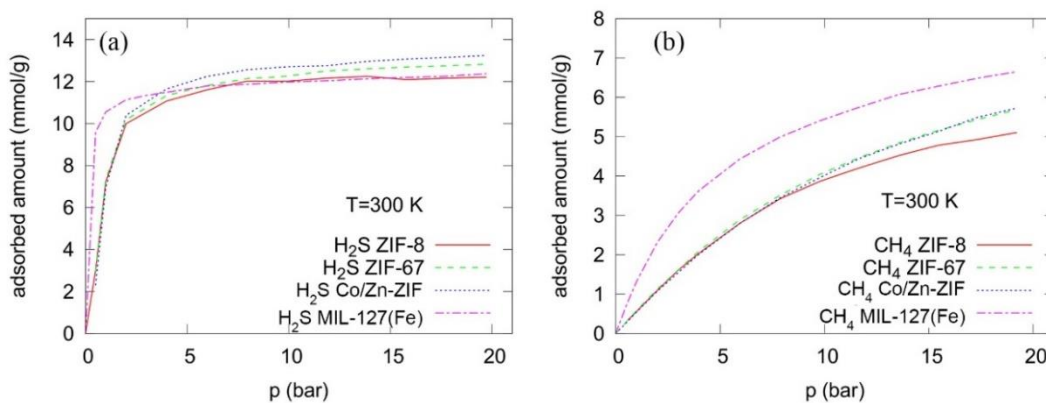


Figure 4.15 Adsorbed amounts of the pure gases (a) H_2S and (b) CH_4 in several materials at 300 K for various pressures.

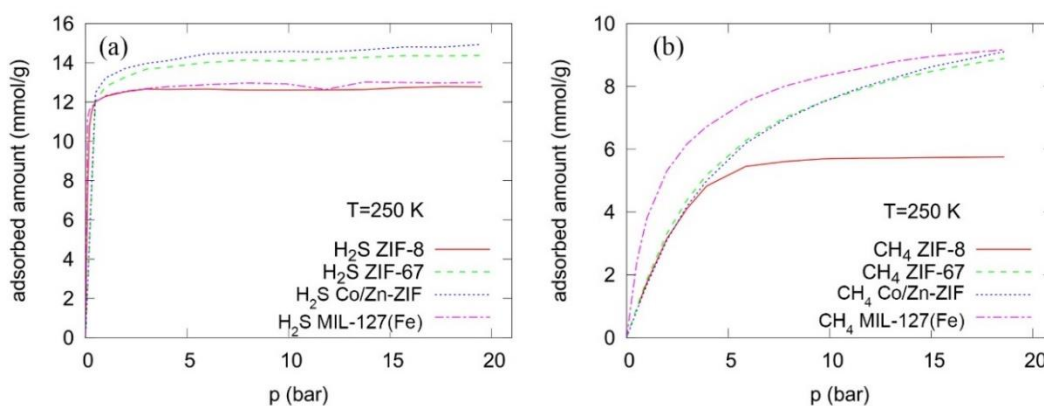


Figure 4.16 Adsorbed amounts of pure gases (a) H_2S and (b) CH_4 in several materials at 250 K for various pressures.

Figure 4.15 shows the adsorbed amounts of pure gases in several materials at 300 K as a function of the pressure. The adsorbed amount of H_2S is larger than that of CH_4 . To obtain an effective separation the difference in the adsorption of the two gases should be as large as possible. Up to 10 bar, the adsorption of CH_4 is almost the same for ZIF-8, ZIF-67 and the mixed metal ZIF. That for MIL-127(Fe) is larger. At low pressure, the adsorption of H_2S in MIL-127(Fe) increases more rapidly with increasing pressure than for the other materials. Hence the separation seems to be most effective if MIL-127(Fe) at low pressure is applied. Nonetheless, it will be interesting to see, if this is also true in the case of competitive co-adsorption in the mixture and with the concentration ratio as it is usually found in natural gas.

Figure 4.16 shows the same at 250 K. As to be expected the adsorption is stronger at the lower temperature. An exception is the adsorption of H_2S , for which saturation is reached at both 250 K and 300 K. The temperature dependence of adsorption at low coverage can be described by the Boltzmann factor for adsorption $\exp(-U_a/kT)$ where U_a is the absolute value of an effective depth of a potential minimum at an adsorbing surface (see F. Keil [92]).

At 250 K at ambient pressure, particularly the mixed metal ZIF seems to be a promising material for the separation while at pressures below 0.5 bar ZIF-8 and MIL-127(Fe) seem to have a better performance. As mentioned above the separation $\text{H}_2\text{S}/\text{CH}_4$ must be investigated at realistic concentrations in the mixture before drawing valid conclusions. It turns out that at 250 K the adsorption of H_2S surprisingly quickly reached saturation. The partial pressure of H_2S in the gas phase is 5% of the total pressure in the equilibrium state for all of our simulations. Hence, the sudden saturation of the adsorption within the porous material has nothing to do with the lack of H_2S in the gas phase.

It may be interesting to compare the amount of adsorbed gases from our simulations with experimental values. We found isotherms of different groups of researchers. Note, however, we found that the adsorption of CO_2 in ZIF-8 which measured adsorption isotherms from 5 different groups showed very different results[91]. The smallest and the largest values differed by a factor of about 2. Hence, such comparisons have to be done with care.

Adsorption isotherms of CH_4 in ZIF-8, ZIF-67 and Co/Zn-ZIF at 273 K up to 1 bar are published[40]. From the graph, we estimate values at 1 bar of about 0.45 mmol/g for ZIF-8, of about 0.54 mmol/g for ZIF-67 and of 0.36 mmol/g for Co/Zn-ZIF. We found in our simulations at 300 K and 1 bar 0.56 mmol/g in ZIF-8, 0.58 mmol/g for ZIF-67 and 0.55 mmol/g for Co/Zn-ZIF. For adsorption isotherms of CH_4 in MIL-127(Fe) at 303K from 1-10 bar are reported[93]. From the illustration, the adsorption capacity at 5 bar and 10 bar are approximately 2.8 and 4.3 mmol/g, respectively. In our simulations at 300 K obtained 4.0 mmol/g for 5 bar and 5.4 mmol/g for 10 bar. The H_2S capacity was investigated for unmodified and modified ZIF-8 at 298K from 1-10 bar[94]. Unmodified ZIF-8 *i.e.* DS-ZIF-8 (dry) and WS-ZIF-8 (suspension in methanol) show adsorption capacities at 10 bar about 9 and 18 mmol/g, respectively. This work demonstrated 12.0 mmol/g at 300K and 10 bar. The

adsorption values from simulations are not fitted to experiments. It is quite frequently the case in such comparisons of simulations and experiments. This disagreement can be caused by transport hindrances in real crystals such as lattice defects, grain boundaries, and pore blocking which do not exist in the ideal crystal of the simulations[95]. The adsorption of e.g. CH_4 and CO_2 in ZIF-68 and ZIF-69 the hypothesis of partial pore blocking was checked. Blocking some pores randomly is the one choice of blocking obtained a very good agreement of simulations with experiment using unfitted generalized force field parameters.

4.2.1.2. $\text{H}_2\text{S}/\text{CH}_4$ Mixture in ZIF-8

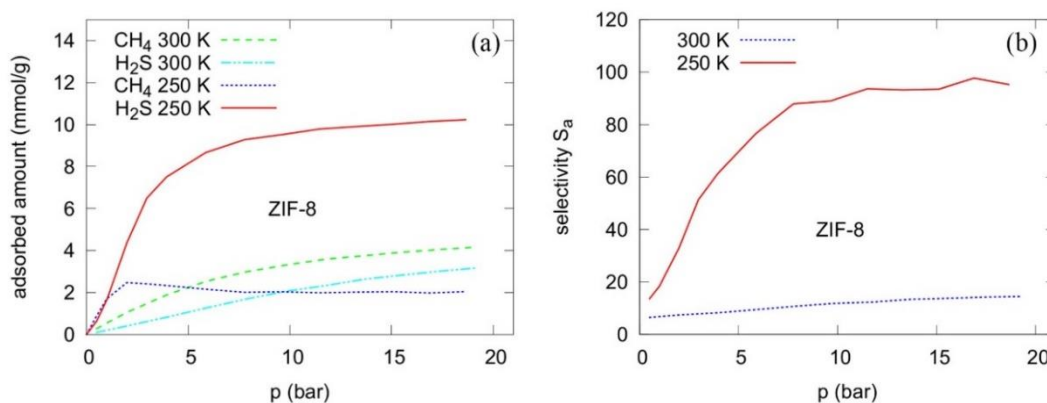


Figure 4.17 (a) Adsorbed amounts and (b) adsorption selectivity of CH_4 and H_2S in ZIF-8 as a function of the pressure and temperature.

Figure 4.17 (a) shows the amount of the gases, that are adsorbed within the ZIF-8 in equilibrium with the gas phase of the mixture mentioned above. Interestingly at 250 K, the adsorbed amount of CH_4 at $p = 2$ bar is larger than at higher pressures. This is clearly the consequence of competitive co-adsorption because for pure substances at constant temperature the adsorbed amount would be a monotonic function of the pressure. The adsorbed amount of CH_4 at 300 K is larger than that of H_2S as to be expected because in the gas phase (box A) the H_2S content is only 5%.

Therefore, also at 300 K, the adsorption selectivity is larger than 1 although more CH₄ than H₂S is adsorbed. This can be seen in Figure 4.17(b). Interestingly, the selectivity increases with increasing pressure. This is in contrast to the separation of CH₄ from air in ZIF-78 as shown by Channajaree *et al.*[71]. The selectivity is calculated by equation (2) where $N_{i,gas} = N_{CH_4,A}$ is the number of CH₄ molecules in box A (gas phase). $N_{j,adsorbed} = N_{CH_4,B}$ is the number of CH₄ molecules in box B (adsorbed phase) and so on. The selectivity increases with increasing pressure.

At 250 K the selectivity as a function of the pressure shows an inflection at about 2-3 bar. For ZIF-8 this inflection is less pronounced than for ZIF-67 and Co/Zn-ZIF. The values for the adsorption selectivity at 1 bar and 10 bar are given in the appendix B.

4.2.1.3. H₂S/ CH₄ Mixture in ZIF-67

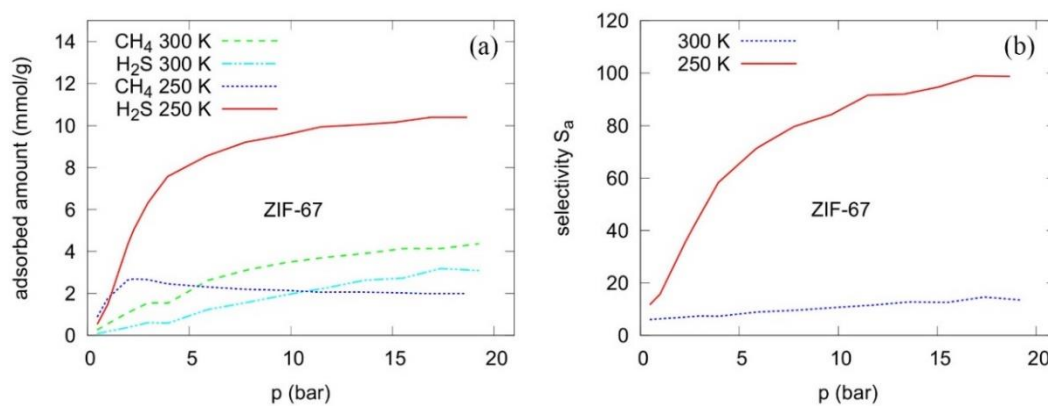


Figure 4.18 (a) Adsorbed amounts and (b) adsorption selectivity of CH₄ and H₂S in ZIF-67 as a function of the pressure and temperature.

Figure 4.18 (a) and (b) show that the adsorption and selectivity for the two gases in ZIF-67 are very similar to the corresponding curves for ZIF-8. The inflection of the selectivity curve at about 2.5 bar is more pronounced for ZIF-67. The reason for a stronger than linear increase of the H₂S adsorption at this pressure is that

'already adsorbed'-H₂S molecules will attract new ones. Note, that the mass of a Zn atom is higher than that of a Co atom. Therefore, an equal amount of adsorbed gas measured in mmol/g corresponds to more adsorbed gas molecules in ZIF-8 as can be seen in Table S5 as shown in the Supporting Material.

4.2.1.4. H₂S/ CH₄ Mixture in Co/Zn-ZIF

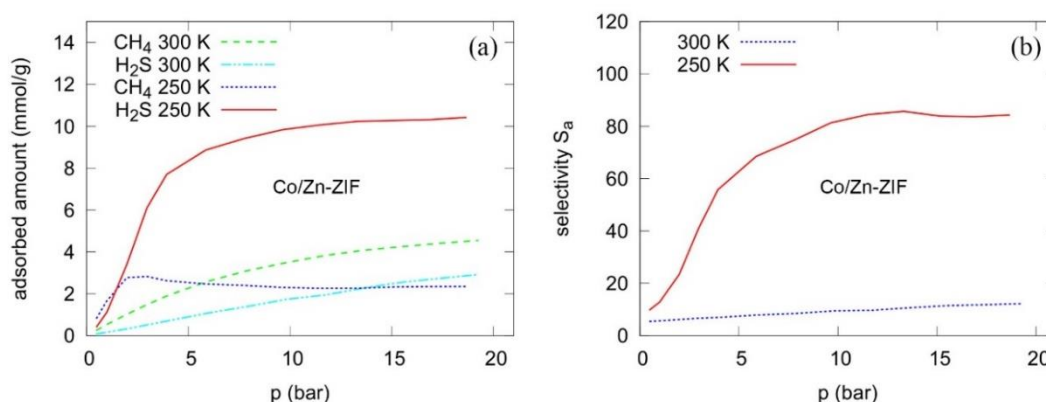


Figure 4.19 (a) Adsorbed amounts and (b) adsorption selectivity of CH₄ and H₂S in Co/Zn ZIF as a function of the pressure and temperature.

Figure 4.19 (a) and (b) show that the adsorption and selectivity for the two gases in the mixed metal ZIF are slightly different from the corresponding curves for ZIF-8 and ZIF-67. This would agree with the (i) structural component *i.e.* metal cluster and organic linker (ii) structural characteristic *i.e.* window aperture, surface area and pore volume. There are no statistical differences between ZIF-8, ZIF-67 and Co/Zn-ZIF as mentioned in appendix B.

The adsorption and selectivity for CH₄/H₂S mixture in ZIFs results (Figure 4.17 - Figure 4.19) are lower than MIL-127(Fe) as shown in Figure 4.20. The explanation is following: (i) The structural feature of ZIFs *i.e.* ZIF-8, ZIF-67 and Co/Zn-ZIF, that have two types of window aperture such as 6-membered ring (~3.4 Å) and 4-membered ring (too small). Whereas MIL-127(Fe) has two types of pores such as an accessible

one-D channel system around 6 Å and cages of cavity around 10 Å accessible through window apertures of around 4 Å that fit well to the kinetic diameter of CH₄ (3.8 Å) and H₂S (3.6 Å) molecules. (ii) Radial distribution functions (in section 3.2) and density plot (in Supporting Material) show the adsorption site of gas molecules in MIL-127(Fe) including –COO cluster, organic linker and pore channels. However, ZIFs no adsorption site near metal cluster (ZnN₄ or CoN₄ or Co/ZnN₄) (iii) Gas molecule could be adsorbed at organic linker in MIL-127(Fe) easier than ZIFs because of space-size of linker, electronegativity of atom (O = 3.44 and N = 3.04) as confirmed by the enthalpy of adsorption between gas and porous materials in Table 1 and no geometric hindrance effects at O atom in MIL-127(Fe). These reasons are also found in Zho's reported[96]. The inflection of the selectivity curve at about 2.5 bar is more pronounced than for ZIF-8. The selectivity at 250 K is about 15 % smaller than for ZIF-8 and ZIF-67.

The numbers of guest molecules that are adsorbed in equilibrium in ZIF-67 and the mixed metal ZIF. Like for ZIF-8 at 1 bar about 3 times more CH₄ than H₂S is adsorbed. Note, however, that in the gas phase that is in equilibrium with these adsorbed species, 95% of the particles are CH₄. In Table 4.4, we compare the numbers of adsorbed particles.

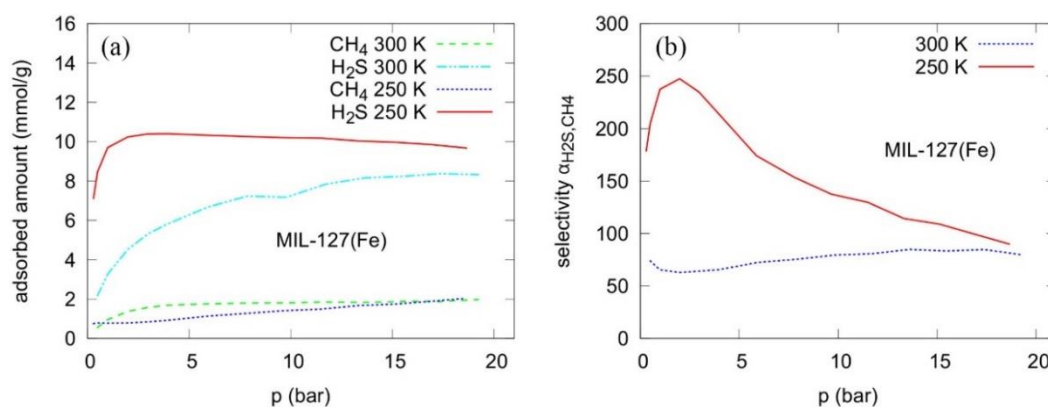
4.2.1.5. H₂S/ CH₄ Mixture in MIL-127(Fe)

Figure 4.20 (a) Adsorbed amounts and (b) adsorption selectivity of CH₄ and H₂S in MIL-127(Fe) as a function of the pressure and temperature.

The adsorption and selectivity for CH₄/H₂S mixture in ZIFs results (Figure 4.17 - Figure 4.19) are lower than MIL-127(Fe) as shown in Figure 4.20. It becomes apparent that the adsorption and selectivity depend on the pore size and window aperture of porous materials. The structural feature of ZIFs *i.e.* ZIF-8, ZIF-67 and Co/Zn-ZIF, have two types of window aperture such as 6-membered ring (~3.4 Å) and 4-membered ring (too small). Whereas MIL-127(Fe) has two types of pores such as an accessible 1D channel system around 6 Å and cages of cavity around 10 Å accessible through window apertures of around 4 Å. Therefore, it is the main reason for increasing adsorption and selectivity.

Figure 4.20 (a) shows the amounts of CH₄ and H₂S, that are adsorbed in MIL-127(Fe), as a function of the pressure and temperature. Interestingly, the numbers of adsorbed CH₄ at T=250 K are smaller than at 300 K. It is well known that adsorption is usually stronger at lower temperature and this can be seen in figure 7 for H₂S. Therefore, the higher selectivity and thus stronger adsorption of H₂S must be the reason for the smaller amount of adsorbed CH₄ at 250 K in MIL-127(Fe). By the way, in order to avoid artifacts due to the strong adsorption of H₂S and the fact that only

5% of the molecules in the gas phase are H_2S the number of molecules in the gas box must be quite high. A typical run includes about 100 H_2S molecules and 2000 CH_4 molecules in the gas phase in equilibrium.

Figure 4.20 (b) shows the adsorption selectivity of the $\text{CH}_4/\text{H}_2\text{S}$ mixture in MIL-127(Fe) as a function of the pressure. At pressures of 1-3 bar the selectivity at 250 K can reach values of about 250. That means that with MIL-127(Fe) it is possible to reach high selectivity at low pressures and that this selectivity is higher than for the other materials examined in this paper. Interestingly, the selectivity does not depend monotonically upon the pressure. This fits the fact that H_2S is adsorbed very strongly at low pressure and reaches its saturation value soon, while the adsorption of CH_4 is much smaller but increases monotonically over the whole region of pressure examined here. Although the highest selectivity occurs at 250 K, even at ambient conditions the selectivity of MIL-127(Fe) is above 50. This may be particularly interesting for industrial applications because it allows separation under ambient conditions.

4.2.2. Enthalpy of adsorption

In order to get some more insight into the high selectivity at 250 K, it may be of interest to evaluate the enthalpy of adsorption at low pressure for this temperature.

Table 4.3 Enthalpy of adsorption in kJ/mol for CH_4 and H_2S at 250 K.

Materials	CH_4	H_2S
ZIF-8	-14.73	-21.76
ZIF-67	-14.73	-21.30
Co/Zn - ZIF	-14.30	-20.15
MIL-127(Fe)	-21.13	-35.36

Table 4.3 shows the enthalpies of adsorption for CH₄ and H₂S at 250 K and at low pressure. The very strong negative enthalpy of adsorption for H₂S, particularly in MIL-127(Fe) illustrates that a high selectivity can be expected.

Note, that the potential energy enters the integrand of the classical canonical partition function in the exponent. This integrand is essentially the probability density of a state in phase space. For example, at 2 bar, 250 K (the region of highest selectivity), the average potential energy of an H₂S molecule in MIL-127(Fe) is -33.29 kJ/mol. The potential energy of a CH₄ molecule in the same run is 20.43 kJ/mol. The integrand of the classical canonical partition function is, of course, much more complicated than a simple Boltzmann factor. Nevertheless, the consideration of a Boltzmann factor may give a feeling for the importance of energy differences in the exponent. The Boltzmann factor $\exp(-U_a/k_B T)$ changes its value by a factor of 486.29 if $U_a = -33.29$ kJ/mol instead of - 20.43 kJ/mol for $T=250$ K.

4.2.3. Radial distribution functions (RDFs)

The radial distribution function, RDF, is the probability to find an atom at a radial distance r from a given reference atom. The evaluation of RDFs between atomic pairs of the binary CH₄/H₂S mixtures and the frameworks yields information about optimal gas-gas and gas-framework distances and possible adsorption sites. RDFs within ZIF-8 may be representative also for ZIF-67 and Co/Zn-ZIF that have the same structure. MIL-127(Fe) has a different structure and it is examined separately. More RDF curves are provided in the appendix B.

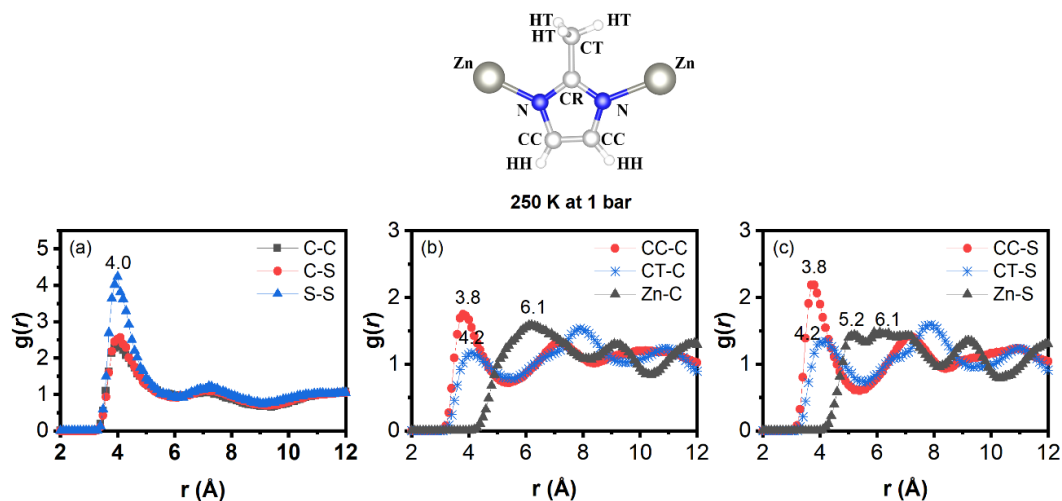
4.2.3.1. H₂S/CH₄ mixture in ZIF-8 at 250 K

Figure 4.21 Radial distribution functions (a) between different atoms of the guest molecules, (b) between the C atom in CH₄ with different atoms of the ZIF-8 lattice, that are defined in the inset picture above, (c) between the S atom of H₂S with these lattice atoms.

Among the three ZIFs with a sodalite crystal structure, ZIF-8 has the best selectivity in the separation of the binary CH₄/H₂S mixtures at all conditions thus it was chosen to represent the structure of each gas inside ZIFs as shown in Figure 4.21 at 250 K and 1 bar. The C and S labels stand for the atoms C and S, which are the centers of mass of the CH₄ molecule and the H₂S molecule respectively. CC and CT are both C atoms, but at different positions within the lattice, with different chemical bonds to their neighbor atoms and hence different properties.

Three sites of the framework atoms have been considered, Zn of the metal part and CC, CT of the imidazolate part. The RDFs in Figure 4.21(a) show that the first maximum of the RDF of the S atom in H₂S with the S atom of another H₂S is somewhat higher than the other two peaks. All of them have the highest maximum at a distance of 4 Å. This is approximately the sum of the two atom radii. But the

height of all three peaks is moderate and hence they result only from the kinetic effect that collisions with other molecules are possible only from outside, if two molecules are close to each other. Such collisions push the two molecules toward each other. No strong attraction and no clustering can be observed. Figure 4.21(b) and (c) show the radial distribution functions of the C and the S atoms with selected lattice atoms. RDFs of the other atoms of the framework with the atoms in guest molecules are available in the Supporting Material. No remarkable adsorption centers can be observed. Hence the strong adsorption of H_2S results from the low potential energy over larger parts of the pores. The spatial restrictions make neighbor shells impossible. Therefore, number integrals would not give much useful information.

4.2.3.2. $\text{H}_2\text{S}/\text{CH}_4$ mixture in MIL-127(Fe) at 250 K

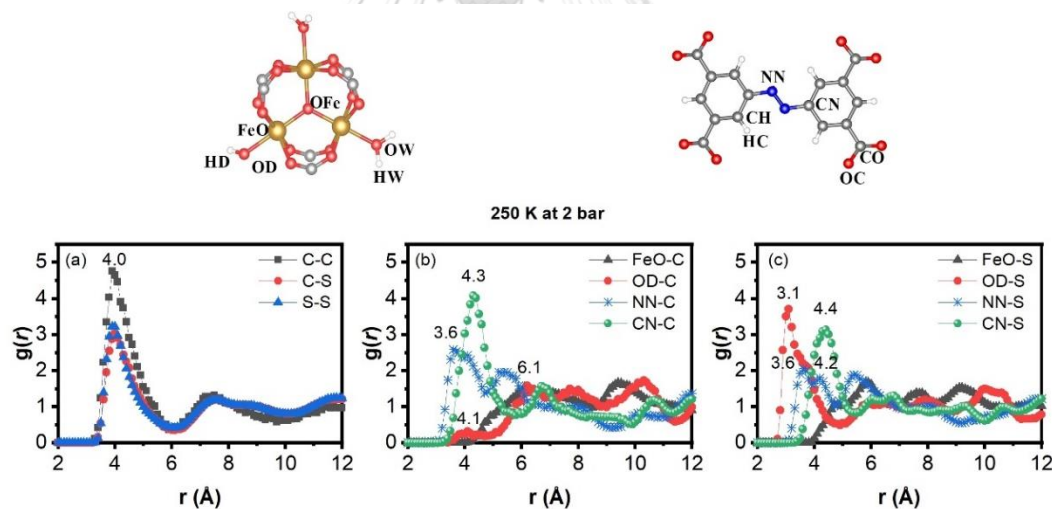


Figure 4.22 Radial distribution functions (a) between different atoms of the guest molecules, (b) between the C atom in CH_4 with different atoms of the MIL-127(Fe) lattice, that are defined in the inlet picture above, (c) between the S atom of H_2S with these lattice atoms.

MIL-127(Fe) has the highest selectivity of separation for the binary $\text{CH}_4/\text{H}_2\text{S}$ mixtures at 250 K and about 2 bar. Therefore, the corresponding RDFs are particularly interesting. They can be found in Figure 4.22. Two regions of the lattice of MIL-127(Fe) at the azobenzenetetracarboxylate (NN and CN) and at the metal cluster (FeO and OD) are examined in Figure 4.22 while the other RDFs of MIL-127(Fe) with guest atoms can be found in the appendix B.

Interestingly, the maximum probability of a close approach between the two C – atoms of different CH_4 is somewhat higher than that of a close approach between two H_2S molecules in MIL-127(Fe) in contrast to ZIF-8. The main difference in the structure of both materials is that the pores of ZIF-8 consist mainly of cavities, connected by bottlenecks, while the pores of MIL-127(Fe) are mainly channels that form a network. Maybe, the smaller diameter of the channels in comparison to the cavities causes this effect. But the moderate height of all peaks leads to the conclusion that there are no remarkable adsorption centers and hence the low potential energy within the channels and pores is more important for the adsorption than accumulation points of the guest molecules.

4.2.4. The average numbers of adsorbed molecules in the ZIFs and MIL-127 materials

The average numbers of adsorbed molecules in the ZIFs and MIL-127 materials that belong to the saturation part of the isotherms of Figure 4.17 - Figure 4.20 are reported in Table 4.4. Thus the ability of the ZIFs and MIL-127 materials for adsorption applications can be compared in this Table. And also it used to be an average number of gas molecules that were loaded in ZIFs and MIL-127 materials for MD simulations by $2 \times 2 \times 2 = 8$ unit cells.

Table 4.4 Average gas adsorption capacities in ZIFs and MIL-127 by GEMC 4x4x4 = 64 unit cells and MD 2x2x2 = 8 unit cells.

Gas molecules	Temp. (K)	Particle Num. in ZIF-8		Particle Num. in ZIF-67		Particle Num. in Co/Zn ZIF		Particle Num. in MIL-127	
		Pressure							
		1 bar	10 bar	1 bar	10 bar	1 bar	10 bar	1 bar	10 bar
GEMC simulation									
CH ₄	250	296.95	354.98	300.37	364.31	284.99	395.42	305.12	554.59
H ₂ S		33.86	359.57	249.14	1614.12	192.40	1692.75	3812.92	4012.21
CH ₄	300	94.38	576.63	93.79	588.25	90.29	600.93	373.26	712.95
H ₂ S		33.86	359.57	31.40	329.28	26.88	298.74	1285.83	2980.46
MD simulation									
CH ₄	250	37	44	38	46	36	24	38	69
H ₂ S		35	208	31	202	49	212	477	502
CH ₄	300	12	72	12	72	11	75	47	161
H ₂ S		4	45	4	45	4	37	89	373

4.2.5. Dynamic property

4.2.5.1. Self-diffusion

The two self-diffusion coefficients D_s of CH_4 and H_2S in their binary mixture adsorbed in ZIFs and MIL-127 as a function of the pressure and temperature as can be seen in Table 4.5. All data were calculated diffusion selectivities by the diffusion coefficient of H_2S divided by that of CH_4 as show in Table 4.6.

Table 4.5 Diffusion of mixture between CH_4 and H_2S in porous materials as a function of the pressure and temperature.

Materials	Temperature (K)	Pressure (bar)	Num. mixture ratio in MD simulations (8 unit cells)	D_s of CH_4 (m^2/sec)	D_s of H_2S (m^2/sec)
ZIF-8	250	1	37 CH_4 : 35 H_2S	8.21×10^{-11}	7.69×10^{-11}
		10	44 CH_4 : 208 H_2S	28.7×10^{-11}	9.01×10^{-11}
	300	1	12 CH_4 : 4 H_2S	20.4×10^{-11}	3.05×10^{-11}
		10	72 CH_4 : 45 H_2S	12.3×10^{-11}	6.25×10^{-11}
ZIF-67	250	1	38 CH_4 : 31 H_2S	6.72×10^{-11}	6.95×10^{-11}
		10	46 CH_4 : 202 H_2S	13.1×10^{-11}	6.07×10^{-11}
	300	1	12 CH_4 : 4 H_2S	2.96×10^{-11}	0.259×10^{-11}
		10	74 CH_4 : 41 H_2S	5.29×10^{-11}	1.49×10^{-11}
Co/Zn-ZIF	250	1	36 CH_4 : 49 H_2S	2.36×10^{-11}	0.413×10^{-11}
		10	24 CH_4 : 212 H_2S	14.7×10^{-11}	7.28×10^{-11}
	300	1	11 CH_4 : 4 H_2S	4.51×10^{-11}	0.260×10^{-11}
		10	75 CH_4 : 37 H_2S	6.02×10^{-11}	0.874×10^{-11}
MIL-127	250	1	38 CH_4 : 477 H_2S	8.66×10^{-11}	10.03×10^{-11}
		10	69 CH_4 : 502 H_2S	5.41×10^{-11}	4.26×10^{-11}

Materials	Temperature (K)	Pressure (bar)	Num. mixture ratio in MD simulations (8 unit cells)	Ds of CH ₄ (m ² /sec)	Ds of H ₂ S (m ² /sec)
	300	1	47CH ₄ : 161H ₂ S	31.1x10 ⁻¹⁰	9.81x10 ⁻¹⁰
		10	89CH ₄ : 373H ₂ S	4.13x10 ⁻¹⁰	2.83x10 ⁻¹⁰

4.2.5.2. Selectivities

The effectivity of separation processes can be expressed by the selectivities. Then the membrane selectivity is calculated from the adsorption selectivity and the diffusion selectivity as shown in Table 4.6.

Table 4.6 Adsorption, diffusion and membrane selectivities of mixture between CH₄ and H₂S in porous materials as a function of the pressure and temperature.

Materials	Temp. (K)	Press. (bar)	Num. mixture ratio in MD simulations (8 unit cells)	Adsorption selectivity ($\alpha_{ij}^{\text{adsorption}}$)	Diffusion selectivity ($\alpha_{ij}^{\text{diffusion}}$)	Membrane selectivity ($\alpha_{ij}^{\text{membrane}}$)
ZIF-8	250	1	37CH ₄ : 35H ₂ S	18.0	0.94	16.86
		10	44CH ₄ : 208H ₂ S	89.0	0.31	27.94
	300	1	12CH ₄ : 4H ₂ S	6.8	0.15	1.02
		10	72CH ₄ : 45H ₂ S	11.8	0.51	6.00
ZIF-67	250	1	38CH ₄ : 31H ₂ S	15.8	1.03	16.34
		10	46CH ₄ : 202H ₂ S	84.2	0.46	39.01
	300	1	12CH ₄ : 4H ₂ S	6.4	0.09	0.56
		10	74CH ₄ : 41H ₂ S	10.6	0.28	2.99
Co/Zn	250	1	36CH ₄ : 49H ₂ S	12.8	0.18	2.24

Materials	Temp. (K)	Press. (bar)	Num. mixture ratio in MD simulations (8 unit cells)	Adsorption selectivity ($\alpha_{ij}^{\text{adsorption}}$)	Diffusion selectivity ($\alpha_{ij}^{\text{diffusion}}$)	Membrane selectivity ($\alpha_{ij}^{\text{membrane}}$)
ZIF		10	24CH ₄ : 212H ₂ S	81.3	0.49	40.26
		1	11CH ₄ : 4H ₂ S	5.7	0.06	0.33
	300	10	75CH ₄ : 37H ₂ S	9.4	0.15	1.36
MIL-127	250	1	38CH ₄ : 477H ₂ S	237.4	1.16	274.96
		10	69CH ₄ : 502H ₂ S	137.4	0.79	108.19
	300	1	47CH ₄ : 161H ₂ S	65.4	0.32	20.63
		10	89CH ₄ : 373H ₂ S	79.4	0.69	54.41

From the results of Table 4.6 we can conclude that MIL-127(Fe) is well suited to separate CH₄ from H₂S in natural gas. The adsorption selectivity and the membrane selectivity at 250 K and 1 bar are significantly high up to 237 and 274, respectively. Moreover, the separation is more effective at lower temperature for all porous materials. MIL-127(Fe) is the most candidate for the removal of H₂S and N₂ from the natural gas.

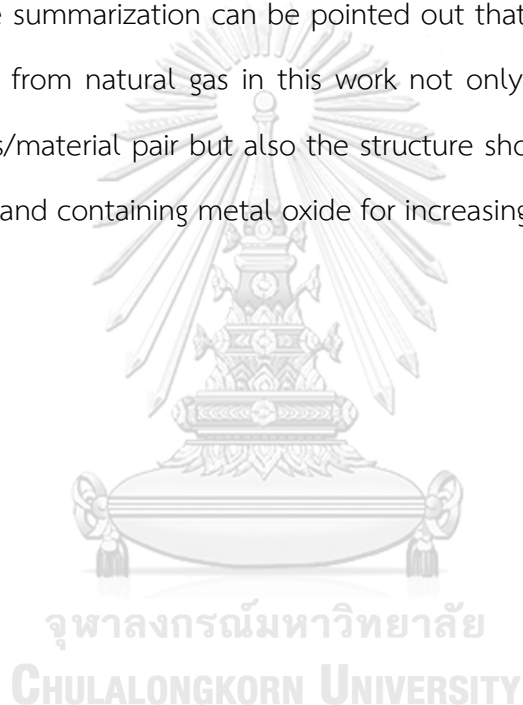
CHAPTER V

CONCLUSIONS

Appropriate force fields of CO₂ and N₂ in ZIF-90 model and information about separation capacity of CO₂/N₂ mixture in term of selectivity, which are useful for the design of ZIF-90 for CO₂ capture application, will be obtained by computational chemistry. The MD simulations of CO₂ in ZIF-90 at various concentrations and temperatures were examined for finding factors of gate-opening effect and adsorption site. For all simulations, the adsorption sites are located on imidazolate-2-carboxyaldehyde linkers and close to the O_OT atom and all C atom of linkers, respectively. The gate-opening effect was considered in terms of 6-membered ring window diameter distributions. When the numbers of CO₂ are increased from 5 to 30 molecules per cage, 6-membered ring window diameter is changed from 3.55 to 4.34 Å at 300K, respectively. Especially, the transition state is captured at 25 molecules per cage. However, the increase of temperature from 100 - 473 K can adjust the window diameter quickly. Finally, it can be concluded that not only the number of CO₂ molecules but also temperatures can induce the gate-opening effect. This effect was not observed for N₂ adsorption but fluctuated slightly to 3.7 Å at high temperature. The separation factor in form of adsorption selectivity of the CO₂/N₂ mixture shows the highest value around 6 at a temperature of 298 K for all CO₂/N₂ ratios.

In addition, the second major feedstock for power plants is natural gas which must be freed from H₂S before it can be used. All porous materials that are investigated in this study (ZIF-8, ZIF-67, Co/Zn-ZIF and MIL-127(Fe)) are suited for separating H₂S from natural gas but the efficiency is different. For the binary mixture CH₄/H₂S, the H₂S is stronger adsorbed than CH₄ in all materials. Due to the larger channels and pores in MIL-127(Fe) the amount of H₂S that is adsorbed is larger than

that in the ZIFs and also the adsorption selectivity is larger. It turned out that MIL-127(Fe) offers also the highest adsorption selectivity. This selectivity reaches its maximum value of 250 at about 2 bar and 250 K. However, even at 300 K the selectivity is between 60 and 80. Therefore, MIL-127(Fe) can be useful for this separation even at room temperature. The other materials considered in this study show very good selectivity of up to nearly 100 at 250 K. For 300 K their selectivity is much smaller. The selectivity of all materials, considered here, is higher at 250 K than at 300 K. The summarization can be pointed out that the important key factors for H₂S separation from natural gas in this work not only depend on the potential energy of each gas/material pair but also the structure should have more free space for gas interaction and containing metal oxide for increasing the adsorption site.



REFERENCES

1. T.C. Merkel, H. Lin, X. Wei and R. Baker, **Power plant post-combustion carbon dioxide capture: An opportunity for membranes.** *Journal of Membrane Science*, 2010. **359**(1-2): p. 126-139. 10.1016/j.memsci.2009.10.041
2. E. Favre, **Carbon dioxide recovery from post-combustion processes: Can gas permeation membranes compete with absorption?** *Journal of Membrane Science*, 2007. **294**(1-2): p. 50-59. 10.1016/j.memsci.2007.02.007
3. X. Zhang, X. He and T. Gundersen, **Post-combustion carbon capture with a gas separation membrane: Parametric study, capture cost, and exergy analysis.** *Energy & Fuels*, 2013. **27**(8): p. 4137-4149. 10.1021/ef3021798
4. Y. Wang, L. Zhao, A. Otto, M. Robinius and D. Stolten, **A review of post-combustion CO₂ capture technologies from coal-fired power plants.** *Energy Procedia*, 2017. **114**: p. 650-665. 10.1016/j.egypro.2017.03.1209
5. R.W. Baker and B.T. Low, **Gas separation membrane materials: A perspective.** *Macromolecules*, 2014. **47**(20): p. 6999-7013. 10.1021/ma501488s
6. K. Ramasubramanian and W.S.W. Ho, **Recent developments on membranes for post-combustion carbon capture.** *Current Opinion in Chemical Engineering*, 2011. **1**(1): p. 47-54. 10.1016/j.coche.2011.08.002
7. Z. Zhang, Y. Zhao, Q. Gong, Z. Li and J. Li, **MOFs for CO₂ capture and separation from flue gas mixtures: The effect of multifunctional sites on their adsorption capacity and selectivity.** *Chem Commun (Camb)*, 2013. **49**(7): p. 653-61. 10.1039/c2cc35561b
8. A. Huang, W. Dou and J. Caro, **Steam-stable Zeolitic Imidazolate Framework ZIF-90 membrane with hydrogen selectivity through covalent functionalization.** *Journal of the American Chemical Society*, 2010. **132**(44): p. 15562-15564. 10.1021/ja108774v
9. A. Huang, Q. Liu, N. Wang and J. Caro, **Organosilica functionalized Zeolitic Imidazolate Framework ZIF-90 membrane for CO₂/CH₄ separation.** *Microporous and Mesoporous Materials*, 2014. **192**: p. 18-22.

- 10.1016/j.micromeso.2013.09.025
10. D. Fairen-Jimenez, S.A. Moggach, M.T. Wharmby, P.A. Wright, S. Parsons and T. Duren, **Opening the gate: Framework flexibility in ZIF-8 explored by experiments and simulations.** *J Am Chem Soc*, 2011. **133**(23): p. 8900-2. 10.1021/ja202154j
 11. *The importance of natural gas industry in malaysia.* 2016 [cited 2020 13 January].
 12. *The global sour gas problem.* 2012 [cited 2022 13 March].
 13. M.S.M. Nurul Noramelya Zulkefli, Jamaliah Jahim, Edy Herianto Majlan, **Overview of h₂s removal technologies from biogas production.** *International Journal of Applied Engineering Research*, 2016. **11**: p. 7.
 14. H. Wu, M. Shen, X. Chen, G. Yu, A.A. Abdeltawab and S.M. Yakout, **New absorbents for hydrogen sulfide: Deep eutectic solvents of tetrabutylammonium bromide/carboxylic acids and choline chloride/carboxylic acids.** *Separation and Purification Technology*, 2019. **224**: p. 281-289. <https://doi.org/10.1016/j.seppur.2019.04.082>
 15. C. Song, Q. Liu, N. Ji, S. Deng, J. Zhao and Y. Kitamura, **Natural gas purification by heat pump assisted MEA absorption process.** *Applied Energy*, 2017. **204**: p. 353-361. <https://doi.org/10.1016/j.apenergy.2017.07.052>
 16. B. Suleiman, A.S. Abdulkareem, Y.O. Abdulsalam, U. Musa, A.S. Kovo and I.A. Mohammed, **Thermo-economic analysis of natural gas treatment process using triethanolamine (TEA) and diethanolamine (DEA) as gas sweeteners.** *Journal of Natural Gas Science and Engineering*, 2016. **36**: p. 184-201. <https://doi.org/10.1016/j.jngse.2016.10.023>
 17. K. Oshima, R. Kadonaga, M. Shiba, M. Sohmiya and S. Satokawa, **Adsorption and catalytic decomposition of dimethyl sulfide on H-BEA zeolite.** *International Journal of Hydrogen Energy*, 2020. **45**(51): p. 27644-27652. <https://doi.org/10.1016/j.ijhydene.2020.07.106>
 18. J. Haider, S. Saeed, M.A. Qyyum, B. Kazmi, R. Ahmad, A. Muhammad and M. Lee, **Simultaneous capture of acid gases from natural gas adopting ionic liquids: Challenges, recent developments, and prospects.** *Renewable and*

- Sustainable Energy Reviews, 2020. **123**: p. 109771.
<https://doi.org/10.1016/j.rser.2020.109771>
19. P.B.S. Rallapalli, K. Cho, S.H. Kim, J.-N. Kim and H.C. Yoon, **Upgrading pipeline-quality natural gas to liquefied-quality via pressure swing adsorption using MIL-101(Cr) as adsorbent to remove CO₂ and H₂S from the gas.** Fuel, 2020. **281**: p. 118985. <https://doi.org/10.1016/j.fuel.2020.118985>
 20. S. Watanabe, **Chemistry of H₂S over the surface of common solid sorbents in industrial natural gas desulfurization.** Catalysis Today, 2020. <https://doi.org/10.1016/j.cattod.2020.05.064>
 21. H.T. Lu, S. Kanehashi, C.A. Scholes and S.E. Kentish, **The impact of ethylene glycol and hydrogen sulphide on the performance of cellulose triacetate membranes in natural gas sweetening.** Journal of Membrane Science, 2017. **539**: p. 432-440. <https://doi.org/10.1016/j.memsci.2017.06.023>
 22. F. Ahmad, H. Mukhtar, Z. Man and B.K. Dutta, **A theoretical analysis of non-chemical separation of hydrogen sulfide from methane by nano-porous membranes using capillary condensation.** Chemical Engineering and Processing: Process Intensification, 2008. **47**(12): p. 2203-2208. <https://doi.org/10.1016/j.cep.2007.11.015>
 23. S. Kanehashi, A. Aguiar, H.T. Lu, G.Q. Chen and S. E. Kentish, **Effects of industrial gas impurities on the performance of mixed matrix membranes.** Journal of Membrane Science, 2018. **549**: p. 686-692. <https://doi.org/10.1016/j.memsci.2017.10.056>
 24. F. Hamad, M. Qahtani, A. Ameen, M. Vaidya, S. Duval, A. Bahamdan and F. Otaibi, **Treatment of highly sour natural gas stream by hybrid membrane-amine process: Techno-economic study.** Separation and Purification Technology, 2020. **237**: p. 116348. <https://doi.org/10.1016/j.seppur.2019.116348>
 25. M. Kárászová, J. Vejražka, V. Veselý, K. Friess, A. Randová, V. Hejtmánek, L. Brabec and P. Izák, **A water-swollen thin film composite membrane for effective upgrading of raw biogas by methane.** Separation and Purification Technology, 2012. **89**: p. 212-216. <https://doi.org/10.1016/j.seppur.2012.01.037>
 26. L. Hertäg, H. Bux, J. Caro, C. Chmelik, T. Remsungnen, M. Knauth and S.

- Fritzsche, **Diffusion of CH₄ and H₂ in ZIF-8**. Journal of Membrane Science, 2011. **377**(1): p. 36-41. <https://doi.org/10.1016/j.memsci.2011.01.019>
27. S.A.S.C. Samarasinghe, C.Y. Chuah, Y. Yang and T.-H. Bae, **Tailoring CO₂/ CH₄ separation properties of mixed-matrix membranes via combined use of two- and three-dimensional Metal-Organic Frameworks**. Journal of Membrane Science, 2018. **557**: p. 30-37. <https://doi.org/10.1016/j.memsci.2018.04.025>
28. I. Erucar and S. Keskin, **High-throughput molecular simulations of metal organic frameworks for CO₂ separation: Opportunities and challenges**. 2018. **5**(4). 10.3389/fmats.2018.00004
29. J.-R. Li, J. Sculley and H.-C. Zhou, **Metal-Organic Frameworks for separations**. Chemical Reviews, 2012. **112**(2): p. 869-932. 10.1021/cr200190s
30. S. Fritzsche, T. Chokbunpiam, J. Caro, S. Hannongbua, W. Janke and T. Remsungnen, **Combined adsorption and reaction in the ternary mixture N₂, N₂O₄, NO₂ on MIL127 examined by computer simulations**. ACS Omega, 2020. **5**(22): p. 13023-13033. 10.1021/acsomega.9b04494
31. S. Wang, D. Wu, H. Huang, Q. Yang, M. Tong, D. Liu and C. Zhong, **Separation science and engineering**. Chinese Journal of Chemical Engineering, 2015. **23**(8): p. 1291-1299. 10.1016/j.cjche.2015.04.017
32. M. Sheikh Alivand, N.H.M. Hossein Tehrani, M. Shafiei-alavijeh, A. Rashidi, M. Kooti, A. Pourreza and S. Fakhraie, **Synthesis of a modified HF-free MIL-101(Cr) nanoadsorbent with enhanced H₂S/CH₄, CO₂/CH₄, and CO₂/N₂ selectivity**. Journal of Environmental Chemical Engineering, 2019. **7**(2): p. 102946. <https://doi.org/10.1016/j.jece.2019.102946>
33. V. Sokhanvaran, M. Gomar and S. Yeganegi, **H₂S separation from biogas by adsorption on functionalized MIL-47-X (X = -OH and - OCH₃): A simulation study**. Applied Surface Science, 2019. **479**: p. 1006-1013. <https://doi.org/10.1016/j.apsusc.2019.02.152>
34. H. Maghsoudi and M. Soltanieh, **Simultaneous separation of H₂S and CO₂ from CH₄ by a high silica CHA-type zeolite membrane**. Journal of Membrane

- Science, 2014. **470**: p. 159-165. <https://doi.org/10.1016/j.memsci.2014.07.025>
35. H.H. Heck, M.L. Hall, R. dos Santos and M.M. Tomadakis, **Pressure swing adsorption separation of H₂S/CO₂/CH₄ gas mixtures with molecular sieves 4A, 5A, and 13X**. Separation Science and Technology, 2018. **53**(10): p. 1490-1497. 10.1080/01496395.2017.1417315
36. A. Phan, C.J. Doonan, F.J. Uribe-Romo, C.B. Knobler, M. O’Keeffe and O.M. Yaghi, **Synthesis, structure, and carbon dioxide capture properties of Zeolitic Imidazolate Frameworks**. Accounts of Chemical Research, 2010. **43**(1): p. 58-67. 10.1021/ar900116g
37. J.-P. Zhang, Y.-B. Zhang, J.-B. Lin and X.-M. Chen, **Metal azolate frameworks: From crystal engineering to functional materials**. Chemical Reviews, 2012. **112**(2): p. 1001-1033. 10.1021/cr200139g
38. S. Park Kyo, Z. Ni, P. Côté Adrien, Y. Choi Jae, R. Huang, J. Uribe-Romo Fernando, K. Chae Hee, M. O’Keeffe and M. Yaghi Omar, **Exceptional chemical and thermal stability of Zeolitic Imidazolate Frameworks**. Proceedings of the National Academy of Sciences, 2006. **103**(27): p. 10186-10191. 10.1073/pnas.0602439103
39. W. Morris, C.J. Doonan, H. Furukawa, R. Banerjee and O.M. Yaghi, **Crystals as molecules: Postsynthesis covalent functionalization of Zeolitic Imidazolate Frameworks**. Journal of the American Chemical Society, 2008. **130**(38): p. 12626-12627. 10.1021/ja805222x
40. K. Zhou, B. Mousavi, Z. Luo, S. Phatanasri, S. Chaemchuen and F. Verpoort, **Characterization and properties of Zn/Co Zeolitic Imidazolate Frameworks vs. ZIF-8 and ZIF-67**. Journal of Materials Chemistry A, 2017. **5**(3): p. 952-957. 10.1039/C6TA07860E
41. S. Wongsakulphasatch, F. Nouar, J. Rodriguez, L. Scott, C. Le Guillouzer, T. Devic, P. Horcajada, J.-M. Greneche, P. Llewellyn, A. Vimont, G. Clet, M. Daturi and C. Serre, **Direct accessibility of mixed-metal (iii/ii) acid sites through the rational synthesis of porous metal carboxylates**. Chemical communications (Cambridge, England), 2015. **51**. 10.1039/c5cc02550h
42. E. Atci and S. Keskin, **Understanding the potential of Zeolite Imidazolate**

- Framework membranes in gas separations using atomically detailed calculations. *The Journal of Physical Chemistry C*, 2012. **116**(29): p. 15525-15537. 10.1021/jp305684d
43. A. Venkatasubramanian, M. Navaei, K.R. Bagnall, K.C. McCarley, S. Nair and P.J. Hesketh, **Gas adsorption characteristics of Metal–Organic Frameworks via quartz crystal microbalance techniques**. *The Journal of Physical Chemistry C*, 2012. **116**(29): p. 15313-15321. 10.1021/jp304631m
44. K. Zhang, A. Nalaparaju, Y. Chen and J. Jiang, **Biofuel purification in Zeolitic Imidazolate Frameworks: The significant role of functional groups**. *Phys Chem Chem Phys*, 2014. **16**(20): p. 9643-55. 10.1039/c4cp00739e
45. V.T. Phuong, T. Chokbunpiam, S. Fritzsche, T. Remsungnen, T. Rungrotmongkol, C. Chmelik, J. Caro and S. Hannongbua, **Methane in Zeolitic Imidazolate Framework ZIF-90: Adsorption and diffusion by Molecular Dynamics and Gibbs ensemble Monte Carlo**. *Microporous Mesoporous Mater.*, 2016. **235**: p. 69-77. <https://doi.org/10.1016/j.micromeso.2016.06.029>
46. Z. Sumer and S. Keskin, **Ranking of mof adsorbents for CO₂ separations: A molecular simulation study**. *Industrial & Engineering Chemistry Research*, 2016. **55**(39): p. 10404-10419. 10.1021/acs.iecr.6b02585
47. T. Chokbunpiam, S. Fritzsche, J. Caro, C. Chmelik, W. Janke and S. Hannongbua, **Importance of ZIF-90 lattice flexibility on diffusion, permeation, and lattice structure for an adsorbed H₂/CH₄ gas mixture: A re-examination by Gibbs ensemble Monte Carlo and Molecular Dynamics simulations**. *J. Phys. Chem. C*, 2017. **121**(19): p. 10455-10462. 10.1021/acs.jpcc.7b02602
48. P. Pongsajanukul, V. Parasuk, S. Fritzsche, S. Assabumrungrat, S. Wongsakulphasatch, T. Bovornratanaraks and T. Chokbunpiam, **Theoretical study of carbon dioxide adsorption and diffusion in MIL-127(fe) Metal Organic Framework**. *Chemical Physics*, 2017. **491**: p. 118-125. <https://doi.org/10.1016/j.chemphys.2017.05.009>
49. R. Jafarzadeh, J. Azamat and H. Erfan-Niya, **Molecular dynamics study for CH₄/H₂S separation through functionalized nanoporous graphyne membrane**. *Petroleum Science and Technology*, 2019. **37**(19): p. 2043-2048.

- 10.1080/10916466.2018.1482321
50. R. Berger, **Computational chemistry. Introduction to the theory and applications of molecular and quantum mechanics.** By errol g. Lewars. Angewandte Chemie International Edition, 2004. **43**(38): p. 4979-4980. <https://doi.org/10.1002/anie.200485057>
 51. F. Jensen, *Introduction to computational chemistry*. 2006: John Wiley & Sons, Inc.
 52. T.R.F.a.I.T.T. W. Smith, *The dl poly classic user manual*. 2012, STFC Daresbury Laboratory, Daresbury, Warrington WA4 4AD, Cheshire, UK.
 53. A.R. Leach, *Molecular modelling : Principles and applications*. 2001, Harlow, England; New York: Prentice Hall.
 54. R. van Santen and P. Sautet, **Computational methods in catalysis and materials science: An introduction for scientists and engineers**. 2009. 10.1002/9783527625482
 55. J.P.J.M.v.d.E. Thijs J.H. Vlugt, Marjolein Dijkstra, Berend Smit, Daan Frenkel, *Introduction to molecular simulation and statistical thermodynamics*. 2008, Delft, The Netherlands.
 56. D.J. Livingstone, **Molecular modelling for beginners by alan hinchliffe.** Wiley, **chichester**, Journal of Medicinal Chemistry, 2004. **47**(12): p. 3328-3328. 10.1021/jm0400698
 57. R. Schneider, A.R. Sharma and A. Rai, *Introduction to molecular dynamics*. Vol. 739. 2008: Lect. Notes Phys.
 58. D. Dubbeldam and R.Q. Snurr, **Recent developments in the molecular modeling of diffusion in nanoporous materials.** Molecular Simulation, 2007. **33**(4-5): p. 305-325. 10.1080/08927020601156418
 59. A.Z. Panagiotopoulos, **Direct determination of phase coexistence properties of fluids by Monte Carlo simulation in a new ensemble.** Molecular Physics, 1987. **61**(4): p. 813-826. 10.1080/00268978700101491
 60. B. Chen, J.I. Siepmann and M.L. Klein, **Direct Gibbs ensemble Monte Carlo simulations for solid-vapor phase equilibria: Applications to**

- Lennard–Jonesium and carbon dioxide.** The Journal of Physical Chemistry B, 2001. **105**(40): p. 9840-9848. 10.1021/jp011950p
61. D.C. Rapaport, *The art of molecular dynamics simulation*. 2 ed. 2004, Cambridge: Cambridge University Press.
62. W. Swope, H. Andersen, P. Berens and K. Wilson, **A computer-simulation method for the calculation of equilibrium-constants for the formation of physical clusters of molecules—application to small water clusters.** The Journal of Chemical Physics, 1982. **76**. 10.1063/1.442716
63. D. Beeman, **Some multistep methods for use in molecular dynamics calculations.** Journal of Computational Physics, 1976. **20**(2): p. 130-139. [https://doi.org/10.1016/0021-9991\(76\)90059-0](https://doi.org/10.1016/0021-9991(76)90059-0)
64. J.A. Gee, J. Chung, S. Nair and D.S. Sholl, **Adsorption and diffusion of small alcohols in Zeolitic Imidazolate Frameworks ZIF-8 and ZIF-90.** The Journal of Physical Chemistry C, 2013. **117**(6): p. 3169-3176. 10.1021/jp312489w
65. P. Vo, T. Chokbunpiam, S. Fritzsche, T. Remsungnen, T. Rungrotmongkol, C. Chmelik, J. Caro and S. Hannongbua, **Methane in Zeolitic Imidazolate Framework ZIF-90: Adsorption and diffusion by molecular dynamics and Gibbs ensemble Monte Carlo.** Microporous and Mesoporous Materials, 2016. **235**. 10.1016/j.micromeso.2016.06.029
66. D. Liu, Y. Wu, Q. Xia, Z. Li and H. Xi, **Experimental and molecular simulation studies of CO₂ adsorption on Zeolitic Imidazolate Frameworks: ZIF-8 and amine-modified ZIF-8.** Adsorption, 2013. **19**(1): p. 25-37. 10.1007/s10450-012-9407-1
67. C.S. Murthy, K. Singer and I.R. McDonald, **Interaction site models for carbon dioxide.** Molecular Physics, 1981. **44**(1): p. 135-143. 10.1080/00268978100102331
68. J.J. Potoff and J.I. Siepmann, **Vapor-liquid equilibria of mixtures containing alkanes, carbon dioxide, and nitrogen.** AIChE Journal, 2001. **47**(7): p. 1676-1682. 10.1002/aic.690470719
69. B. Zheng, M. Sant, P. Demontis and G.B. Suffritti, **Force field for Molecular Dynamics computations in flexible ZIF-8 framework.** The Journal of Physical

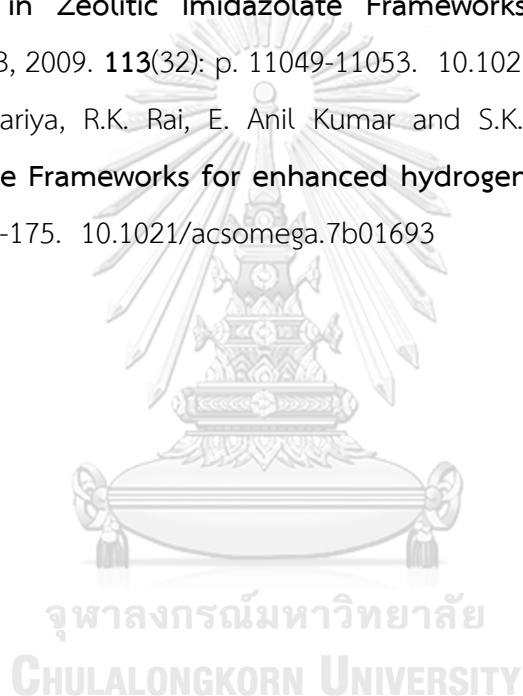
- Chemistry C, 2012. **116**(1): p. 933-938. 10.1021/jp209463a
70. X. Wu, J. Huang, W. Cai and M. Jaroniec, **Force field for ZIF-8 flexible frameworks: Atomistic simulation of adsorption, diffusion of pure gases as CH₄, H₂, CO₂ and N₂**. RSC Advances, 2014. **4**(32): p. 16503-16511. 10.1039/C4RA00664J
71. R. Chanajaree, T. Chokbunpiam, J. Kärger, S. Hannongbua and S. Fritzsche, **Investigating adsorption- and diffusion selectivity of CO₂ and CH₄ from air on Zeolitic Imidazolate Framework-78 using molecular simulations**. Microporous Mesoporous Mater., 2019. **274**: p. 266-276. <https://doi.org/10.1016/j.micromeso.2018.07.023>
72. T. Chokbunpiam, R. Chanajaree, J. Caro, W. Janke, T. Remsungnen, S. Hannongbua and S. Fritzsche, **Separation of nitrogen dioxide from the gas mixture with nitrogen by use of ZIF materials; computer simulation studies**. Comput. Mater. Sci., 2019. **168**: p. 246-252. <https://doi.org/10.1016/j.commatsci.2019.05.025>
73. P. Schierz, S. Fritzsche, W. Janke, S. Hannongbua, O. Saengsawang, C. Chmelik and J. Kärger, **Md simulations of hydrogen diffusion in ZIF-11 with a force field fitted to experimental adsorption data**. Microporous and Mesoporous Materials, 2015. **203**: p. 132-138. <https://doi.org/10.1016/j.micromeso.2014.10.031>
74. T. Chokbunpiam, S. Fritzsche, V. Parasuk, J. Caro and S. Assabumrungrat, **Molecular simulations of a CO₂/CO mixture in MIL-127**. Chem. Phys. Lett., 2018. **696**: p. 86-91. <https://doi.org/10.1016/j.cplett.2018.02.032>
75. F. van Gunsteren Wilfred and J.C. Berendsen Herman, **Computer simulation of molecular dynamics: Methodology, applications, and perspectives in chemistry**. Angewandte Chemie International Edition in English, 1990. **29**(9): p. 992-1023. 10.1002/anie.199009921
76. C.J. Fennell and J.D. Gezelter, **Is the ewald summation still necessary? Pairwise alternatives to the accepted standard for long-range electrostatics**. The Journal of Chemical Physics, 2006. **124**(23): p. 234104. 10.1063/1.2206581
77. L. Zhang, G. Wu and J. Jiang, **Adsorption and diffusion of CO₂ and CH₄ in**

- Zeolitic Imidazolate Framework-8: Effect of structural flexibility.** The Journal of Physical Chemistry C, 2014. **118**(17): p. 8788-8794. 10.1021/jp500796e
78. T.R.F.a.I.T.T. W. Smith, *DL poly classic*.
79. K.S. Park, Z. Ni, A.P. Côté, J.Y. Choi, R. Huang, F.J. Uribe-Romo, H.K. Chae, M. O'Keeffe and O.M. Yaghi, **Exceptional chemical and thermal stability of Zeolitic Imidazolate Frameworks.** Proceedings of the National Academy of Sciences, 2006. **103**(27): p. 10186. 10.1073/pnas.0602439103
80. H. Hayashi, A.P. Côté, H. Furukawa, M. O'Keeffe and O.M. Yaghi, **Zeolite a imidazolate frameworks.** Nature materials, 2007. **6**(7): p. 501-6. 10.1038/nmat1927
81. S. Wongsakulphasatch, F. Nouar, J. Rodriguez, L. Scott, C. Le Guillouzer, T. Devic, P. Horcajada, J.M. Grenèche, P.L. Llewellyn, A. Vimont, G. Clet, M. Daturi and C. Serre, **Direct accessibility of mixed-metal (iii/ii) acid sites through the rational synthesis of porous metal carboxylates.** Chemical Communications, 2015. **51**(50): p. 10194-10197. 10.1039/C5CC02550H
82. T. Chokbunpiam, R. Chanajaree, O. Saengsawang, S. Reimann, C. Chmelik, S. Fritzsche, J. Caro, T. Remsungnen and S. Hannongbua, **The importance of lattice flexibility for the migration of ethane in ZIF-8: Molecular Dynamics simulations.** Microporous and Mesoporous Materials, 2013. **174**: p. 126-134. <https://doi.org/10.1016/j.micromeso.2012.12.047>
83. P. Li, B.P. Roberts, D.K. Chakravorty and K.M. Merz, Jr., **Rational design of particle mesh ewald compatible Lennard-Jones parameters for +2 metal cations in explicit solvent.** Journal of chemical theory and computation, 2013. **9**(6): p. 2733-2748. 10.1021/ct400146w
84. P. Krokidas, M. Castier, S. Moncho, D.N. Sredojevic, E.N. Brothers, H.T. Kwon, H.-K. Jeong, J.S. Lee and I.G. Economou, **ZIF-67 framework: A promising new candidate for propylene/propane separation. Experimental data and molecular simulations.** The Journal of Physical Chemistry C, 2016. **120**(15): p. 8116-8124. 10.1021/acs.jpcc.6b00305
85. Z. Hu, L. Zhang and J. Jiang, **Development of a force field for Zeolitic Imidazolate Framework-8 with structural flexibility.** The Journal of Chemical

- Physics, 2012. **136**(24): p. 244703. 10.1063/1.4729314
86. M.G. Martin and J.I. Siepmann, **Transferable potentials for phase equilibria. 1. United-atom description of n-alkanes.** J. Phys. Chem. B, 1998. **102**(14): p. 2569-2577. 10.1021/jp972543+
87. R. López-Rendón and J. Alejandre, **MolecularDynamics simulations of the solubility of H₂S and CO₂ in water.** Journal of the Mexican Chemical Society, 2008. **52**: p. 88-92.
88. A.K. Rappe, C.J. Casewit, K.S. Colwell, W.A. Goddard and W.M. Skiff, **UFF a full periodic table force field for Molecular Mechanics and Molecular Dynamics simulations.** J. Am. Chem. Soc., 1992. **114**(25): p. 10024-10035. 10.1021/ja00051a040
89. C. Gücüyener, J. van den Bergh, J. Gascon and F. Kapteijn, **Ethane/ethene separation turned on its head: Selective ethane adsorption on the Metal–Organic Framework ZIF-7 through a gate-opening mechanism.** J. Am. Chem. Soc., 2010. **132**(50): p. 17704-17706. 10.1021/ja1089765
90. S. Aguado, G. Bergeret, M.P. Titus, V. Moizan, C. Nieto-Draghi, N. Bats and D. Farrusseng, **Guest-induced gate-opening of a Zeolite Imidazolate Framework.** New J. Chem., 2011. **35**(3): p. 546-550. 10.1039/C0NJ00836B
91. T. Chokbunpiam, S. Fritzsche, C. Chmelik, J. Caro, W. Janke and S. Hannongbua, **Gate opening effect for carbon dioxide in ZIF-8 by Molecular Dynamics – confirmed, but at high CO₂ pressure.** Chem. Phys. Lett., 2016. **648**: p. 178-181. <https://doi.org/10.1016/j.cplett.2016.01.060>
92. F. Keil, *Diffusion und chemische reaktionen in der gas/feststoff-katalyse.* 1 ed. 1999: Springer, Berlin, Heidelberg.
93. N. Chanut, A.D. Wiersum, U.H. Lee, Y.K. Hwang, F. Ragon, H. Chevreau, S. Bourrelly, B. Kuchta, J.-S. Chang, C. Serre and P.L. Llewellyn, **Observing the effects of shaping on gas adsorption in Metal-Organic Frameworks.** European Journal of Inorganic Chemistry, 2016. **2016**(27): p. 4416-4423. <https://doi.org/10.1002/ejic.201600410>
94. A.A. Jameh, T. Mohammadi, O. Bakhtiari and M. Mahdyarfar, **Synthesis and modification of Zeolitic Imidazolate Framework (ZIF-8) nanoparticles as**

highly efficient adsorbent for H₂S and CO₂ removal from natural gas. Journal of Environmental Chemical Engineering, 2019. 7(3): p. 103058. <https://doi.org/10.1016/j.jece.2019.103058>

95. R. Babarao, S. Dai and D.-e. Jiang, **Effect of pore topology and accessibility on gas adsorption capacity in Zeolitic-Imidazolate Frameworks: Bringing molecular simulation close to experiment**. The Journal of Physical Chemistry C, 2011. **115**(16): p. 8126-8135. 10.1021/jp1117294
96. M. Zhou, Q. Wang, L. Zhang, Y.-C. Liu and Y. Kang, **Adsorption sites of hydrogen in Zeolitic Imidazolate Frameworks**. The Journal of Physical Chemistry B, 2009. **113**(32): p. 11049-11053. 10.1021/jp904170s
97. D.K. Panchariya, R.K. Rai, E. Anil Kumar and S.K. Singh, **Core-shell Zeolitic Imidazolate Frameworks for enhanced hydrogen storage**. ACS Omega, 2018. **3**(1): p. 167-175. 10.1021/acsomega.7b01693





APPENDICES

จุฬาลงกรณ์มหาวิทยาลัย
CHULALONGKORN UNIVERSITY

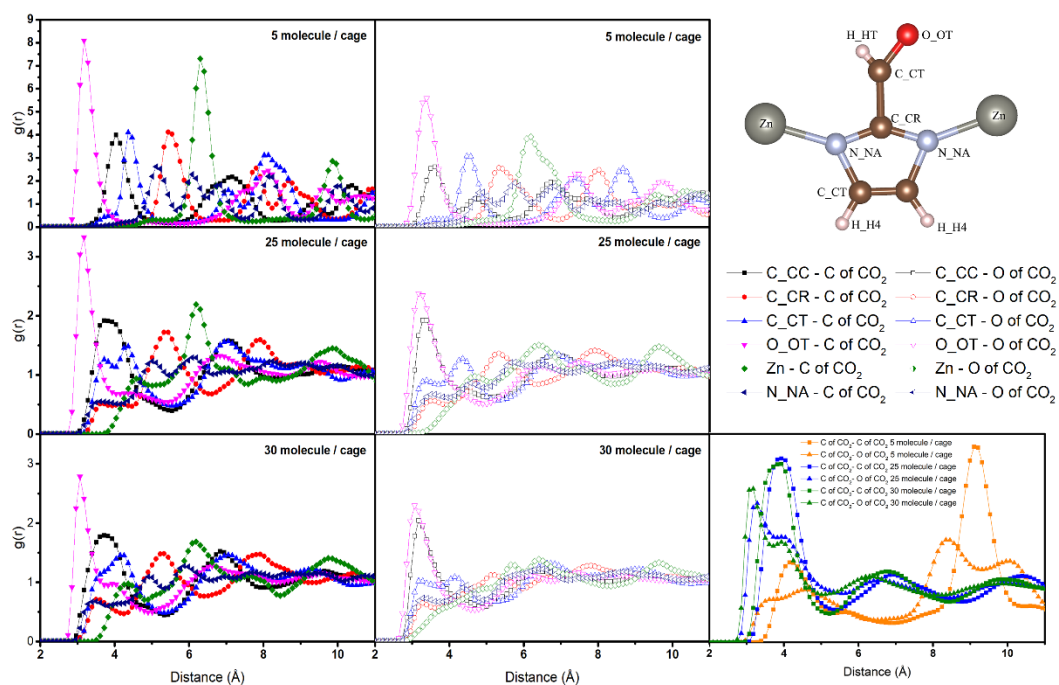
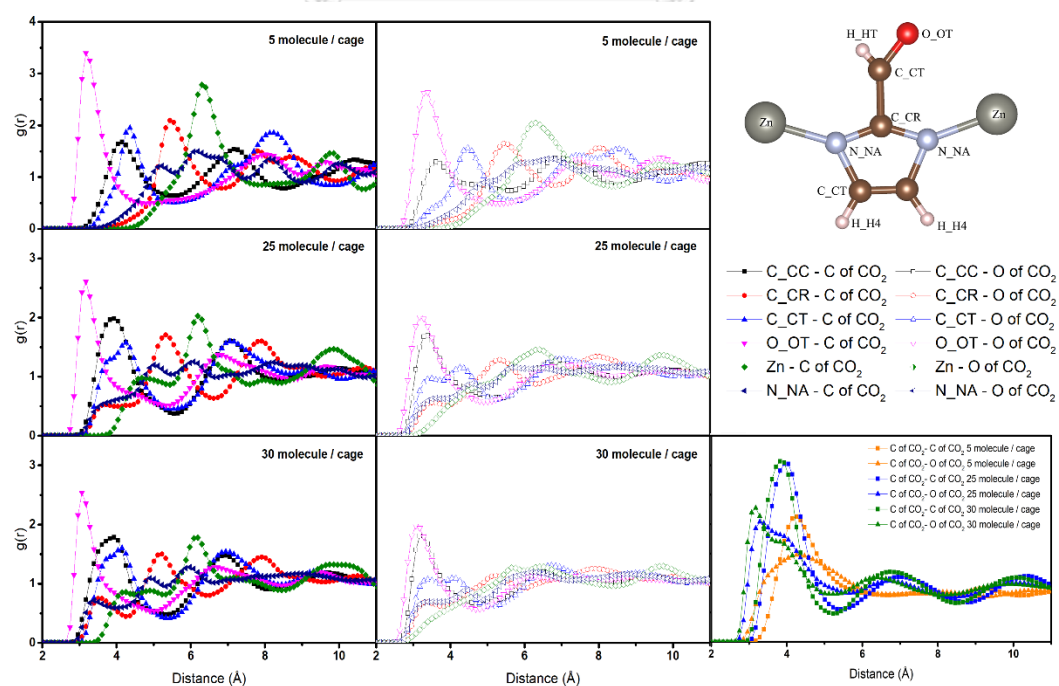


APPENDIX A

CO₂ induced swing effect at imidazolate of zeolitic imidazolate framework-90
using molecular simulations

จุฬาลงกรณ์มหาวิทยาลัย
CHULALONGKORN UNIVERSITY

Radial Distribution Functions

Figure A1 The Radial Distribution Functions (RDF) for CO₂ in ZIF-90 at 100 KFigure A2 The Radial Distribution Functions (RDF) for CO₂ in ZIF-90 at 200 K

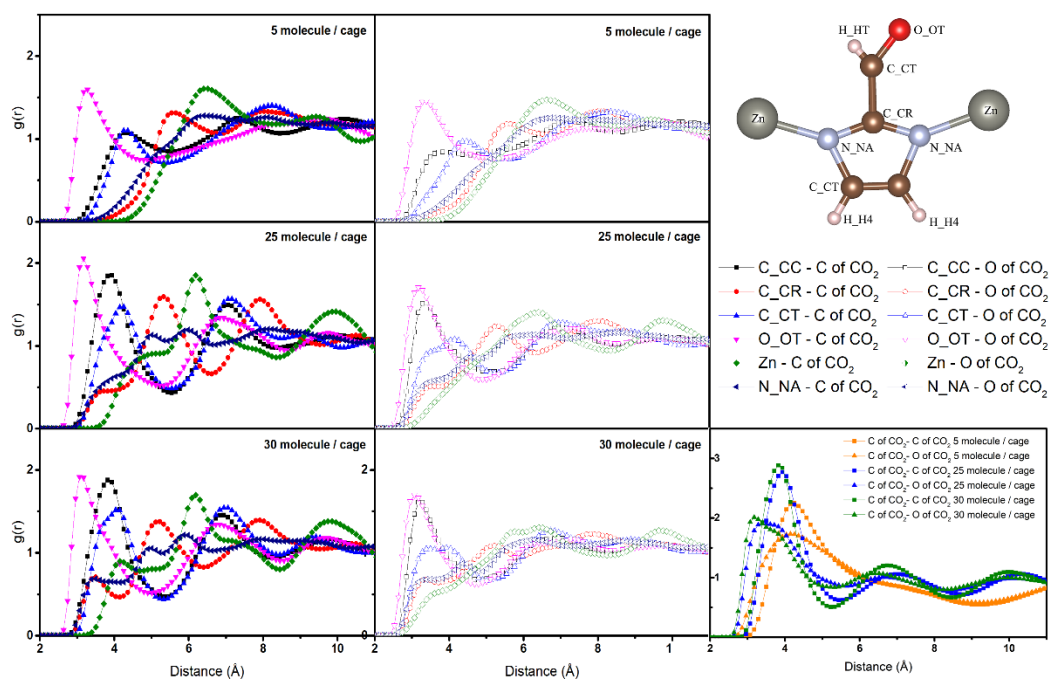


Figure A3 The Radial Distribution Functions (RDF) for CO₂ in ZIF-90 at 373 K

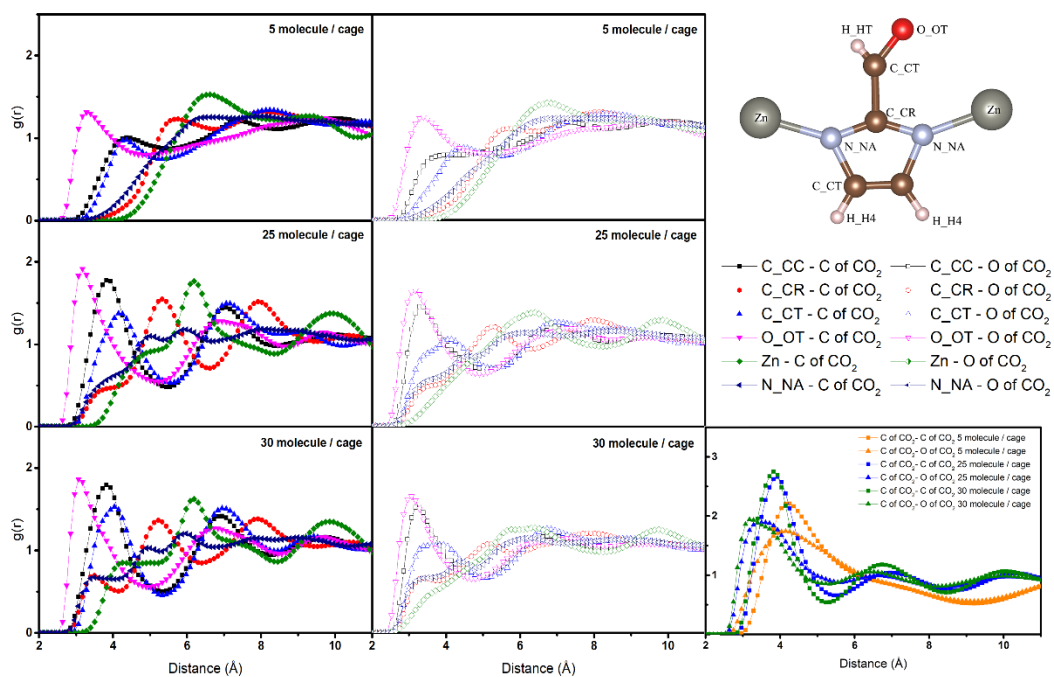


Figure A4 The Radial Distribution Functions (RDF) for CO₂ in ZIF-90 at 473 K



APPENDIX B

Porous Material Adsorbents ZIF-8, ZIF-67, Co/Zn-ZIF and MIL-127(Fe)
for separation of H₂S from a H₂S /CH₄ Mixture

จุฬาลงกรณ์มหาวิทยาลัย
CHULALONGKORN UNIVERSITY

Porous materials

Structural characteristics of ZIFs

Table B1. Structural characteristics of ZIFs.

ZIF materials	Window aperture diameter (Å)		$S_{\text{BET}[97]}$ (m ² /g)	$V_{\text{p}[97]}$ (cm ³ /g)	$S_{\text{BET}[40]}$ (m ² /g)	$V_{\text{p}[40]}$ (cm ³ /g)
	6-membered ring	4-membered ring				
ZIF-8	~ 3.4	~ 0.8	~ 1323	~ 0.76	~1821	~0.66
ZIF-67			~ 1295	~ 0.73	~1888	~0.71
Co/Zn-ZIF			~ 1392	~ 0.69	~1864	~0.62

* S_{BET} = Surface area

* V_{p} = Pore Volume (by Horvath-Kawazoe method)



Figure B1 Atom types of ZIF materials.

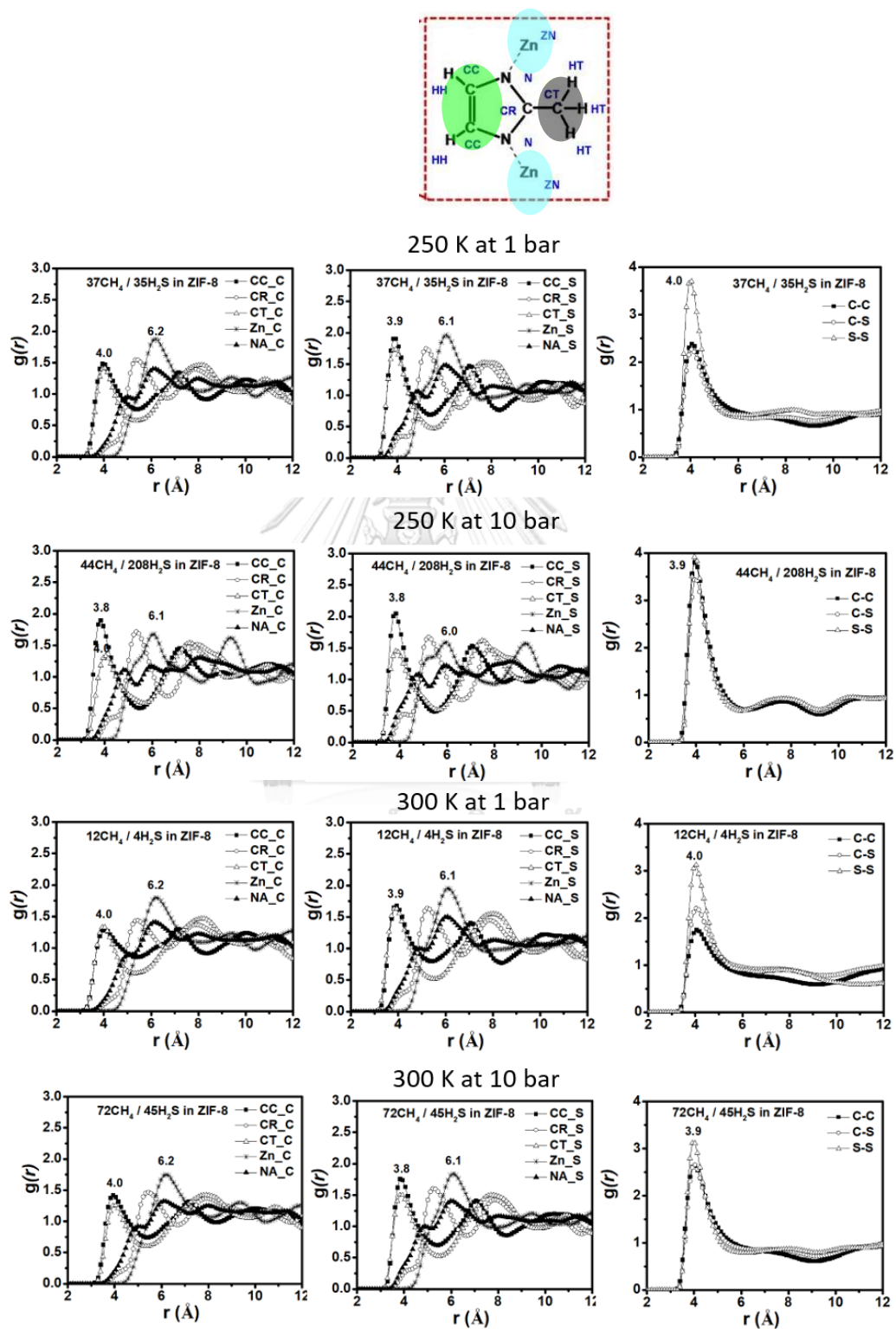
Structural characteristics of MIL-127(Fe)

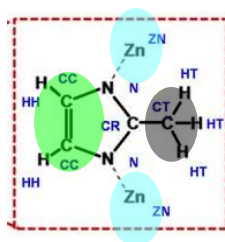
MIL-127(Fe) has two types of pores such as an accessible 1D channel system around 6 Å and cages of cavity around 10 Å accessible through window apertures of around 4 Å. It has surface area and pore volume around 1400 m²/g and 0.7 cm³/g, respectively.



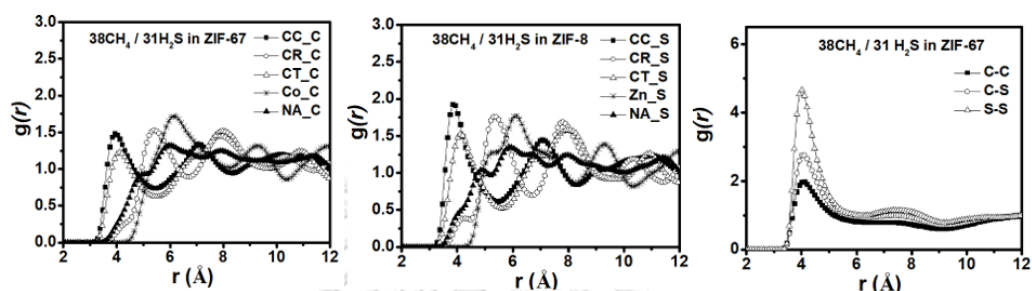
Figure B2 Atom types of MIL-127(Fe) material.

Radial distribution functions (RDFs)

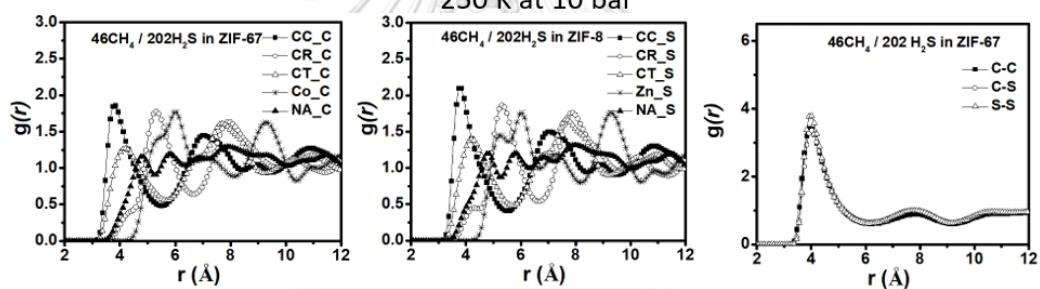
 $\text{H}_2\text{S}/\text{CH}_4$ mixture in ZIF-8Figure B3 RDFs of mixture CH_4 and H_2S and guest-guest in ZIF-8.

H₂S/CH₄ mixture in ZIF-67

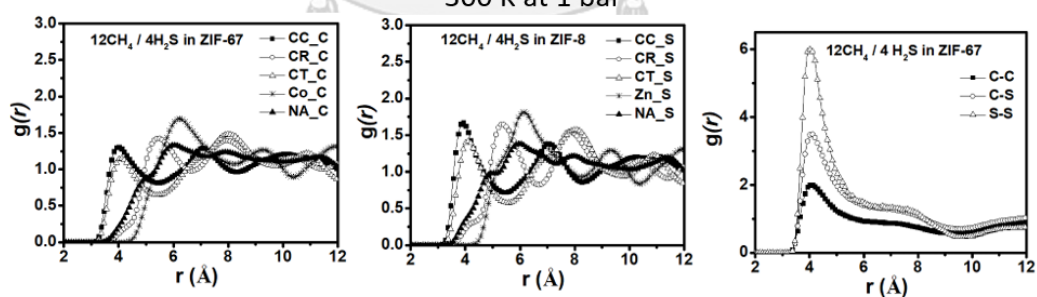
250 K at 1 bar



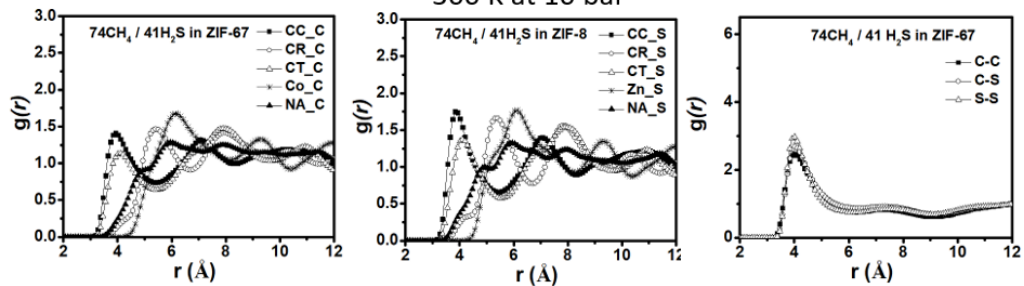
250 K at 10 bar

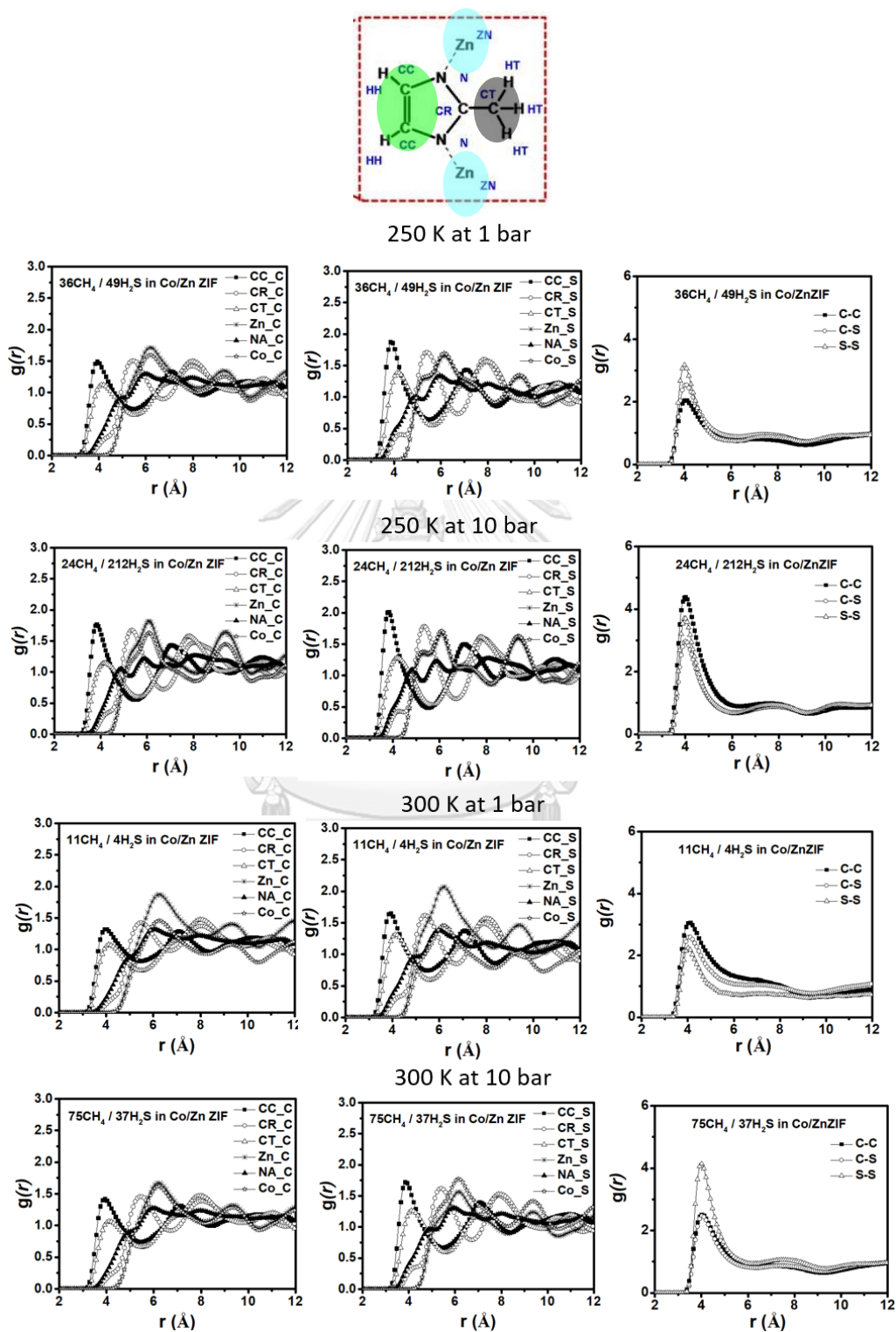


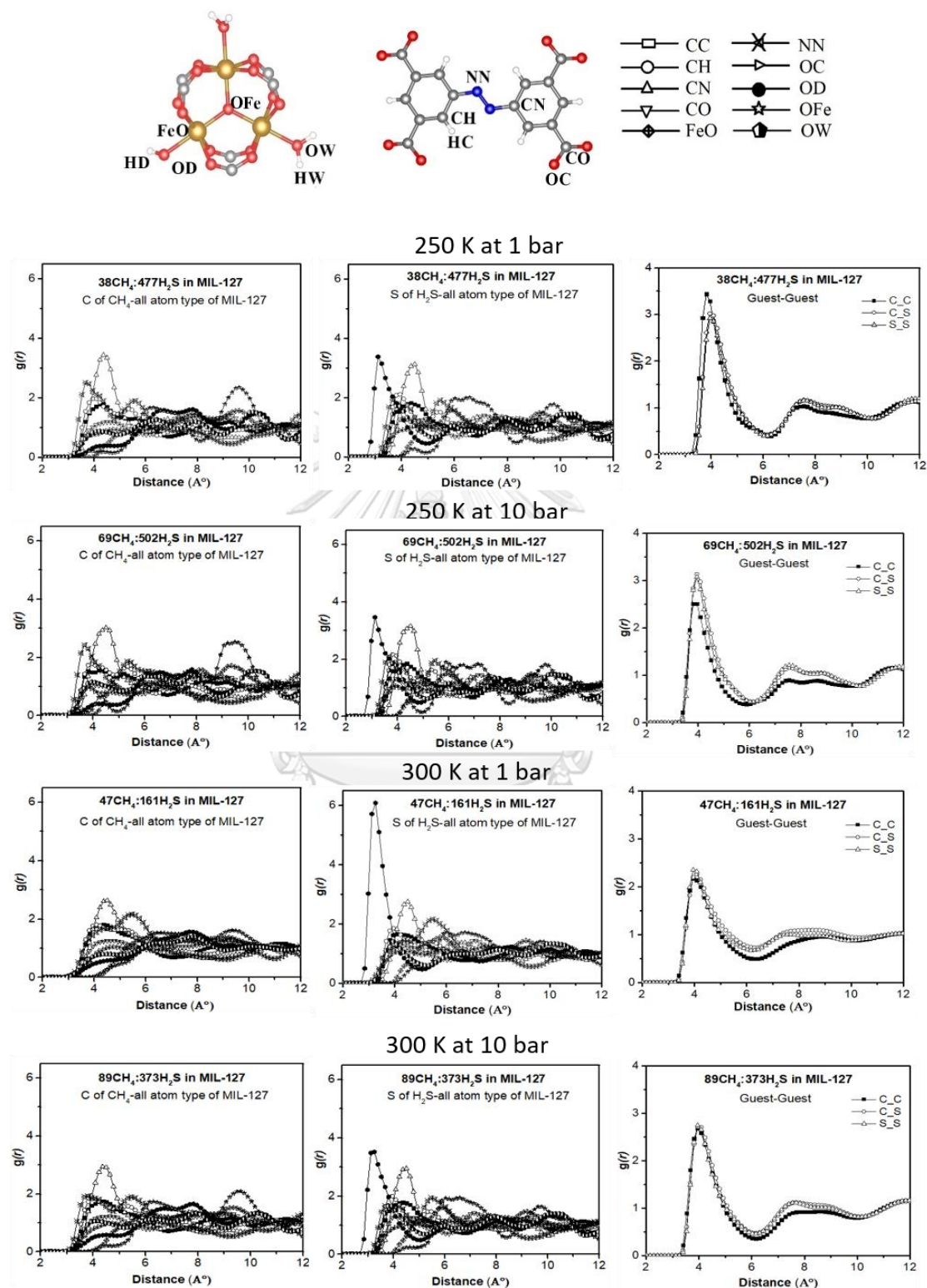
300 K at 1 bar



300 K at 10 bar

Figure B4 RDFs of mixture CH₄ and H₂S and guest- guest in ZIF-67.

H₂S/CH₄ mixture in Co/Zn-ZIFFigure B5 RDFs of mixture CH₄ and H₂S and guest-guest in Co/Zn ZIF.

H₂S/CH₄ mixture in MIL-127(Fe)Figure B6 RDFs of mixture CH₄ and H₂S and guest- guest in MIL-127(Fe).

The comparison of some results from GEMC with results from GCMC

In order to learn about the usability of GEMC and GCMC we have carried out additional GCMC calculations. Since the adsorption and the selectivity are the strongest at 250 K we have investigated the selective adsorption in ZIF-8 for three pressures at 250 K.

Table B2 Comparison of results from GEMC and GCMC for the CH₄/H₂S mixture at 250 K and at various pressures.

Pressure (bar)	GCMC H ₂ S adsorbed in mmol/g	GCMC CH ₄ adsorbed in mmol/g	GEMC H ₂ S adsorbed in mmol/g	GEMC CH ₄ adsorbed in mmol/g	Selectivity GEMC	Selectivity GCMC
1.99	2.45	4.49	2.47	4.36	33.44	34.87
9.66	9.58	2.01	9.52	2.03	89.00	90.16
18.49	10.30	1.94	10.23	2.04	95.26	101.23

The results agree quite well. The GCMC calculations seem to yield slightly higher selectivity, but the differences are still in the range of fluctuations. The fugacities that were needed for GCMC have been calculated by the Peng-Robinson equation of state. The cross correction contributions in the Peng-Robinson equation for mixtures have been neglected. The fugacities are given in Table B3

Table B3 Fugacities that have been used in GCMC for the mixture of 95% CH₄ and 5% H₂S at 250 K.

Pressure (bar)	Fugacity of CH ₄ (bar)	Fugacity of H ₂ S (bar)
1.99	1.87	0.097
9.66	8.84	0.44
18.49	16.36	0.76

The Density Plot of CH₄ and H₂S in MIL-127(Fe), ZIF-8, ZIF-67 and Co/Zn-ZIF at 10 bar and 300 K.

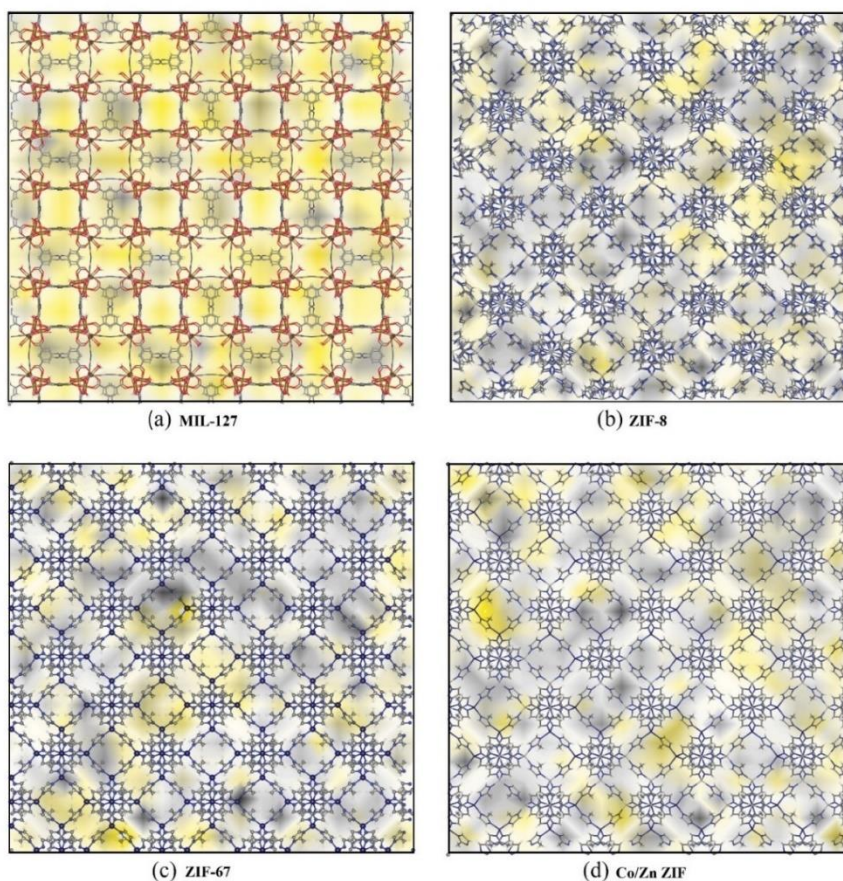


Figure B7 The density plot of CH₄ (gray region) and H₂S (yellow region) for (a) MIL-127(Fe) (b) ZIF-8 (c) ZIF-67 and (d) Co/Zn-ZIF materials at 10 bar and 300 K.

The snapshots of CH_4 and H_2S inside MIL-127(Fe), ZIF-8, ZIF-67 and Co/Zn-ZIF.

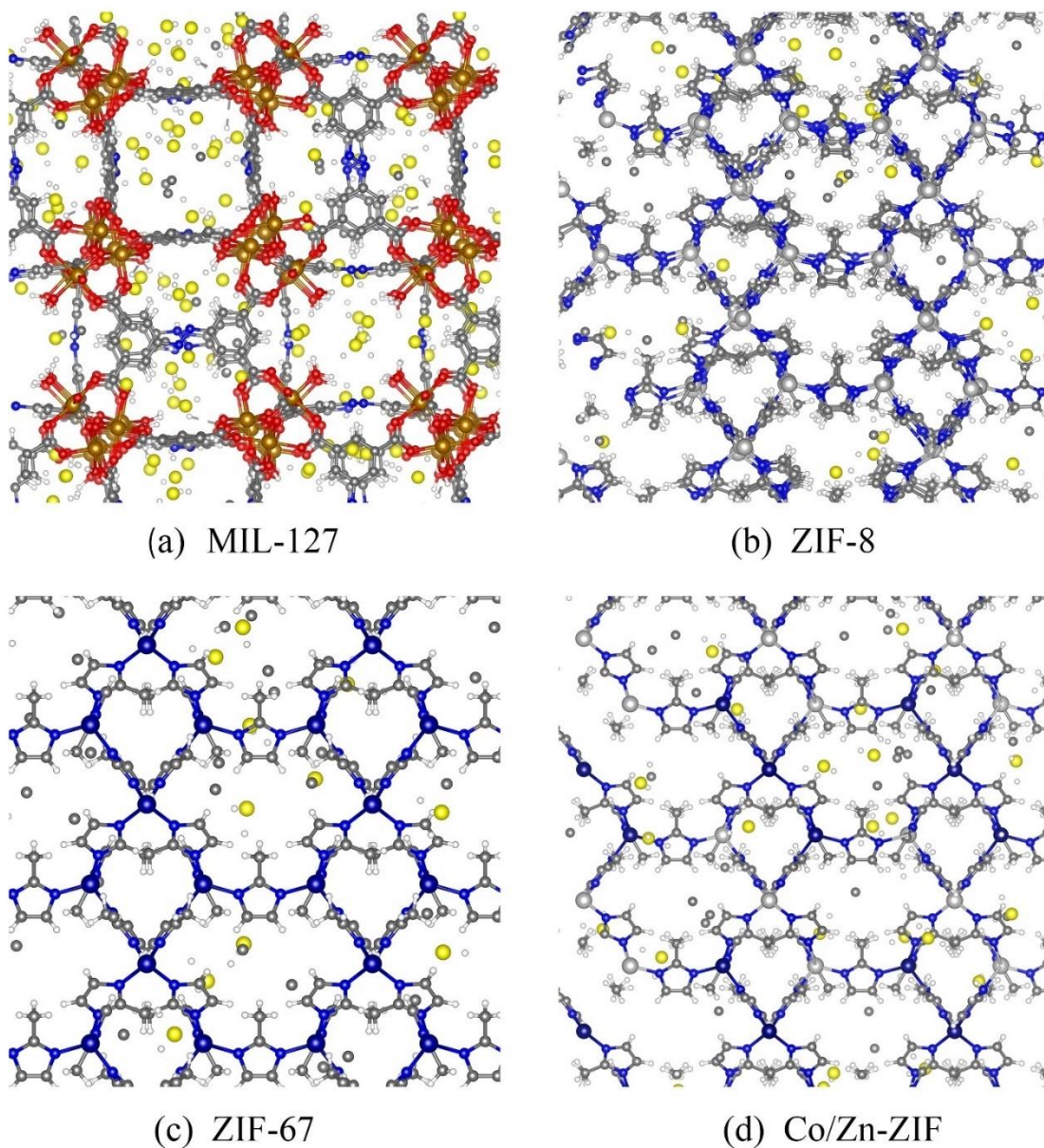


Figure B8 The snapshots of CH_4 (gray circle) and H_2S (yellow circle) for (a) MIL-127(Fe) (b) ZIF-8 (c) ZIF-67 and (d) Co/Zn-ZIF materials at 10 bar and 300 K.

VITA

NAME Tanawut Ploymeerusmee

DATE OF BIRTH 13 January 1983

PLACE OF BIRTH Bangkok

INSTITUTIONS ATTENDED

1989-1995	Nakprasith School, Nakhon Pathom
1995-2001	Nakprasith School, Nakhon Pathom
2001-2005	B. Sc. in Chemistry, Department of Chemistry, Faculty of Science, Chulalongkorn University, Bangkok
2006-2009	M. Sc. in Petrochemistry and Polymer Science, Faculty of Science, Chulalongkorn University, Bangkok
2015-2022	Ph.D. in Petrochemistry, Faculty of Science, Chulalongkorn University, Bangkok

HOME ADDRESS 101 M5 Klongmai Sampran Nakhonpathom

PUBLICATION

Pianwanit, C. Kritayakornupong, A. Vongachariya, N. Selphusit, T. Ploymeerusmee, T. Remsungnen, D. Nuntasri, S. Fritzsche and S. Hannongbua, The optimal binding sites of CH₄ and CO₂ molecules on the metal-organic framework MOF-5: Oniom calculations. *Chemical Physics*, 2008. 349(1): p. 77-82.

T. Ploymeerusmee, S. Fritzsche, S. Hannongbua and T. Chokbunpiam, CO₂ induced swing effect at imidazolate of zeolitic imidazolate framework-90 using molecular simulations. *Theoretical Chemistry Accounts*, 2019. 138(10): p. 118.

T. Ploymeerusmee, W. Janke, T. Remsungnen, S. Hannongbua and T. Chokbunpiam, Porous material adsorbents ZIF-8, ZIF-67, Co/Zn-ZIF and MIL-127(Fe) for separation of H₂S from a H₂S/CH₄ mixture. *Molecular Simulation*, 2022. 48(5): p. 417-426.

